ISSN 0915-6348

NATIONAL INSTITUTE FOR FUSION SCIENCE

Physics and Application of High Density Z-pinches

(Received – June 7, 1993)

NIFS-PROC-14 July 1993

RESEARCH REPORT
NIFS-PROC Series

NAGOYA, JAPAN

Physics and Application of High Density Z-pinches

Edited by T. Miyamoto and K. Takasugi

Keywords: z-pinch, plasma focus, soft x-ray, x-ray laser, pulse power

PREFACE

This publication is a collection of papers presented at the research meeting on "Physics and Application on Z-pinches" held at National Institute for Fusion Science in December 11-12, 1992, in which thirty-seven persons attended from the eighteen organizations, and eighteen lectures were given. The Z-pinch is an old subject that has been studied since 1950's, but recently, is noticed in a new point of view again. The classical Z-pinch is characterized by discharging in a dilute gas filled in the glass tube and by applying the relatively low discharge voltage of few 10 kV. On the other hand, the modern Z-pinches is characterized by puffing a gas into a vacuum vessel or using a solid fiber, and also by applying the relatively high discharge voltage, i.e., more than several hundred kV. Hence, the pulse power device is often used instead of the capacitor bank, and permits to generated the Z-pinch using a solid narrow wire for which the discharge is explosive in few 10 kV. The modern Z-pinch researches give a prospect in the important field, i.e., the discharge excitation of short wave length lasers, the production of a fusion plasma and etc.. Nevertheless, it is reglettable that there is no Z-pinch research group in Japan that equips the pulse power device. One of the puposes of this meeting was to stimulate the reasearches on Z-pinches and relating subjects.

This report includes the macroscopic behaviors and radiation measurements on gas-puff and metal-vapor Z-pinches

which were presented by Nihon University and Tokyo Institute of Technology, soft X-ray measuring methods and deta processing by Gunma University, the related technical problems on voltagee amplification and closing switch by Himeji Institute of Technology and Kumamoto University, and unstable motion of toroidal Z-discharge plasma by Utsunomiya University. In the meeting several review talks (on pulsed power technology and X-ray laser) and other problems were given besides the above papers.

Tetsu Miyamoto

May, 1993

CONTENTS

LIST OF ATTENDEES

H. Akiyama	Kumamoto University
J. Du	Gunma University
T. Fujimi	Nihon University
M. Fukao	Shizuoka University
S. Furuya	Tokyo Institute of Technology
Y. Hashimoto	Himeji Institute of Technology
K. Hirano	Gunma University
K. Hoshina	Tokyo Institute of Technology
K. Ikuta	Japan Steel Works
K. Imasaka	Kumamoto University
S. Ishii	Tokyo Institute of Technology
K. Iwai	Gunma University
Y. Kato	Osaka University
K. Matsumoto	Utsunomiya University
K. Matsuura	Utsunomiya University
H. Matsuzawa	Yamanashi University
T. Miyamoto	Nihon University
K. Moriyama	Nihon University
K. Nagakawa	Himeji Institute of Technology
H. Nakamura	Nihon University
T. Nakano	Hamamatsu Photonics
Y. Nonami	Shizuoka University
M. Oba	Hamamatsu Photonics
M. Sato	Himeji Institute of Technology
H. Seki	Hitachi Ltd.

K. Shibata	Oyama Polytechnic College
N. Shimizu	Utsunomiya University
H. Suemitsu	Kyoto University
H. Suzuki	Nihon University
Y. Takahama	Gunma University
K. Takasugi	Nihon University
T. Tazima	National Institute for Fusion Science
A. Tokuchi	Nichikon Co.
R. Yamamoto	Himeji Institute of Technology
T. Yamamoto	Gunma University
K. Yatsui	Nagaoka University of Technology
M. Yokoyama	Kinki University

VOLTAGE AMPLIFICATION EXPERIMENT WITH SMALL COAXIAL MAGNETICALLY INSULATED SWITCH

Tadashi Yamamoto, Morihiko Sato,

Mitsuyasu Yatsuzuka and Sadao Nobuhara

Department of Electrical Engineering,

Himeji Institute of Technology,

Shosha, Himeji, Hyogo 671-22, Japan

ABSTRACT

In most of pulsed power generators, the voltages applied to loads drop from the output voltages of the generators. As one of the solution, we tried voltage amplification by using a small coaxial magnetically insulated switch. In the experiment, the "Inverse Pinch Ion Diode" was used as a load, and the voltage applied to the diode increased from 130 to 260 kV.

§1. Introduction

The voltages applied to loads generally drop from the output voltages of pulsed power generators due to effect of the inductance between the pulsed power generators and the loads. One of the good solution to remove this effect is to use the plasma erosion opening switch[1]. As the other solution, we propose the method to use a small coaxial magnetically insulated switch (MIS).

This switch consists of an inner and an outer conductor of which diameters are several millimeters, and the lengths of them are approximately 10 to 20 mm. For operation of MIS, only these conductors are placed between a pulsed power generator and a load.

Figures 1 (a) and (b) show the schematic drawings of MIS and a small pinched relativistic electron beam (REB) diode. When a pulsed high voltage is supplied from a pulsed power generator, MIS initially plays a role of an electron beam diode,

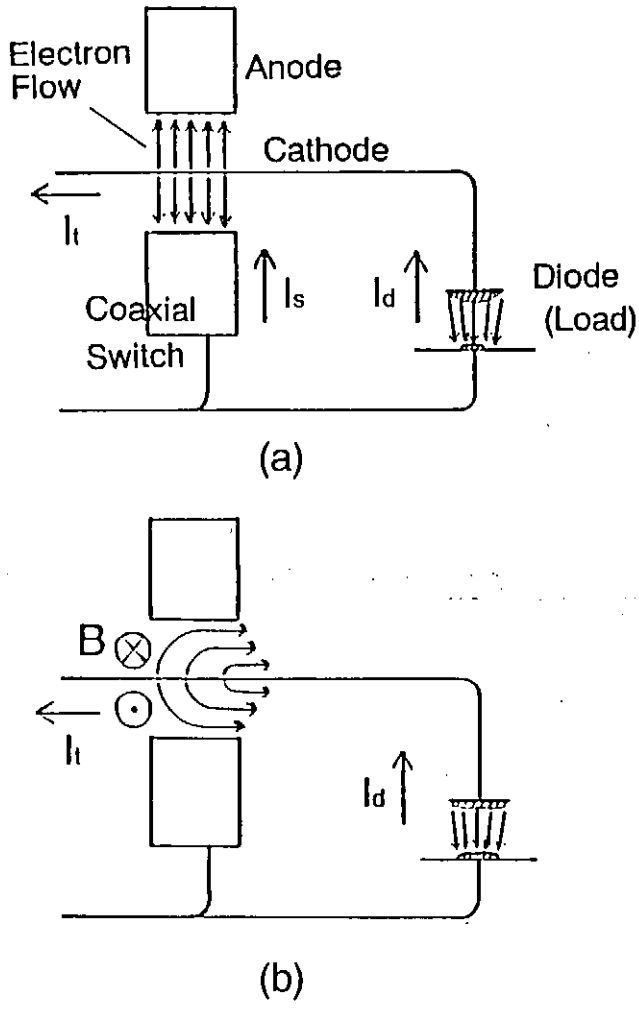

Fig. 1. Schematic drawings of arrangement in voltage amplification experiment with MIS: initial phase (a) and after magnetic insulation (b).

i.e. an electron current flows between the conductors. The currents flowing in MIS and the load increase slowly, and the summation of these currents exceed the critical current in MIS. At this time magnetic insulation is completed. By magnetic insulation, the current flowing in MIS transfer to the load, and the voltage across the load becomes high. In this method, a voltage amplification factor is not so high, but the method itself is very simple and easy way.

The experiments were made with the pulsed power generator "HARIMA-II". The "Inverse Pinch Ion Diode" (IPD)[2] and a small pinched REB diode [3] were used as the loads. In the case of IPD, the maximum voltage measured at the diode increased from 130 to 260 kV by operation of MIS. The small pinched REB diode was used to estimate the current flowing in MIS. From the experimental results, it was verified that the current flowing in MIS decreased after magnetic insulation was completed. In this paper we present the results of these experiments with MIS.

§2. Experimental Setup

The pulsed power generator "HARIMA-II" (400 kV, 3 Ω, 50 ns) was used as the power supply in the experiments reported here. The small pinched REB diode and IPD were used as the loads of MIS. Figures 2 (a) and (b) show the schematic drawings of IPD and its experimental setup, respectively. In Fig. 2 (a), a rod which held the cathode of IPD was also used as the inner conductor of MIS. The inner surface of the aperture located at the center of a ring anode was used as the outer conductor of MIS. Each size of the electrodes is shown in Fig. 2 (a), and a gap length between these two conductors (Δ) was varied from 0.5 to 3.5 mm. The length of MIS (outer conductor) was also varied from 6 to 24 mm. An anode-cathode gap length (δ) was set at 3 mm. The experiments were carried out with 60 % of the maximum output voltage of the "HARIMA-II".

In the experiment with the small pinched REB diode, MIS consisted of the same electrodes used as IPD. The cathode was the 10 mmϕ circular plate attached at the end of the rod shown in Fig. 2 (a). The anode was the 50 × 50

mm square plate located at 3 mm from the cathode surface. The "HARIMA-II" was used at 50 % of the maximum output voltage.

Figure 2 (b) shows the experimental setup arranged at the end of the "HARIMA-II". A voltage was measured at the diode (V_d) with a resistive voltage divider. A total current (I_t) and a diode current (I_d) were measured with Rogowski coils. Here I_d was only measured in the case of the small pinched REB diode, because the Rogowski coil was not able to be located between the diode and MIS in the case of IPD. A biased ion collector (BIC) was used to measure the total current of the ion beam. In front of BIC, a grounded plate was placed, and its transparency was 0.2 %. A charge collector located in BIC was biased at -450 V to remove the accompanying electrons. A Thomson-parabola ion spectrometer[4] was employed for analyzing the

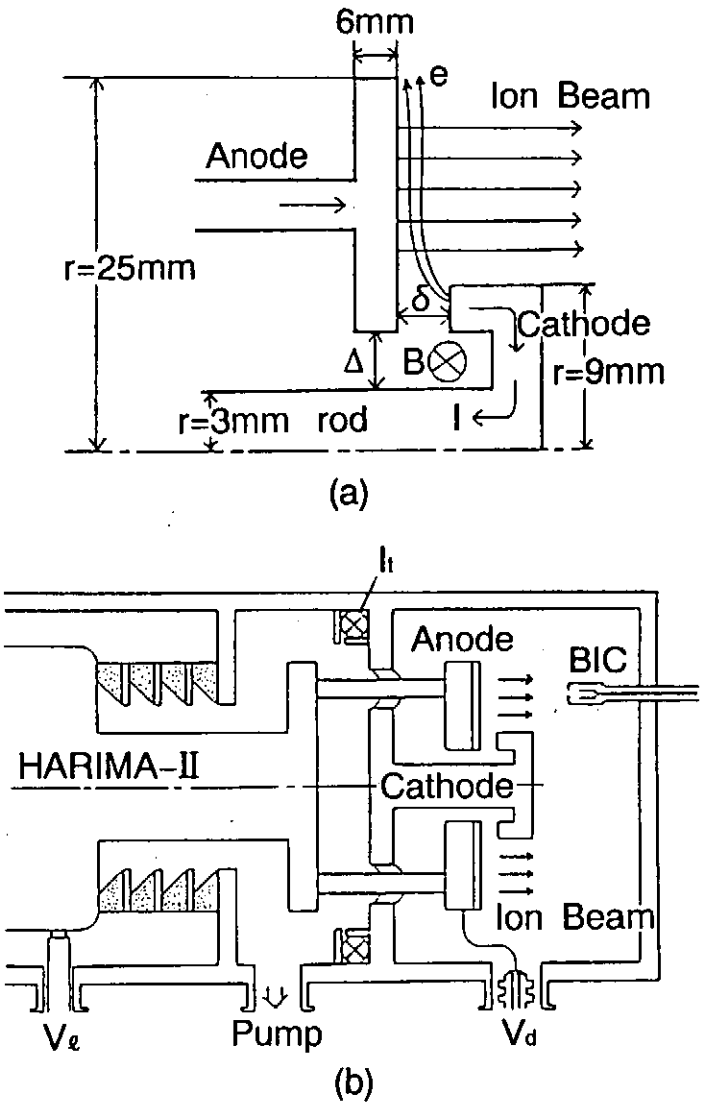

Fig. 2. Schematic drawings of the "Inverse Pinch Ion Diode" (a) and its experimental setup (b).

species and those energies of the ion beam generated with IPD.

§3. Experimental Results

3.1 Voltage Amplification by Magnetic Insulation

Typical wave-forms obtained with IPD are shown in Figs. 3, because voltage amplification is clearly observed in the case of IPD. Figures 3 (a), (b) and (c) show the wave-forms of the diode voltage (V_d), the diode current (I_d) and the total current of the ion beam (I_i), respectively. In Figs. 3, the wave-forms obtained with operation (Δ=1mm) and without operation (effectively Δ=6mm) of MIS are shown in the left and the right side, respectively. Without switch

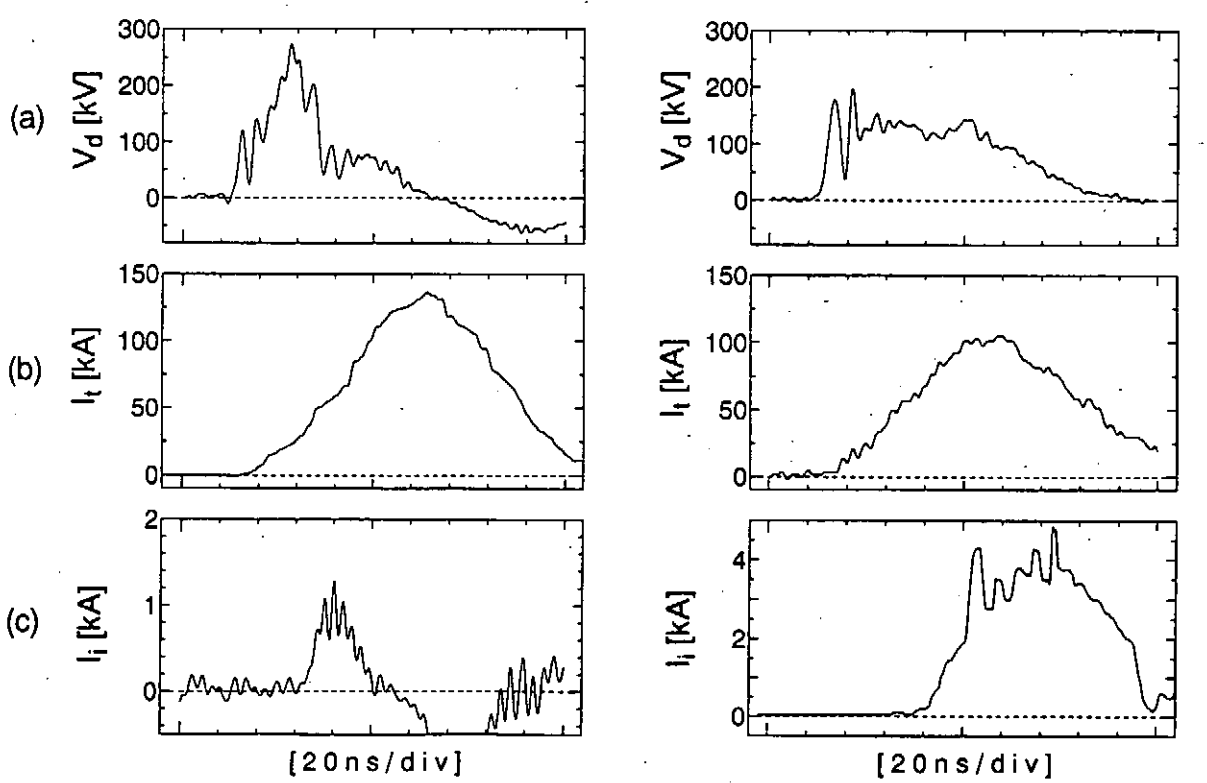

Fig. 3. Typical wave-forms obtained with IPD: V_d (a), I_t (b) and I_i (c). The figures placed at the left side were obtained with switch operation, and the other figures were obtained without switch operation.

operation, the wave-form of V_d has the over-shoot (180kV) and a flat top (130kV). In contrast to these values, with switch operation, the over-shoot becomes low (120kV) and the maximum value of V_d becomes high (260 kV). Moreover the pulse width of V_d becomes short and the flat top is not seen. These changes in the voltage are due to operation of MIS, and shortening of the pulse width is due to closure (shorting) of the gap in MIS by expansion of electrode plasmas[5].

Without switch operation, I_d increases linearly up to the maximum value of 100 kA in Fig. 3 (b). With switch operation, the diode current linearly increases up to about 50 kA. From this time, the rate of increase in I_d changes, and reaches to the maximum value of 130 kA. This change is also caused by shorting of the gap in MIS. The current and the pulse width of I_i become low and short by switch operation. These facts are caused by shortening of the pulse width of V_d and decreasing of I_d (I_t) when the ion beam is generated.

Figure 4 shows the dependence of voltage amplification factors on

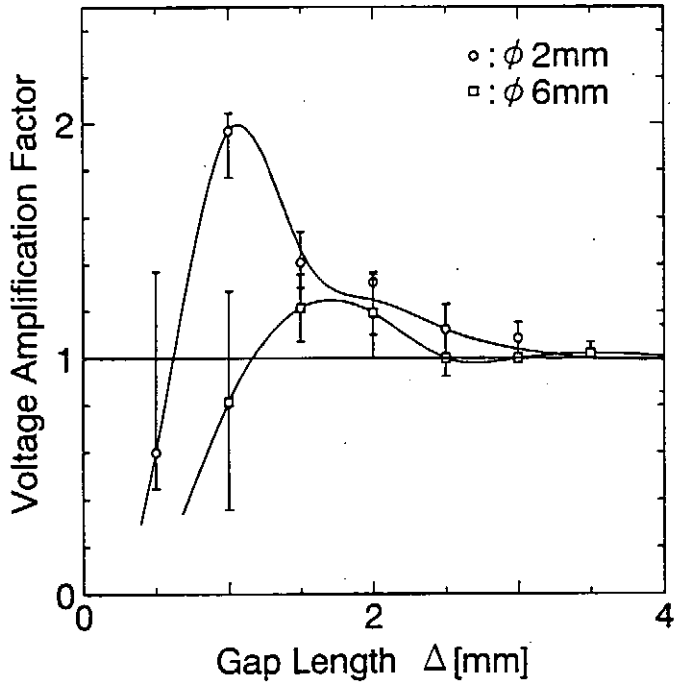

Fig. 4. Dependence of voltage amplification factors on gap length between conductors of MIS (Δ).

the gap length between the electrodes of MIS (Δ). Here the voltage amplification factor is defined as dividing the diode voltage obtained at each Δ by that obtained without MIS (effectively Δ=6mm). In Fig. 4, the data obtained with two different inner conductors (2,6mmϕ) are displayed. The experimental setup was same as that shown in Fig. 2 (a), except that the lengths of MIS were 24 (2mmϕ) and 12 (6mmϕ) mm. The higher voltage amplification factor is obtained at a short gap length, and is obtained with more slender inner conductor.

3.2 Energy Analysis of Ion Beams

The species and the energies of the ion beams were analyzed with the Thomson-parabola ion spectrometer. The magnetic and the electric field were set at 0.1 T and 3 kV/cm, respectively. Since the traces obtained on the film CN-85 are not clear, the outlines of the traces are copied to transparency films, and are shown in Figs. 5. The traces shown in Figs. 5 (a) and (b) are obtained with (Δ=1mm) and without switch operation,

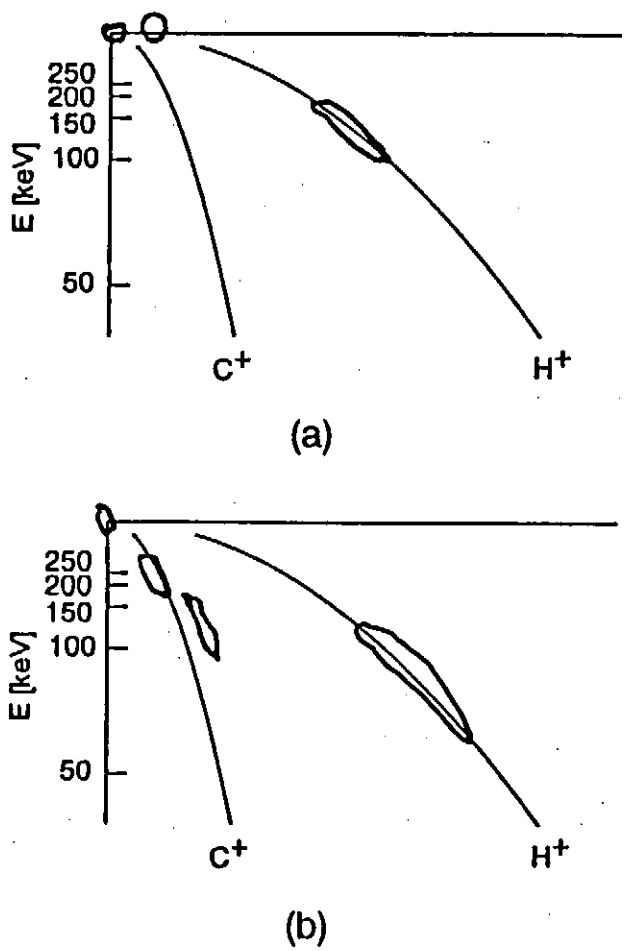

Fig. 5. Traces on film CN-85: with switch operation (a) and without switch operation (b).

respectively. In Figs. 5, the vertical lines correspond to the energies of the ions, and the lines calculated to protons and the carbon ions are displayed.

With switch operation, the protons and the neutral particles (the trace located on the top of the vertical line) are detected, and the energies of the protons range from 100 to 200 keV. Without switch operation, the protons, the carbon ions and the neutral particles are detected, and the energies of the protons range from 60 to 110 keV. The energy of 110 keV corresponds to the flat top voltage of V_d in this shot. Although the carbon ions are only detected in Fig. 5 (b), this might be caused by the longer duration of V_d. However increasing of the diode voltage is verified from the energies of the protons.

3.3 Comparison between total current and diode current

In order to obtain the switch current flowing in MIS, the total and the diode current were measured with the small pinched REB diode. The wave-forms of the diode voltage V_d, the total current I_t, the diode current I_d and the switch current I_s (I_t-I_d) are shown in Figs. 6 (a), (b), (c) and (d), respectively. In this shot, the gap length Δ of MIS was set at 2 mm. The wave-form of V_d is similar to that shown in the right side of Fig. 3 (a) (without switch operation), but increasing of the diode voltage is seen at the center of the wave-form. The flat top and the maximum voltage of V_d are 170 and 240 kV, respectively.

In Fig. 6 (b), I_t increases linearly up to 30 kA, and increases slowly up to 85 kA. At this turning point, magnetic insulation is completed. Initially

I_d does not flow, but increases rapidly after magnetic insulation is completed. The maximum current of I_d is approximately same as that of I_t. The switch current I_s was estimated by subtracting the diode current from the total current. The switch current decreases slowly after magnetic insulation is completed.

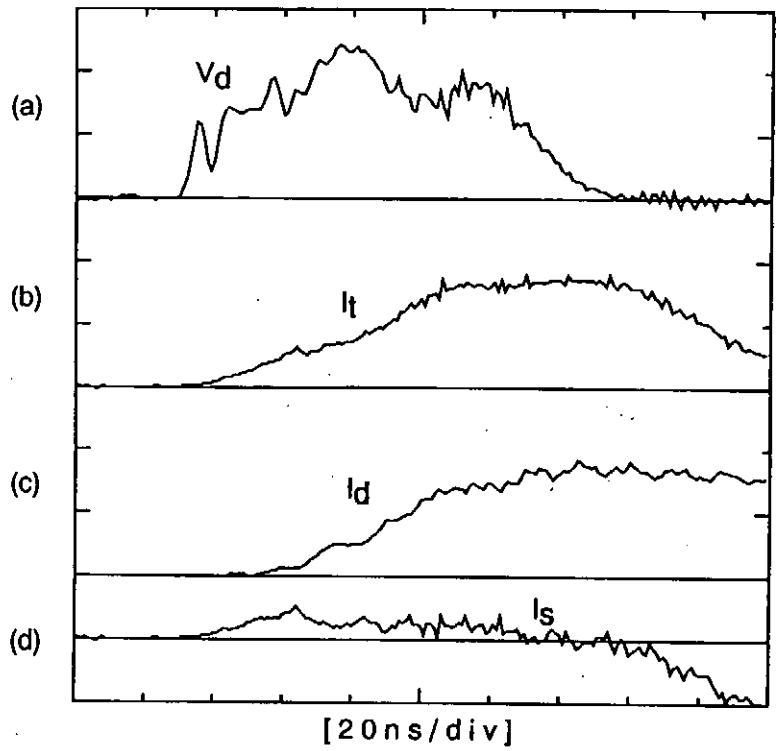

Fig. 6. Typical wave-forms obtained with REB diode: V_d (a), I_t (b), I_d (c) and I_s (d). The vertical scale in (a) is 100 kV/div, and those in (b), (c) and (d) are 50 kA/div.

It seems that this small current is caused by the ion current flowing from the electrode plasma generated by bombardment of electrons in MIS. From these results, it is verified that voltage amplification is occurred after I_s starts to decrease by magnetic insulation.

§4. Summary

We tried amplification of diode voltages by using the small magnetically insulated switch (MIS). As the loads of MIS, the "Inverse Pinch Ion Diode" (IPD) and the small pinched REB diode were used. The major results are followings:

1. By operation of MIS, the diode voltage increased from 130 to 260 kV in the case of IPD.
2. Increasing of the diode voltage was also verified by the experiments carried out to estimate the energies of the ion beams with the Thomson-parabola ion spectrometer.
3. From the experimental results with the small pinched REB diode, it was verified that voltage amplification was occurred after the current flowing in MIS started to decrease by magnetic insulation.

Acknowledgement

This work was partly supported by grand in aid of culture of Japan.

References

1) For example:

R. A. Meger, R. J. Commisso, G. Cooperstein and S. A. Goldstein: Appl. Phys. Lett. 42 (1983) 943.

2) Y. Hashimoto, M. Sato, M. Yatsuzuka and S. Nobuhara: Proc. 8th IEEE Int. Pulsed Power Conf., San Diego, (1991) 578.

3) M. Sato, J. Mizui, H. Yonezu and T. Tazima: Jpn. J. Appl. Phys. 25 (1986) 601.

4) M. Sato: Jpn. J. Appl. Phys. 26 (1987) 927.

5) M. Sato, Y. Hashimoto, M. Yatsuzuka and S. Nobuhara: Proc. 8th Int. Conf. High-Power Particle Beams, Novosibirsk (1990) 1070.

Effect of Adsorbed Matters on Generation of Ion Beams

Yoshiyuki Hashimoto, Morihiko Sato, Mitsuyasu Yatsuzuka,

and Sadao Nobuhara

Department of Electrical Engineering,

Faculty of Engineering,Himeji Institute of Technology

ABSTRACT

Improvement of purity of ion beams produced by a pulse power generator has been studied. Carbon ion beams were successively produced with an inverse pinch ion diode with the anode of a teflon(CF_2=CF_2) plate without breaking vacuum. The main components of the ion beams were carbon, fluorine and hydrogen ions. A current of impurity, hydrogen, decreased after an initial few shots. The carbon ion current of 3 kA in the fourth shots was measured. A few of initial shots without breaking vacuum was found to be useful for improvement of purity in the ion beams. Changing the residual gas pressure in the range of 10^{-2}-10^{-3} Pa was little effect on the ion beam purity.

§1. INTRODUCTION

Recently, material developments using an intense pulsed ion beam(IPIB) have attracted special interest since the IPIB has characteristics of a high power and a short pulse duration compared with conventional ion extractors in material developments.[1-4] On

the occasion that the IPIB is used for the ion implantation in material developments, the IPIB of good quality is required. However, the quality of the IPIB is generally lower than that of ion beams generated by the conventional ion extractors. The quality of the IPIB is dependent on two factors, energy spread and purity. The energy spread results from diode configurations and characteristics of the pulse power generator, and a deterioration of the purity is caused by absorbed matters on the anode surface.

In this paper, we report on effects of the matters absorbed upon the anode surface on the purity of the IPIB. Improvement of the ion beam purity by successive shots without breaking vacuum is studied experimentally. The experimental setup and measurement methods are described in §2, and experimental results and some discussions are presented in §3. And some conclusions are presented in §4.

§2. EXPERIMENTAL SETUP AND MEASUREMENT SYSTEM

The schematic drawing of an experimental setup is shown in Fig.1. An inverse pinch ion diode(IPD)[5-7] was used for generation of ion beams. The diode is located at the end of a pulsed power generator "HARIMA-II" (400kV, 3Ω, 50ns) at the Himeji Institute of Technology. The inner and the outer diameters of the anode were 10 mm and 50 mm, respectively. The inner and the outer diameters of the cathode were 10 mm and 14 mm, respectively. The A-K gap length was 3 mm. A 2mm-thick teflon(CF_2=CF_2) plate was attached to the anode surface as an ion source.

A resistive voltage divider and a Rogowski coil were used for

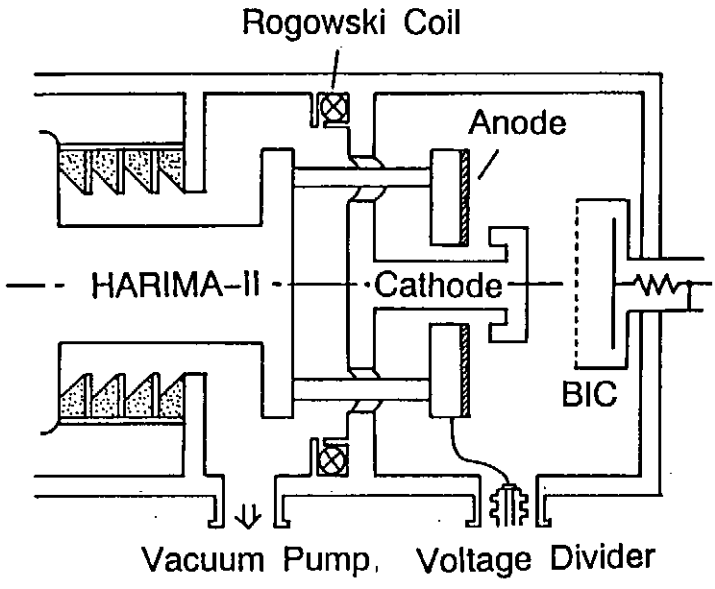

Fig.1 A schematic diagram of an experimental setup.

measurement of a diode voltage(V_d) and a diode current(I_d), respectively. A biased ion-collector(BIC) was used to estimate ion beam currents. The BIC consists of a ground plate with small apertures (transparency = 5%) and an ion collector plate, and is used to estimate the total current of the ion beams. The BIC was located at 150 mm behind the anode. The collector of the BIC was biased at voltage of -450 V to remove accompanying electrons. Energies and species of the ion beams were analyzed using a thomson-parabola ion spectrometer. The thomson-parabola ion spectrometer consists of three sections; a collimator section, electric and magnetic deflection section, and an ion detector section. The collimator has two pinholes of which diameters are 0.2 and 0.5 mm, respectively. The maximum value of the magnetic and electric fields are 0.5 T and 6 kV/cm, respectively. The film CR-39 was used for detection of analyzed ions.

§3. EXPERIMENTAL RESULTS AND DISCUSSION

3.1. Diode characteristics

Figure 2(a) and 2(b) show a typical time history of V_d and I_d, respectively. As seen in Fig.2(a), V_d reaches to the top value of 130 kV in 10 ns, and the pulse width is 80 ns (FWHM: full width at half maximum). The diode current rises up in 10 ns after V_d is initiated, and reaches its peak value of 120 kA by 80 ns. Figure 2(c) shows the waveform of the total ion current(I_i) measured with the BIC at the fourth shot. The peak value of I_i is found to be 3 kA in Fig.2(c). Using the peak value of I_i and the value of I_d, the generation efficiency is estimated to be 2.5%.

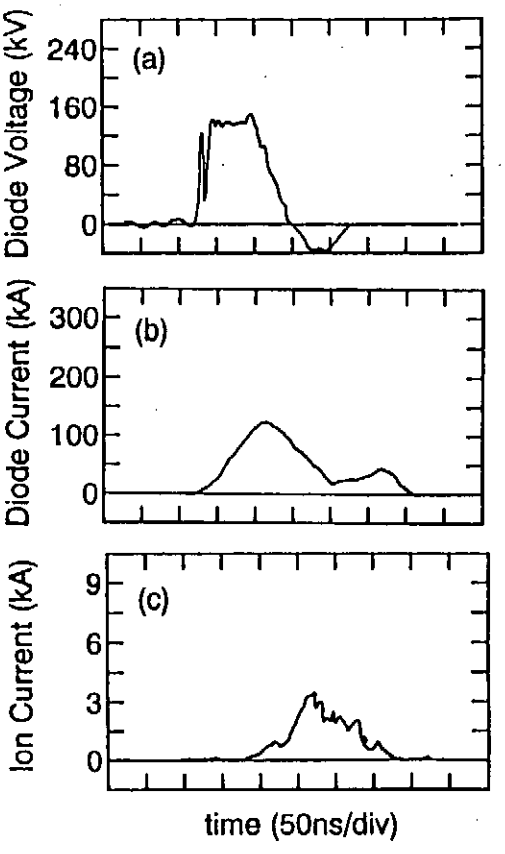

Fig.2 Typical time history of (a)diode voltage, (b)diode current and (c)total ion current.

3.2 Analysis of ion species with Thomson-parabola ion spectrometer

Figure 3 shows a photograph of the film CR-39 which indicates mass and energy distributions of the ion beams measured by the Thomson-parabola ion spectrometer where the magnetic and the electric fields were 0.1 T and 3 kV/cm, respectively. In this shot,

the residual gas pressure in the diode chamber was 3×10^{-3} Pa. As shown in Fig.3, the main components of the ion beams are found to be hydrogen, carbon and fluorine. The hydrogen ions originate from adsorbed water vapor on the anode surface. An energy of hydrogen ions corresponds to V_d of 130 kV measured with the voltage divider. The carbon and fluorine components were found to be two to four times higher energies than the hydrogen components. These high-energy ions are able to be produced through charge exchange process in the diode region.

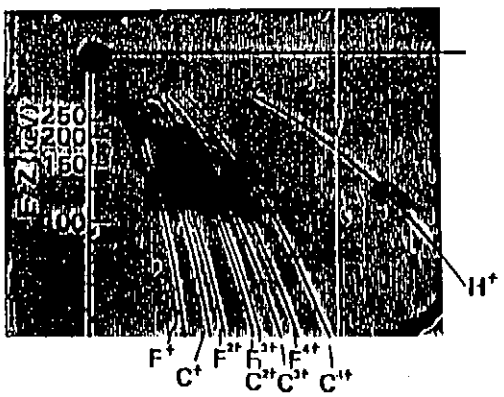

Fig.3 Typical traces on the CR-39 film located in the Thomson-parabola ion spectrometer with the magnetic field of 0.1T and the electric field of 3kV/cm.

3.3 Effect of extraneous matters on purity of ion beams

Impurities of the ion beams generated by the pulsed power generator mainly originate from adsorbed matters on the anode. The adsorbed matters can be classified two types: (a)the matters adsorbed and stuck on the anode when the anode is left in the air for a long time (extraneous matters); and (b)the matters adsorbed instantaneously on the anode in a vacuum (quickly-adsorbed matters). In this section, effects of the extraneous matters upon the anode on the purity of the ion beams will be studied experimentally.

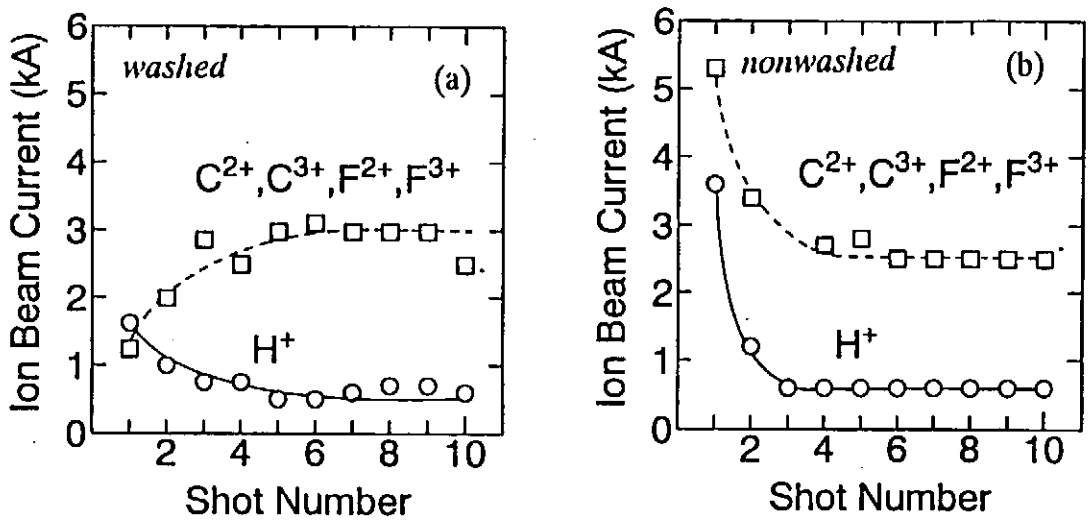

Fig.4 Ion currents as a function of a shot number in case of (a)washed teflon plate and (b)nonwashed teflon plate.

Two types of teflon plates were prepared as an ion source in this experiment. The one was a teflon plate washed with methanol(washed teflon plate) and another was a teflon plate not washed(nonwashed teflon plate). Since the extraneous matters such as oils and dusts are removed by washing with methanol, effects of the extraneous matters on the purity of the ion beams can be clarified by comparing the ion beams using the washed teflon plate with those using the nonwashed teflon plate. In the experiments mentioned below, the A-K gap length was 3 mm and the diode chamber was exhausted by a vacuum pump to 4×10^{-3} Pa. The ion beams were produced by successive shots at intervals of 7 minutes, and the ion beam current for each shot was measured with the BIC. Figure 4(a) and 4(b) show the ion currents as a function of a shot number in cases of the washed teflon plate and the nonwashed teflon plate, respectively, where a solid line indicates a component of hydrogen ions and a broken line indicates components of carbon and fluorine

ions. From Fig.4(a) and 4(b), it is found that the ion current with the nonwashed teflon plate is larger than that with the washed teflon plate in the first several shots. This result shows that the extraneous matters upon the anode are removed by washing the teflon plate with methanol. In Fig.4(a) and 4(b), a decrease in hydrogen ion current with increasing shot number is ascribed to the removal of the extraneous matters by the electron bombardment. However, a small amount of the hydrogen-ion current continues to appear after several shots because residual gases in the diode chamber instantaneously adsorb on the anode surface. Therefore, the removal of the adsorbed matters from the anode surface is important for producing of high-quality ion beams.

Next, it is found that currents of the carbon and fluorine ions with the washed teflon plate(Fig.4(a)) increases with shot numbers. On the other hand, the ion beams with the nonwashed teflon plate(Fig.4(b)) decreases after repeating shots. This results implies that the carbon and fluorine ions are initially extracted from the extraneous matters and that the carbon and fluorine ions are extracted from the teflon plate after a few shots.

From these results above, it is clarified that a cleaning of the anode surface by a few initial successive shots is useful for removal of the extraneous matters on the anode surface and for generation of high-purity ion beam.

3.4 Effect of residual gas pressure on ion beam generation

It is considered that the density of molecules adsorbed on the anode was dependent on the residual gases pressure in the diode

chamber. Therefore, the ion current for each shot is estimated from data of the BIC for various residual gases pressures in the diode chamber(Fig.5). The currents of hydrogen ions, and carbon and fluorine ions are plotted as a function of shot number in Fig.5(a) and 5(b), respectively. In Fig.5, we see that the currents of the hydrogen ions and the carbon and fluorine ions are independent on the change in the residual gas pressure range from 1×10^{-2} to 4×10^{-3} Pa. As a result, a change in one order of the residual gas pressure is found to be little effect on the current of the ion beams.

From these studies, it is considered that generation of the ion beams of high purity needs a high vacuum in the diode chamber.

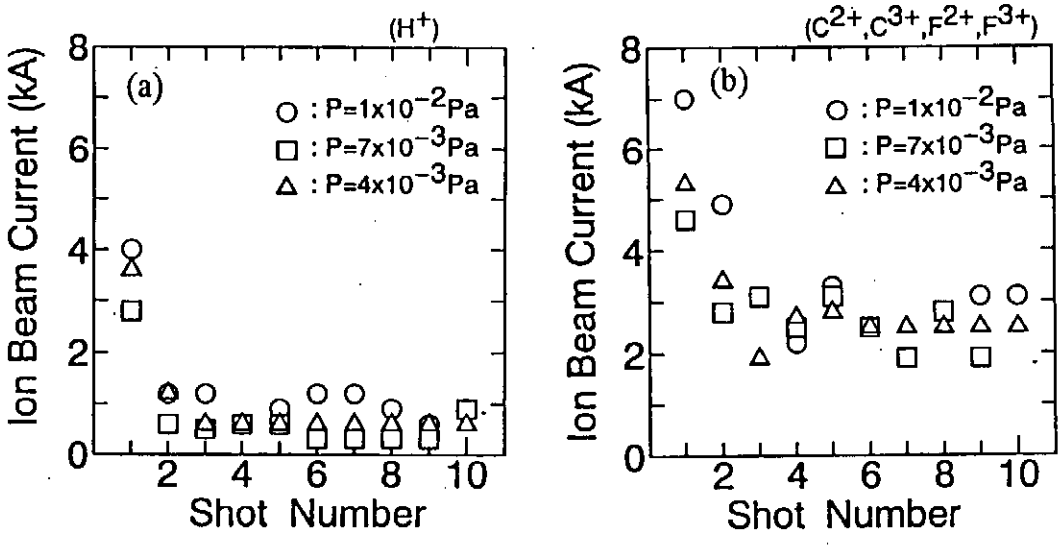

Fig.5 Current of (a)H^+ and (b)C^{2+},C^{3+},F^{2+},F^{3+} are plotted as a function of a shot number in various gas pressure.

§4. Conclusions

Generation of intense ion beams of a high-quality has been studied experimentally. The results are summarized as follows: The

intense carbon-beam was produced using the inverse pinch ion diode with the anode of the teflon plate. It was found that the deterioration of ion beam purity was caused by adsorbed matters on the anode surface. A few of initial successive shots without breaking vacuum was found to be useful for improvement of purity in the ion beams. A change in the residual gas pressure ranging 10^{-2} to 10^{-3} Pa was little effect on the ion beam purity.

References

1) K.Yatsui and K.Masugata : Ceramics 19 (1984) 666 [in Japanese].

2) Y.Shimotori, M.Yokoyama, H.Isobe, S.Harada, K.Masugata and K.Yatsui : J. Appl. Phys. 63 (1988) 968.

3) K.Yatsui : Laser & Particle Beams 7 (1989) 733.

4) Y.Nakagawa, T.Ariyoshi, H.Hanjo, S.Tsutsumi, Y.Fuji, M.Itami, A.Okamoto, S.Ogawa, T.Hamada and F.Fukumaru : Nucl. Instrum. & Methods. B39 (1989) 603.

5) J.P.VanDevender, J.P.Quintenz, R.J.Leeper, D.J.Johnson and J.T.Crow : J. Appl. Phys. 52 (1981) 4.

6) S.Miyamoto, A.Yoshinouchi, T.Ozaki, S.Higaki, H.Fujita, K.Imasaki, S.Nakai, and C.Yamanaka : Jpn. J. Appl. Phys. 22 (1983) L703.

7) Y.Hashimoto, M.Sato, M.Yatsuzuka, and S.Nobuhara : Jpn. J. Appl. Phys. 31 (1992) 1922.

Gas-Puff Triggered Closing Switch

Kiminobu Imasaka, Hidenori Akiyama, Sadao Maeda

Kumamoto University,Kumamoto 860

ABSTRACT

Gas-puff triggered closing switch uses the discharge of the annular gas injected into the vacuum switch region. The large current flows through the annular plasma, which moves toward the axis. The advantages of this closing switch are large dielectric strength of vacuum, low plasma inductance and small erosion on the surfaces of both electrodes by the moving plasma.

§ 1 INTRODUCTION

Pulsed power technology is remarkably developing and is useful in a wide variety of fields. The basis of pulsed power generation is to take out the stored energy in a moment and then transmit it to the load. So it would not be going too far to say that the ability of pulsed power generation depends on the switching technology[1,2], which can control high power. Especially, closing switches are important to pulsed power generators and the energy transmission to the load.

The closing switches are initially in the state of insulation, and then become conductive by triggering the switch or applying the voltage over a value. There are a lot of

variety of closing switches, for example, spark gap, thyratron, ignitron (discharge tubes), thyristor (semiconductor), and magnetic switch.

Characteristics required as closing switches are generally to be able to flow sufficient charge and current, small jitter, low inductance and resistance at closing, repeatability, fast voltage drop during closing, small erosion on the surfaces of the two electrodes and so on.

In this paper, a new method of triggered closing switch, that is, "gas-puff triggered closing switch" is proposed, and the characteristics of this closing switch, for example, jitter, plasma inductance and plasma resistance obtained by solving the circuit equation, are investigated.

§ 2 EXPERIMENTAL SETUP

Fig.1 shows the schematic configuration of the experimental apparatus. After charging capacitor of 6.39μF, an annular gas with 2mm thickness is injected from cathode to anode through the fast opening valve. The two electrodes are made of brass and the separation between them is 10mm. The diameter of the annular gas is 50mm. The fast opening valve is operated by the piston, which moves by the magnetic force generated by the coil current from the gas puff actuator. The hollow-shaped plasma is produced between two electrodes, and a high current flows through the plasma. The hollow plasma is contracted toward the inside of the radial direction by the J $\times$ B force, and finally the soft x-ray is emitted. Experimental contents are the measurements of jitter and the plasma

inductance, and the calculation of plasma resistance.

The discharge current is measured by the Rogowski coil, and the coil current is measured by the $\dot{B}$ probe. The image converter camera is used to observe the discharge phenomena. The soft x-ray is detected by the Pin-photo diode.

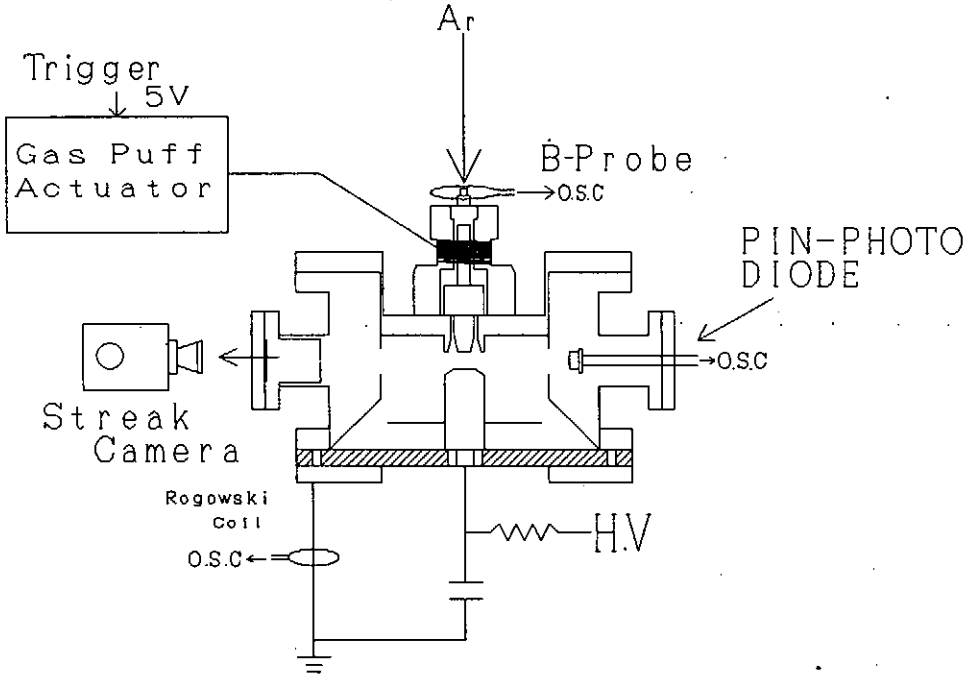

Fig.1 Schematic configuration of the experimentalapparatus.

§ 3 RESULTS AND DISCUSSIONS

Measurement of jitter

Fig.2 shows the waveforms of coil and discharge currents. The standard deviation σ of operating time is expressed as

$$\sigma = \sqrt{\frac{1}{N-1}\sum_{i=1}^{N}(\Delta t_i - \overline{\Delta t})^2} \qquad (1)$$

where Δt_i is the difference of times when the coil current and the discharge current begin to flow, N is the total shot number, and $\overline{\Delta t}$ is the mean value of Δt_i. The gas-puff

pressure is 1.5atm.

Fig.3 shows the dependence of the jitter on the voltage V of gas-puff actuator. The jitter is about 10μs at V=600V. Though this value is large, it would be possible to decrease the jitter by increasing V.

Measurement of plasma inductance

Figs.4(a) and (b) show the streak photograph of the discharge and the waveforms of the soft x-ray and the discharge current, respectively. Fig.5 shows the distribution of the gradation of Fig.4(a). From Fig.4(a) and Fig.5, the contraction of the hollow plasma is observed. A soft x-ray pulse is also measured at around the maximum contraction of the plasma, as shown in Fig.4(b).

Plasma inductance L(t) is given by the following equation;

$$L(t) = \frac{\mu_0 l}{2\pi} \ln\left(\frac{R_R}{r(t)}\right) \qquad (2)$$

where l, R_R, r(t), are the separation between two electrodes, the distance between the center of the electrodes and the return cylinder, and the plasma radius, respectively. When r(t) becomes small, that is, the hollow plasma contracts, L(t) becomes larger.

Fig.6 shows the dependence of $L(t)/L_0$ on $r(t)/r_0$, where L_0 and r_0 are the initial plasma inductance and radius. The plasma inductance increases rapidly around the maximum contraction($r(t)/r_0=0$). Practically, since the diameter of the hollow-shaped gas or the maximum current is adjusted, all stored energy is transferred to the load before the maximum contraction occurs.

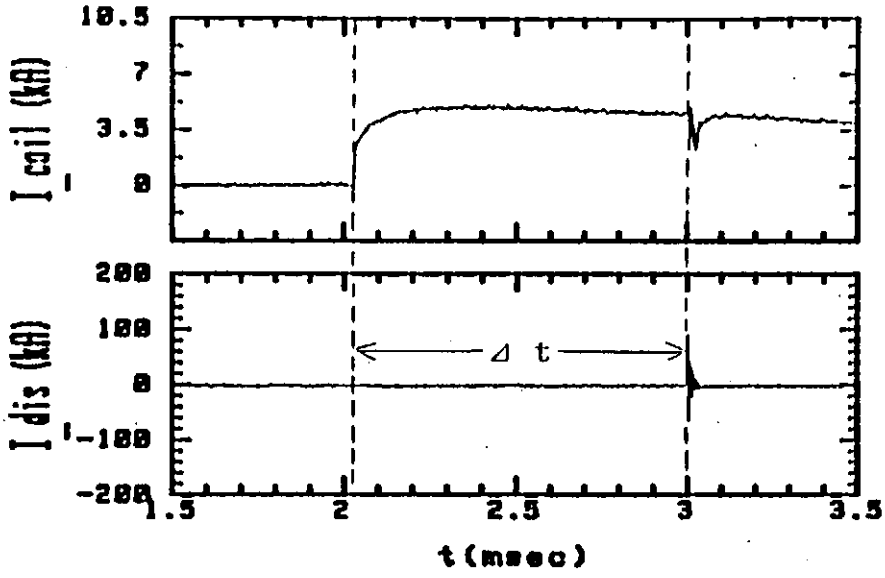

Fig.2 Waveforms of coil and discharge currents.

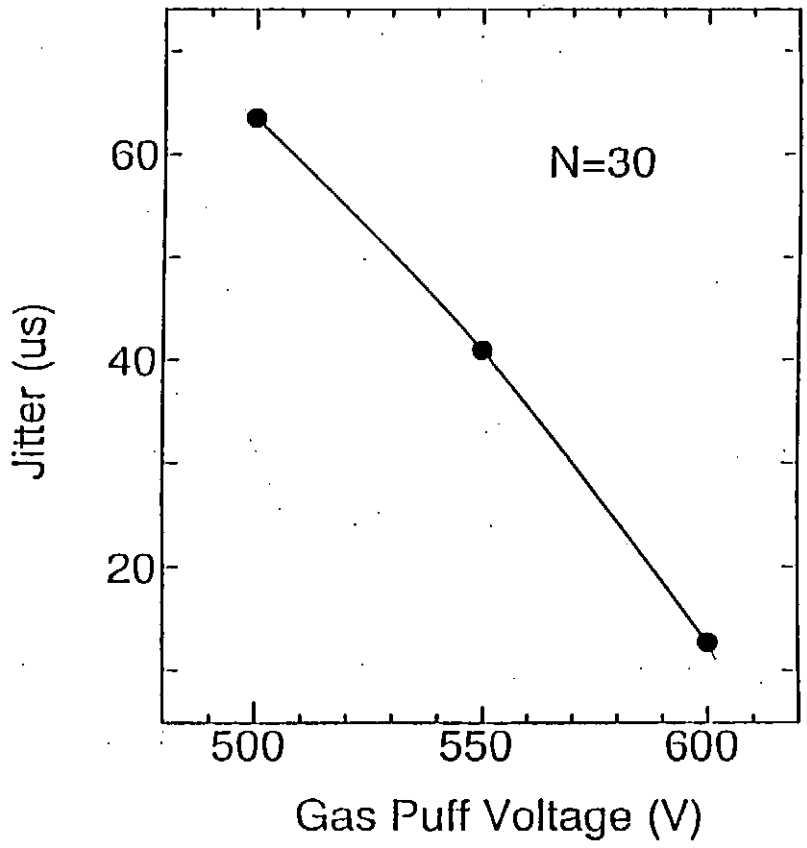

Fig.3 Dependence of the jitter on voltage of gas-puff actuator.

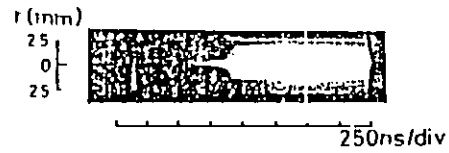

(a) Streak photograph.

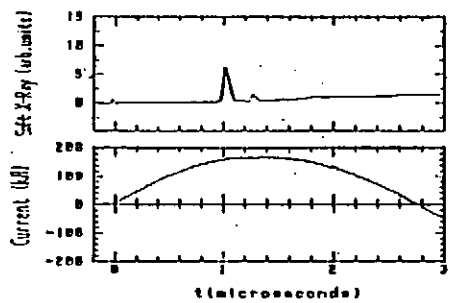

(b) Waveforms of soft x-ray and current.

Fig.4 Discharge phenomena.

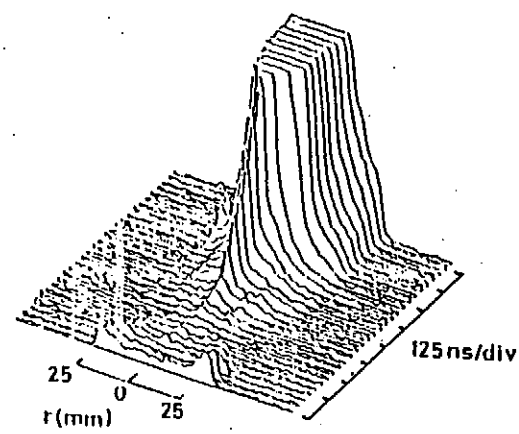

Fig.5 Distribution of gradation of Fig.4(a).

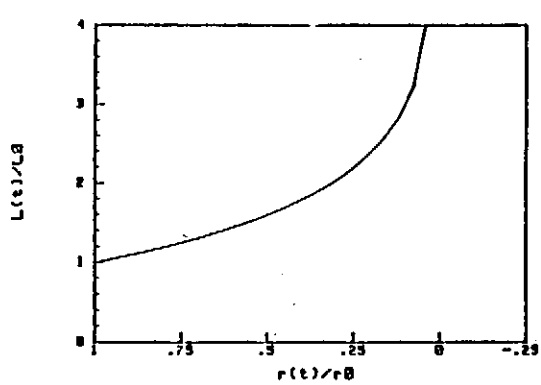

Fig.6 Dependence of $L(t)/L_0$ on $r(t)/r_0$.

Calculation of the plasma resistance

Fig.7 shows the equivalent circuit of the experimental setup shown in Fig.1. The plasma resistance, $R_p(t)$, is calculated using the following equation,

$$R_p(t) = \frac{1}{i(t)} \left[V_b - \frac{1}{C} \int i(t)dt - \frac{d}{dt} \{L0 + L(t)\} i(t) - R_0 i(t) \right] \quad (3)$$

where V_b, $i(t)$, R_0, L_0, C and $L(t)$ are the breakdown voltage, the discharge current, the circuit resistance, the inductance except for the discharge itself, the capacitance of the condensor, and the plasma inductance respectively. $L(t)$ is given by eq.(2). The value of $r(t)$ is calculated from the snow plow model expressed by the following equation;

$$m \frac{d^2 r(t)}{dt^2} = - \frac{\mu_0 i(t)^2}{4 \pi r(t)} + 2 \pi r_0 P \quad (4)$$

where m and P are the plasma mass per unit length and the plasma pressure, respectively.

Fig.8 shows the discharge current $i(t)$ and the plasma resistance $R_p(t)$. $R_p(t)$ decreases rapidly when the current increases, and then it becomes the minimum value of about 10mΩ. Then R_p increases rapidly again.

Fig.9 shows the power loss by plasma, which is calculated from $R_p(t)i^2(t)$. The power loss during half cycle of the discharge current becomes about 300J.

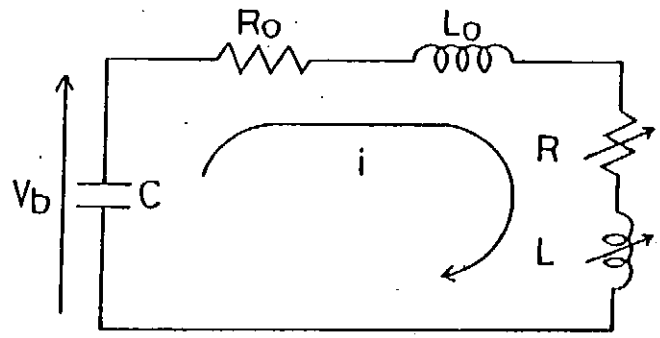

Fig.7 Equivalent circuit of Fig.1.

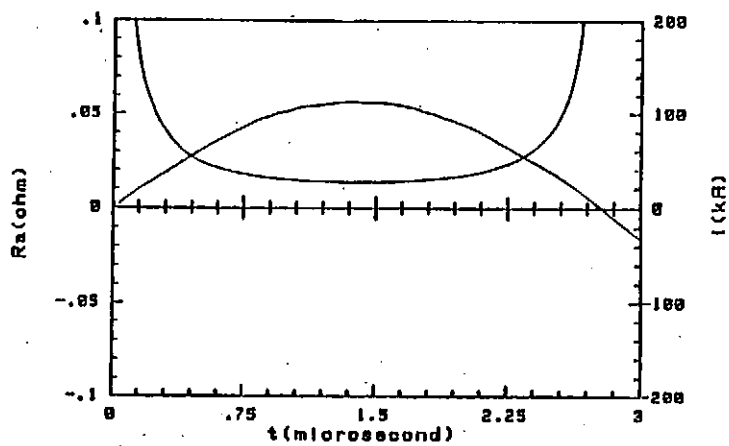

Fig.8 Waveforms of plasma resistance and discharge current.

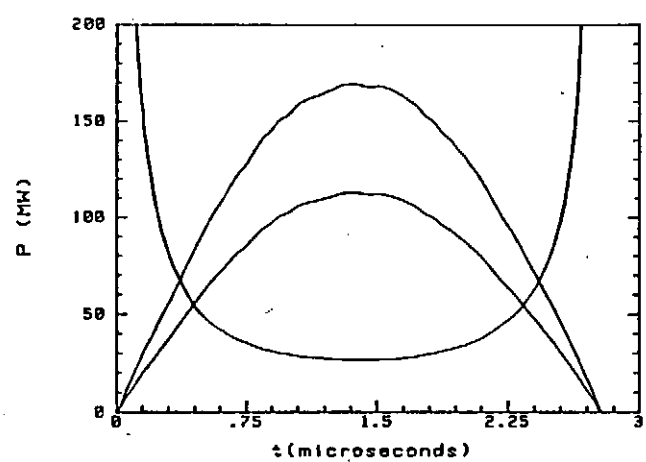

Fig.9 Power loss by plasma.

§ 4 SUMMARY

The gas-puff triggered closing switch for high current was proposed and its characteristics was investigated.

The jitter of the closing switch triggered by the gas-puff depends on the ability of the fast opening valve mainly. A method to reduce the jitter is to increase the voltage of the gas-puff actuator. The plasma inductance is small except when the soft x-ray is emitted from pinched plasma. Plasma resistance rapidly decreases with the increase of the discharge current, and then keeps almost the constant value of 10mΩ. After that it rapidly increases with the decrease of the discharge current. The power loss by plasma during half cycle of the discharge current was about 300J.

REFERENCES

1) G.Schaefer, M.Kristiansen and A.Guenther, "Gas Discharge Closing switches", Vol.2. New York: Plenum, 1990.

2) I.M.Vitkovitsky, "High Power Switching", New York: Van Nostrand Reinhold, 1987.

An Unstable Motion of Plasma in Toroidal Z-pinch Discharge

Norio Shimizu, Kanetoshi Shibata+
and Kenya Matsuura

Faculty of Engineering, Utsunomiya University
+Department of Electronic Technology, Oyama
Polytechnic College

ABSTRACT

The MHD instabilities in a z-pinch discharge have experimentaly investigated with a toroidal plasma device. The investigations are mainly made by measuring poloidal magnetic fields with a poloidal array of small coils. Especially, the motions of the center of plasma column are observed in relation to m=1 poloidal mode. The experimental results in the unstable case of the low bias magnetic field show that the plasma column experiences a large toroidal drift in the initially rising stage of plasma current and oscillates after that stage. The experimental values for the periods of the oscillatory motions of plasma column are in good accordance with the theoretical values given by MHD theory.

§ 1. Introduction

In the early stage of nuclear fusion research, the observations with streak photographs in ZETA device reported that the plasma column in the toroidal discharge was unstable and gave rise to a oscillatory motion[1-2]. After that, such an unstable, oscillatory motion has not been pursued systemati-

cally in many experiments of nuclear fusion research, because the main objects of the experiments was to confine magnetically the plasma in stable. However, if we take interest in physical phenomena of the magnetically confined plasma which is in unstable state, the re-examinations for the unstable motion of the plasma column may be valuable. In this report, we investigate the unstable motion of plasma column in a toroidal z-pinch discharge. The observations of it are made by measuring the poloidal components of magnetic field with arrays of small magnetic coils.

In the case of discharge with a high plasma current and a low bias magnetic field, the plasma column experiences a large toroidal drift in the initially rising stage of the current and the center of the column oscillates about the center of cross-section of the dischage tube after that stage. The physical picture of such an oscillation is in the following. The initially outward motion of plasma column due to the toroidal drift brings about the compression of the poloidal magnetic field between the plasma and the conducting wall. If the restoring force arising from such a compression of the field balances the driving force of the toroidal drift, the plasma column has a MHD equiliblium state at a position shifted outwardly from the center of the wall. However, in the case of plasma column having the large toroidal drift motion, the force of inertia in the drift motion is required in addition to the above two forces and then the center of the column gives rise to the oscillatory motion around the equilibrium position.

The outline of experiments is described in Section 2 and the method of measurements is stated in Section 3. The experimental results are presented in Section 4. The discussions are given in Section 5.

§ 2. Experiments

Figure 1 shows the shematic view of the toroidal pinch device. The device consists of a dischage tube surrounding by copper shell (conducting wall), a z-coil to carry plasma current and a θ-coil to produce bias magnetic field. The major and minor radii of the tube are 25cm and 5cm, respectively. The energy of z-discharge capacitor bank has the value of 6kJ.

The plasma was produced by the discharge in helium gas with the initial pressure of 60 mtoor. The experiments were carried out in the range of time of t=36—76 μsec corresponding to the second half-period in the discharge. The first half-period in it was used as the preionization stage. The plasma current and the initial bias magnetic field in the experiments were in the range of I_p=16.2—28.0 kA and B_b=400—832 gauss, respectively. The typical wave forms of the plasma current, the loop voltage and the bias magnetic field in the second half-period of the discharge of I_p=21,45 kA and B_b=400 gauss are shown in Fig.2. The field has been measured by a magnetic probe at the center of the conducting wall with circular cross-section. We see from Fig.2(c) that the bias magnetic field is trapped inside the plasma and its maximum value increases to approximately five times the initial value. Through this report, the specification of the bias magnetic field is made with the initial value.

§ 3 Measurements

The unstable behaviour of plasma column were analyzed by observing the poroidal distributions of the poloidal magnetic field, which is denoted by $B_p(\theta, t)$. Here, θ is a poloidal angle and t is a time. The observations were made by measureing the poloidal field with a poloidal array of small

magnetic coils at 16 equally spaced angles[3]. The coils were placed in the interspace between the discharge tube and the conducting wall. The distributions $B_p(\theta, t)$ are Fourier decomposed in poloidal angles θ, which are given by the expression

$$B_p(\theta, t) = B_{op}(t) + \sum_{m \geq 1} B_m(t) \cos(m\theta - \phi_m). \qquad (3.1)$$

Here, B_{op} is an average value of the poloidal field, B_m is an amplitude of the field for the instabilitiy of poloidal mode number m and ϕ_m is a phase of it. We have the descrete data of 16 coils at each time. Therefore, B_m and ϕ_m are given by

$$B_m = \sqrt{a_m^2 + b_m^2},$$
$$\phi_m = \tan^{-1}\frac{b_m}{a_m}, \qquad (3.2)$$

where a_m and b_m are defined by

$$a_m = \frac{2}{N} \sum_{k=1}^{N} B_p(k,t) \cos m\theta_k,$$
$$b_m = \frac{2}{N} \sum_{k=1}^{N} B_p(k,t) \sin m\theta_k. \qquad (3.3)$$

Here, we have $\theta_k = 2\pi(k-1)/N$ and N=16. The average value B_{op} is also given by

$$B_{op} = \frac{1}{N} \sum_{k=1}^{N} B_p(k,t). \qquad (3.4)$$

The signals from the magnetic coils have been observed by

a digital oscilloscope of the sampling time of 0.025μsec.

We can experimentally investigate a shift of the center of plasma column by using the signals from the magnetic coils in the poloidal array. We assume that the center of plasma column with circular cross-section of radius a shifts from the center of the circular conducting wall with radius b and the magnitude of the shift is denoted by the distance Δ in radial direction and the angle α in poloidal one. Then, the poloidal magnetic field outside the plasma column can be calculated by Maxwell's equations. Using coordinates (r, θ) in which the origin is taken the center of the conducting wall, the calculated result for thefield is given as

$$B_{p\,cal}(r,\theta) = \frac{a}{r} B_a + \frac{a\,\Delta\,B_a}{b^2 - a^2}\left(1 + \frac{b^2}{r^2}\right)\cos(\theta - \alpha) + \frac{a\,B_a}{2R}\left\{\frac{b^2}{a^2 - b^2}\left(1 + \frac{a^2}{r^2}\right)\ln\frac{b}{a} + \ln\frac{r}{a} - 1\right\}\cos\theta , \qquad (3.5)$$

where R is the major radius of the toroidal discharge tube and B_a is the poloidal magnetic field at r=a. In the calculation, we have used a technique of series expansion for the inverse aspect ratio. Now, the quantities Δ and α are determined by using the least-squares method which minimizes

$$S = \sum_{k=1}^{N}\{B_{p\,cal}(\theta_k) - B_p(\theta_k)\}^2 , \qquad (3.6)$$

where $B_p(\theta_k)$ is the observed value of the poloidal magnetic field given by the k-th coil[4]. It is noted here that the behaviours for the shifts of plasma column obtained with the above treatments are deeply related to the m=1 mode of instabilities.

The experimental estimations of the plasma radius are required in the determinations of Δ and α. The estimations are made with requiring that the flux of the toroidal magnetic field inside the plasma column is conserved. The measurements of the field are carried out by a magnetic probe inserted into the plasma. Such estimations of the plasma radius may approximately be good in a pinch discharge.In the experiments,the radial positions of the magnetic coils are r=5.3 cm and the radius of the conducting wall is b=5.5 cm.

In the next section, the obtained values of Δ and α will be presented as the quantities Δ_x and Δ_y, which are defined by

$$\Delta_x = \Delta \cos\alpha \ ,$$
$$\Delta_y = \Delta \sin\alpha \ . \qquad (3.7)$$

The quantity Δ_x means the shift in a horizontal direction and Δ_y does in a vertical direction.

§ 4 Experimental results

Figure 3 shows the experimental results for Δ_x , Δ_y and B_m at three different values of the initial bias magnetic field . Here, the values of B_m have been given by normalizing with B_{op} . The motions of Δ_x in the initial stage from 36μsec to about 46μsec are the outwardly toroidal drift of plsma column which is well-known in a toroidal discharge.The toroidal drift becomes larger with decreasing the bias magnetic field. In the case of the lowest bias magnetic field of 400 gauss, the center of plasma column begins to return

to the position near the center in the cross-section of the conducting wall after the large toroidal drift and subsequently has a oscillatory motion. On the other hand, the plasma column shifts downwards initially in the cross section of conducting wall as seen from the motions of Δ_y in the figure. Subsequently,in the case of the lowest bias magnetic field, it has the same oscillatory motion as in Δ_x . The results for B_m also show us that the amplitudes of m=1 mode rapidly change with time in the case of the lowest bias magnetic field. This fact for the amplitudes corresponds to the motions of Δ_x and Δ_y .

The experimental results for Δ_x and Δ_y at five diffrent values of the plasma current are shown in Fig.4. The initial bias magnetic field has been fixed in 400 gauss. The horizontally toroidal drifts of the plasma column become larger with increasing with plasma current and the subsequent oscillatory motions become also clearer. The motions of Δ_y in the figure also show us that the initially downward shifts in the vertical direction become not necessarily larger with increasing the plasma current and are nearly equal in magnitude. However, for the cases of the higher plasma current,the motions of Δ_y subsequent to the downward shifts have the same clearer features of oscillatory motion as in Δ_x.

We can experimentally obtain the periods of the oscillatory motions of the plasma column from the results for Δ_x and Δ_y. Figure 5 shows the dependences of the plasma current on the periods. In the figure, the values of periods obtained from Δ_x have been expressed by the closed circles and those obtained from Δ_y have been done by the open circles. The period decreases with increasing the plasma current.

In Fig.6, we also present the Fourier decomposed ampli-

tudes of the magnetic field, B_m , at three diferent values of the plasma current. For all the cases, the m=1 instabilities may be noticeable.

§ 5 Discussions

The period of oscillatory motion of the plasma column subsequent to the toroidal drift in the horizontal direction can theoretiaclly be calculated according to MHD theory[5]. The period T is given by

$$T = \pi \sqrt{\frac{2Mc^2(b^2-a^2)}{I_p^2}} \qquad (5.1)$$

in cgs Gaussian unit. Here, M is the mass per unit length of the plasma column, c is the light speed and Ip is the plasma current. It can also be verified by calculation that, if the column initially moves downward or upward in the vertical direction, the period of the subsequently oscillatory motion are given by the same expression as in eq.(5.1). Using the values of plasma current observed with a Rogowski coil, the values of the period calculated from eq.(5.1) have been presented by the solid curve in Fig.5. In the calculation, we have assumed that the ionization degree of the plasma was 80% . We seem that this assumption for the ionization degree may approximately be acceptable as seen from the results of the other experiments in the discharge of our device. The agreements between the experiments and the calculations for the period may be quite good.

For the initial shifts of plasma column in the vertical direction, we have stated in § 3 that the magnitudes of those are nearly independent of the values of plasma current .The shifts may be regarded as one of the unstable motions

of the plasma column. However, the origin of those is not yet clear.

Lastly, we make reference to the toroidal modes of instabilities. The measurements of the poloidal magnetic field with a toroidal array of the magnetic coils show us that the n=1 instability is noticeable.

REFERENCES

1) E.P.Butt et al. ; Proc. 2nd U. N. Conf. on Peaceful Uses of Atomic Energy, 32 (1958) 42.
2) P.C.Thonemann, E.P.Butt, R.Carruthers, A.N.Dellis, D.W. Fry, A.Gibson, G.N.Harding, D.J.Lees, R.W.P.McWhirter, R.S.Pease, S.A.Ramsden, and S.Ward ; Nature, 181 (1958) 217.
3) I.H.Hutchinson, M.Malacarne, P.Noonan and D.Brotherton-Ratcliffe ; Nucl. Fusion, 24 (1984) 59.
4) H.Ji, H.Toyama, S.Shinohara, A.Fujisawa, and K.Miyamoto; Plasma Phys. Control Fusion 32 (1990) 79.
5) V.S.Mukhovatov and V.D.Shafranov ; Nucl. Fusion, 11 (1971) 605.

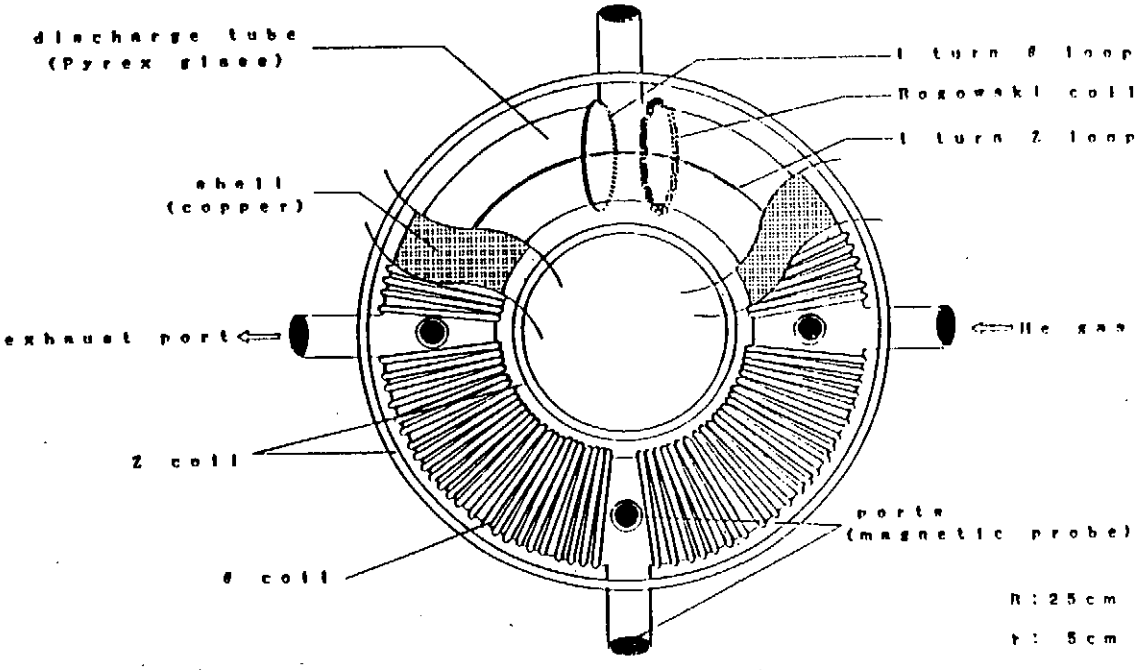

Fig. 1 Schematic view of the toroidal pinch device.

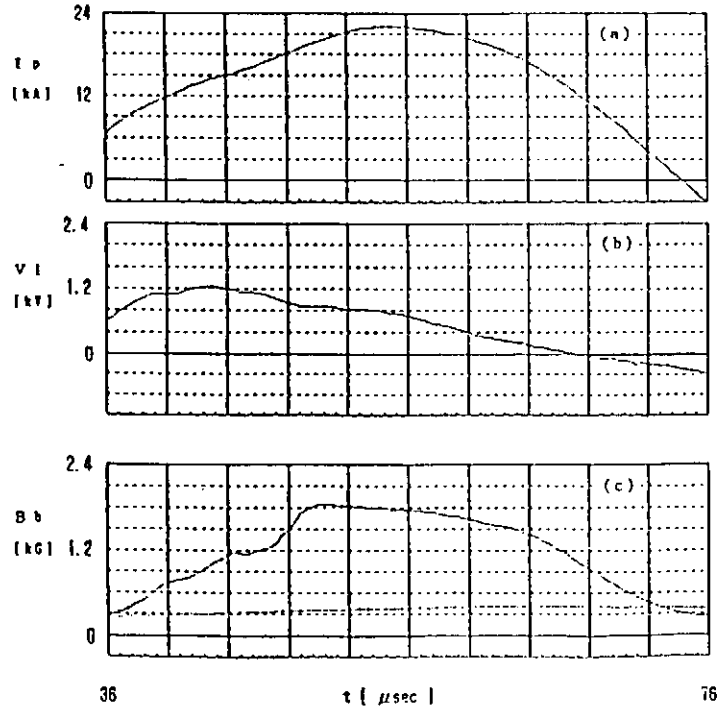

Fig.2 Temporal waveforms in a typical discharge. (a) plasma current. (b) Loop voltage. (c) Bias magnetic field at the center of plasma column (The dotted line is the field in the absence of plasma).

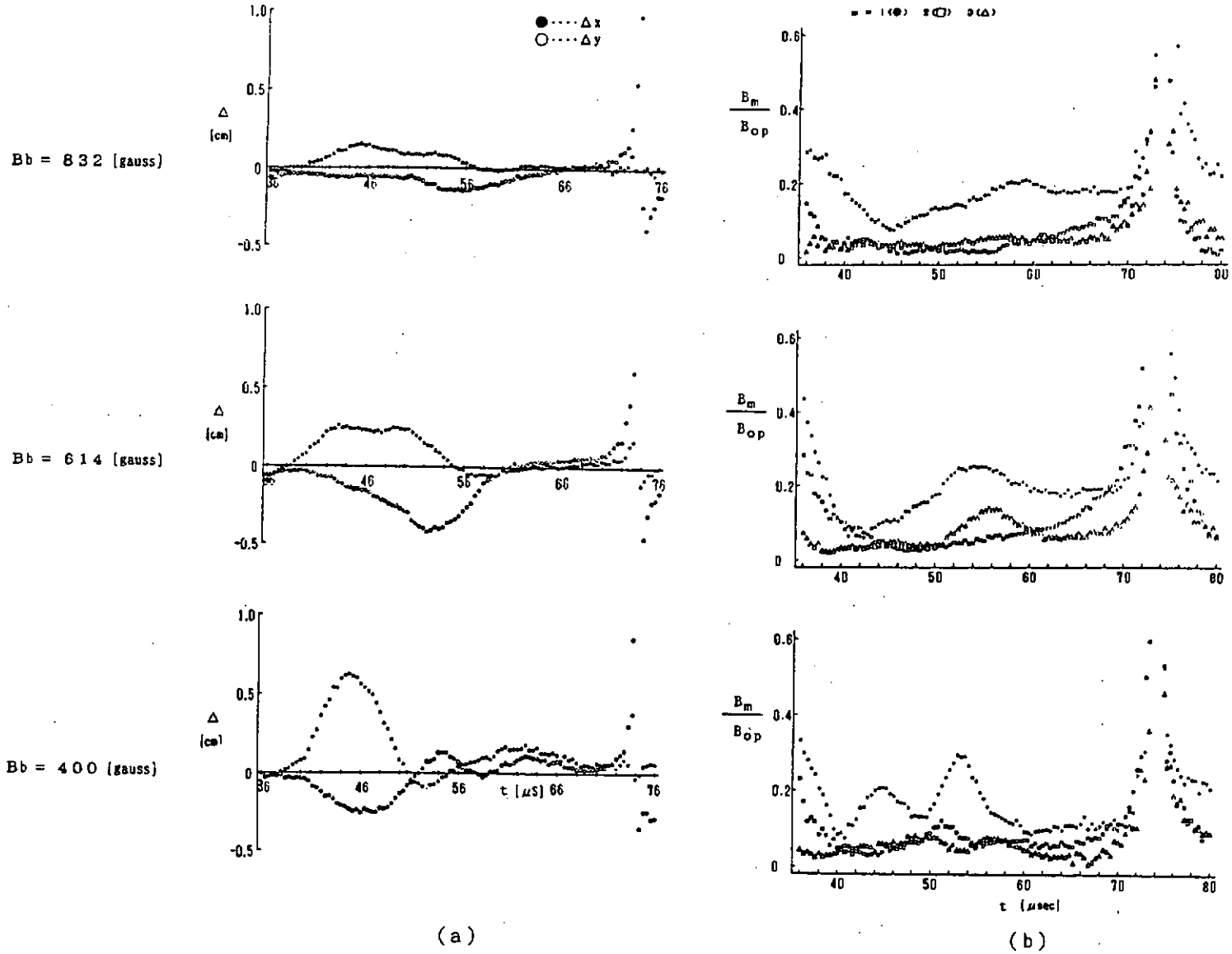

Fig.3 Time variations of (a) the shifts of the plasma column, Δ_x and Δ_y, and (b) the Fourier decomposed amplitudes, B_m, at three different values of the initial bias magnetic field.

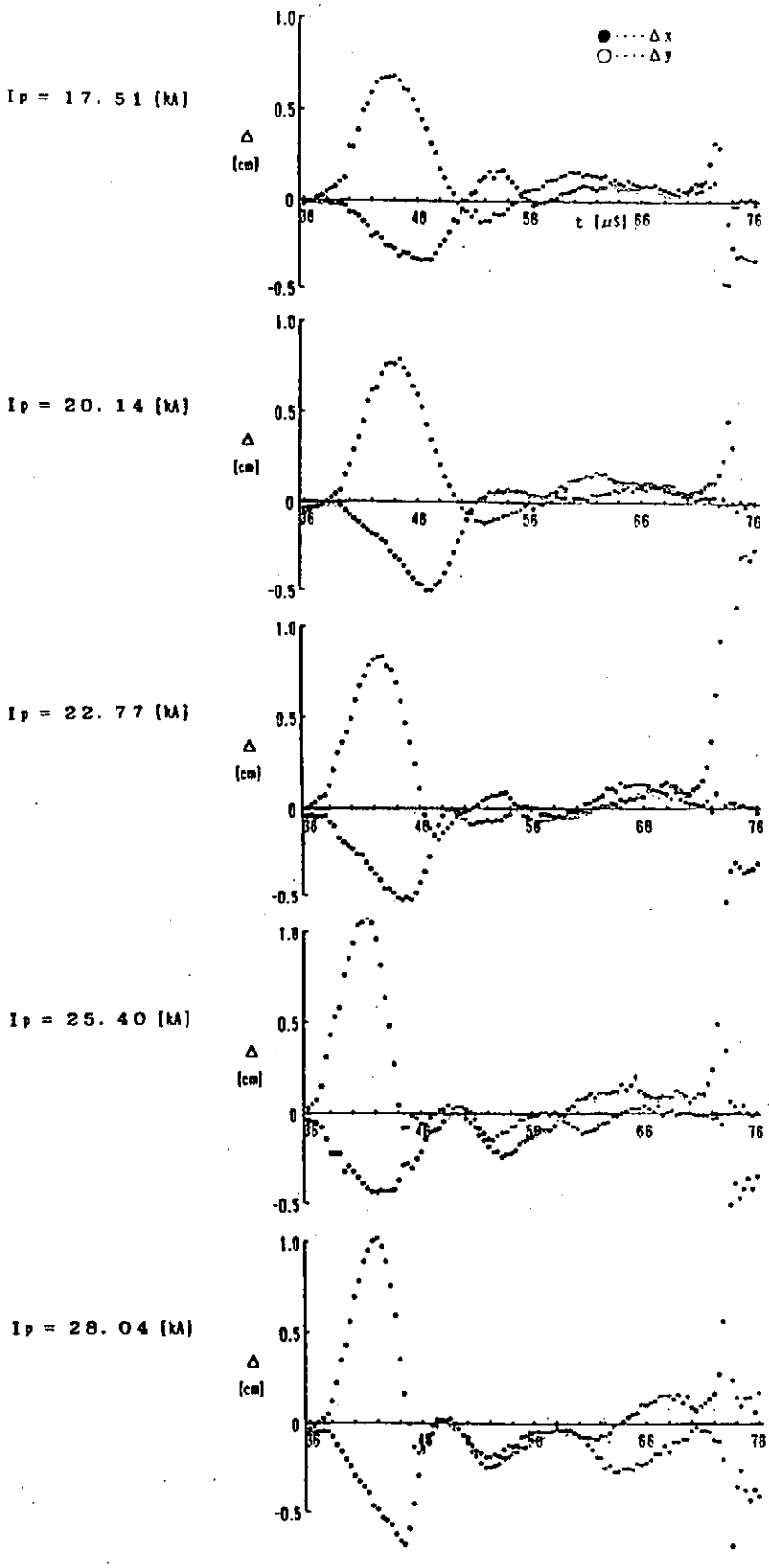

Fig.4 Time variations of the shifts of the plasma column, Δ_x, Δ_y, at five different values of the plasma current.

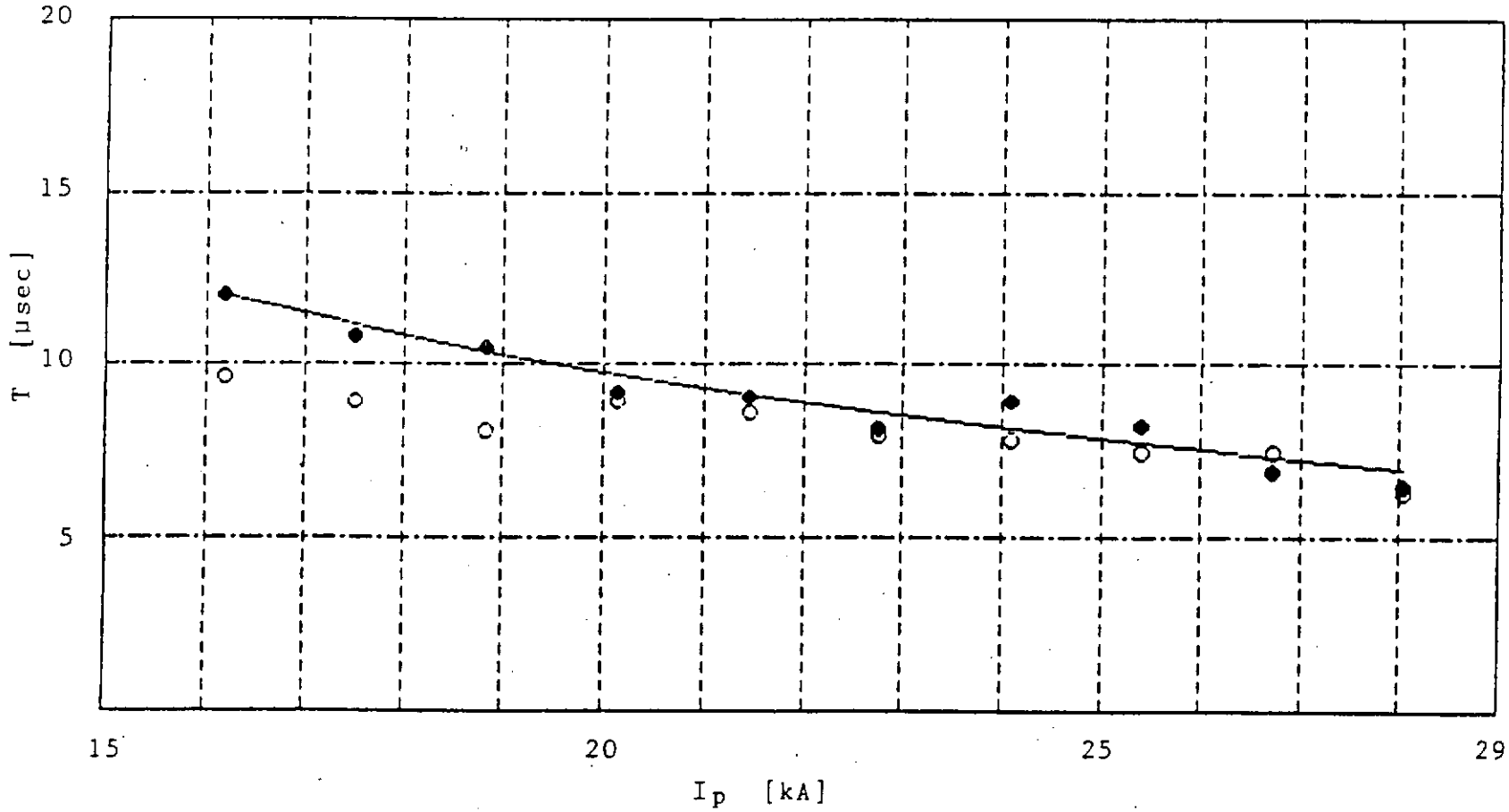

Fig.5 Dependences of the plasma current on the periods for the oscillatory motions of plasma column.

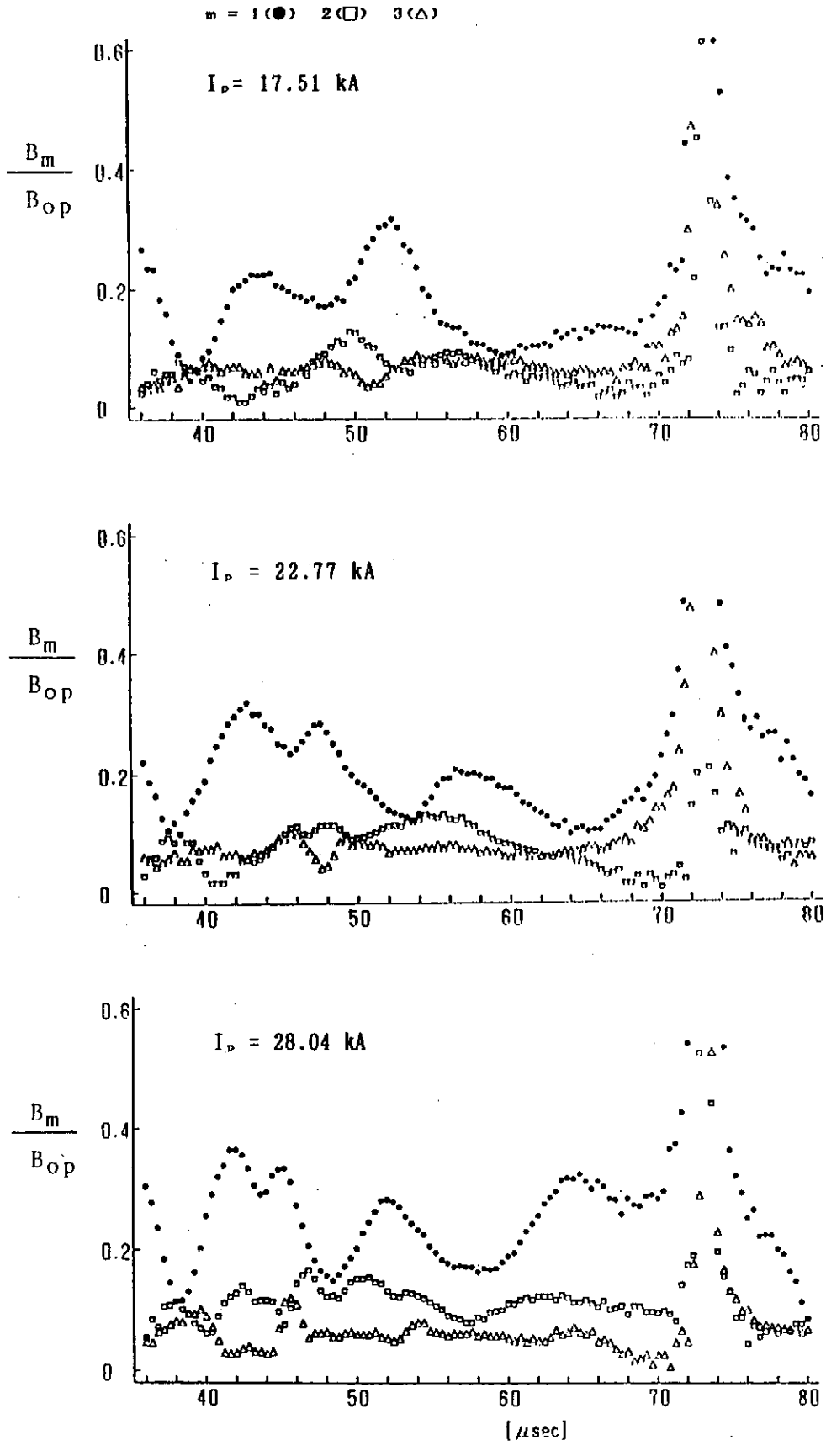

Fig.6 Fourier decomposed amplitudes at three diffrent values of the plasma current.

Dynamic Behavior of a Gas-puff Z-pinch Plasma and X-ray Radiation

Kinya Moriyama,[+] Keiichi Takasugi, Hideaki Suzuki[+] and Tetsu Miyamoto

Atomic Energy Research Institute, Nihon University

[+]College of Science and Technology, Nihon University

ABSTRACT

A gas-puff z-pinch plasma was produced in the SHOTGUN device, in which a hollow initial gas is injected through an annular nozzle on the anode. The contracting plasma showed nonuniformity along the column axis. As the rippling develops, the plasma column is separated into sections, which shrinks by turns from the gas nozzle. The spot images in the x-ray photograph corresponds to the nodes of the rippling.

I. INTRODUCTION

The gas-puff z-pinch[1] is one of the high energy density plasmas which are available in laboratory, and it has been applied to intense pulsed x-ray and XUV light source. The z-pinch is full of unstable MHD modes. The stabilization of z-pinch and understanding of mechanism of neutron emission has been important subjects in the nuclear fusion research. Particle acceleration due to the instability was shown,[2] and

accelerated electron beam was detected from a z-pinch.[3] The instabilities play important role not only for nuclear fusion but also for x-ray generation. The understandings of the z-pinch dynamics is important for both purposes.

Here macroscopic behavior of the collapsing z-pinch is observed using a N_2 laser measurement, and the relation between the axial nonuniformity and the x-ray spot formation is investigated. The micropinches formed in the z-pinch column are shown to have some relation to the instability.

II. Experimental Setup

Figure 1 is the experimental setup of "SHOTGUN" z-pinch device.[4] The anode has a hollow laval nozzle with inner diameter 26 mm and outer diameter 30 mm. Supersonic gas is injected between two electrodes. Both electrode are made of carbon. Spacing of the electrodes is 25 mm. The plasma currents are measured by Rogowskii coils placed around two electrodes as shown in Fig.1.

The diagnostics are located azimuthally to the plasma axis as shown in Fig. 2. Scintillation probes with various x-ray filters are used to detect radiation from the pinched plasma. An NE-102A scintillator is installed in each probe. An x-ray pinhole camera is used to take time-integrated picture of x-ray image. The Kodak DEF x-ray film placed in He atmosphere is used for taking soft x-ray image.

A N_2 laser shadowgraphy is used for monitoring the plasma density profile. The laser light is once focused on a pinhole before a camera after passed through the plasma in order to

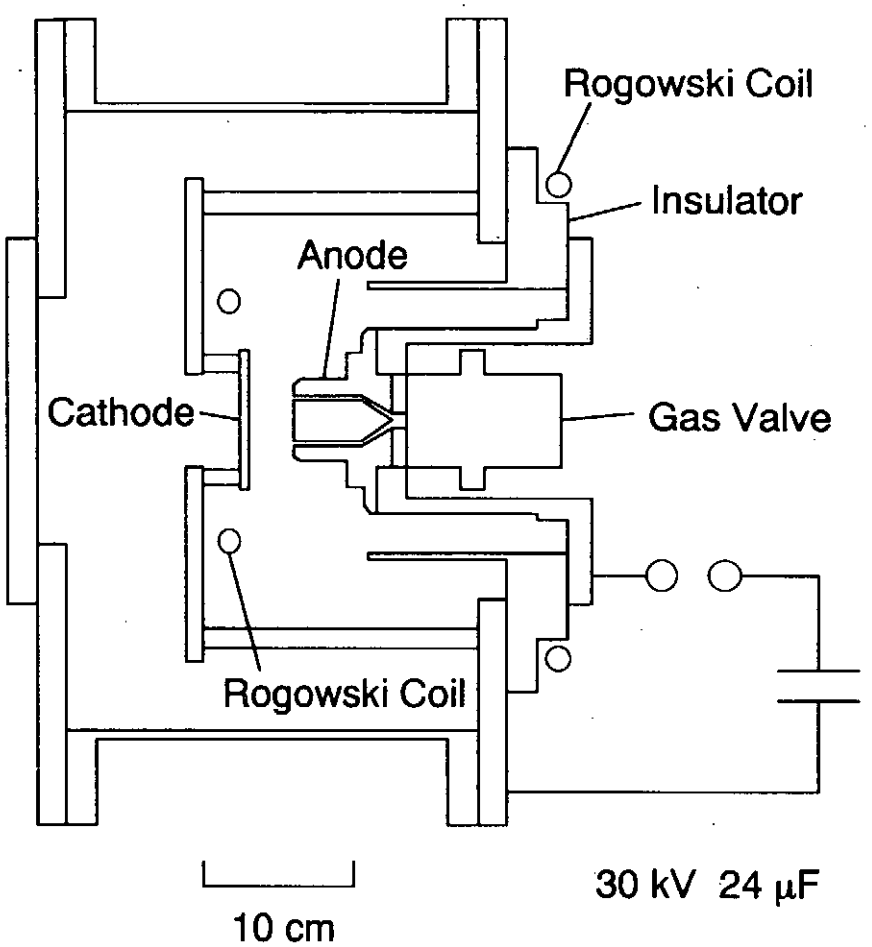

Fig. 1. Experimental setup of the SHOTGUN z-pinch device.

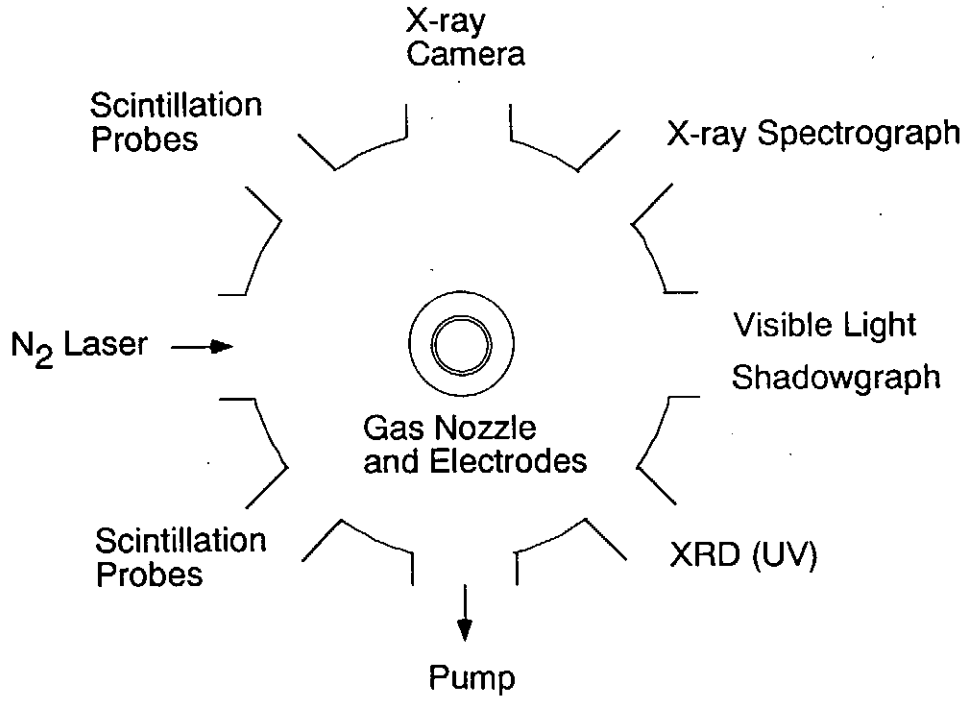

Fig. 2. Diagnostic arrangements in azimuthal direction.

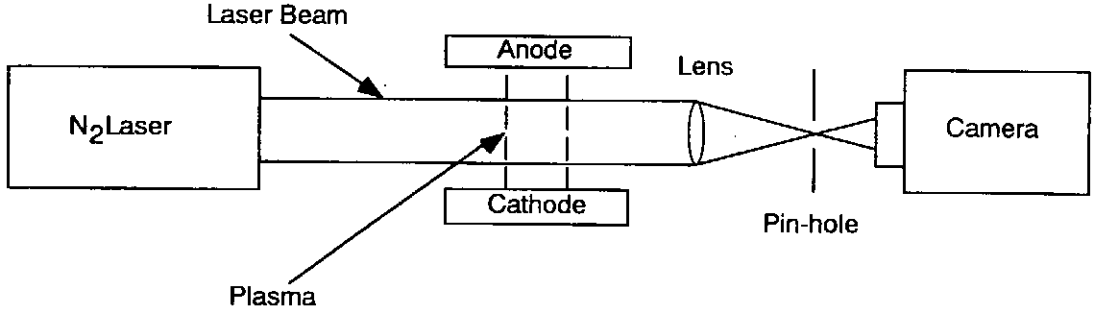

Fig. 3. Schematic diagram of the laser shadowgraphy.

reject plasma light (Fig. 3). Although the size of the pinhole rejector is large enough for the beam, it may possibly act as a schlieren knife edge. Anyway the resultant photograph shows the density profile, because the plasma has a steep boundary.

III. Dynamic Behavior during Implosion

The dynamic behavior of the plasma in the contraction is shown in a series of shadowgraphs of Fig. 4. The photographs were taken in different shots. As the phenomena were well reproducible, the moment of laser firing was counted from the beginning of the discharge and shown in the same current trace (top). The time sequence of the plasma behavior was observed as follows.

(a) The plasma of contracting thin current layer is observed. The plasma has already exhibited nonuniformity in the z-direction. The wavelength is smaller than that observed in the continuing photographs.

(b) The nonuniformity with a large wavelength (5 - 6 mm) devolops, and makes the first node at about 5 mm apart from the anode.

(c) The plasma between the node and the anode collapses rapidly and forms a divided small z-pinch column.

(d) The second divided contraction is observed. The small contraction occurs one after another from the anode (gas nozzle). It may be understood as a kind of zippering effect due to initial gas distribution. In the first divided pinch column, the plasma is heated, and has a instability like a sousage mode.

(e) After passing through the maximum pinch (current

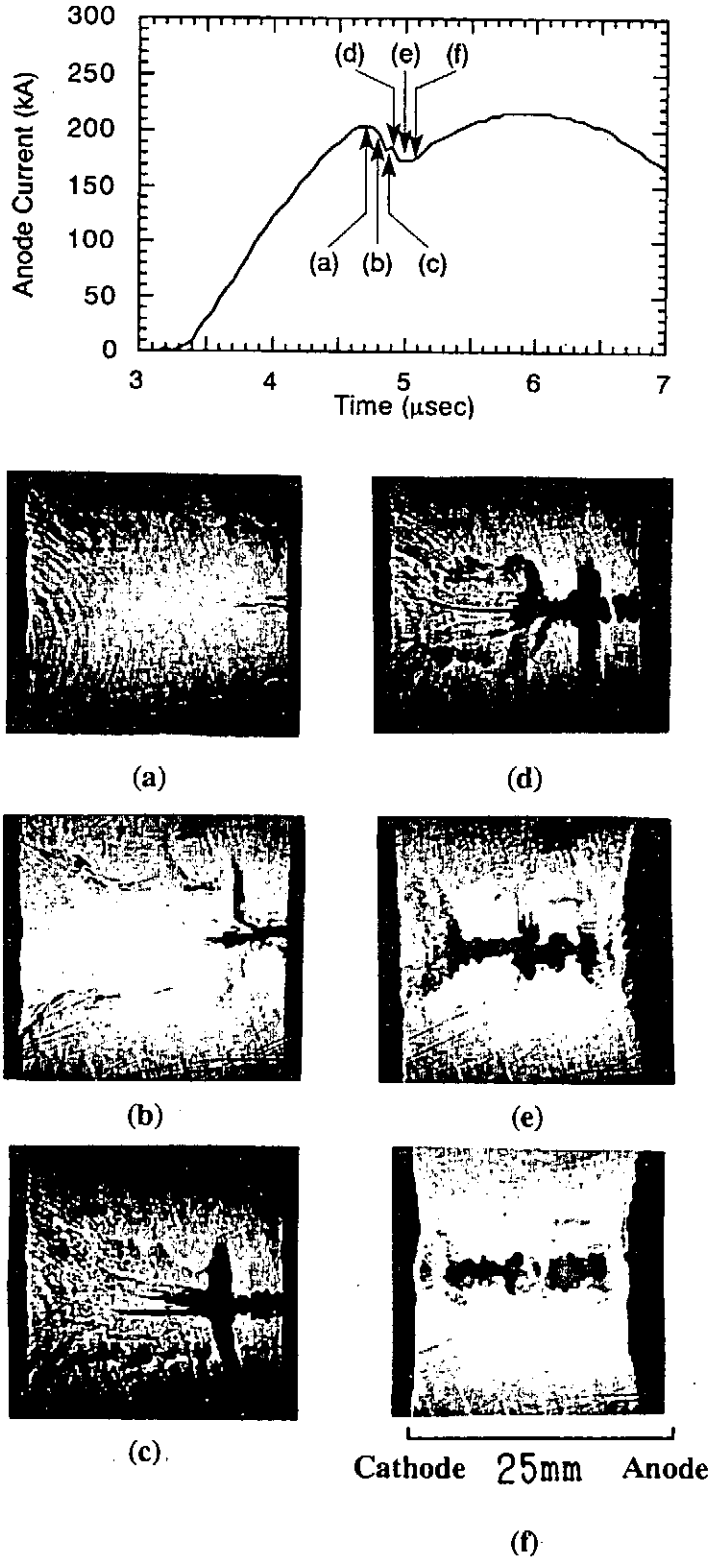

Fig. 4. Time sequence of radial contraction of the plasma. The plasma is divided into sections.

minimum), an averaged z-pinch column is formed between the electrodes. The column diameter is about 3 mm, however, the boundary and the density distribution are not exactly uniform. Expansion of the column has already started.

(f) The locally constricted part of the column grows up to form helical structure (m = 1 mode). After this the amplitude of the instability becomes comparable to its length. Finally the plasma expand to the wall and disappears from the view, while the plasma current continues.

IV. X-RAY RADIATION

Figure 5 shows (a) the shadowgraph and (b) the pinhole x-ray photograph taken in a same shot of Kr dicharge. X-ray images are classified into two types, one of which is spot and the other is cloud. Some of x-ray spots spatially corresponds to the nodes of rippling observed in the shadowgraph, and the other are observed in local pinches. X-ray clouds are also observed between the spots, but no evident relation with radial motion was found. Figure 5.(c) shows the x-ray signals filterd by 0.2 mm polyethylene (PE) and 0.1 mm Al. Two x-ray spikes were observed, and those peak intensity ratios do not change much. As the x-ray image is time-integrated, we cannot say which spike corresponds to which spot or cloud.

V. SUMMARY AND DISCUSSION

The dynamic and spatial behavior of the z-pinch plasma was investigated using the N_2 laser measurement, the x-ray photography and the x-ray emission detected by scintillation

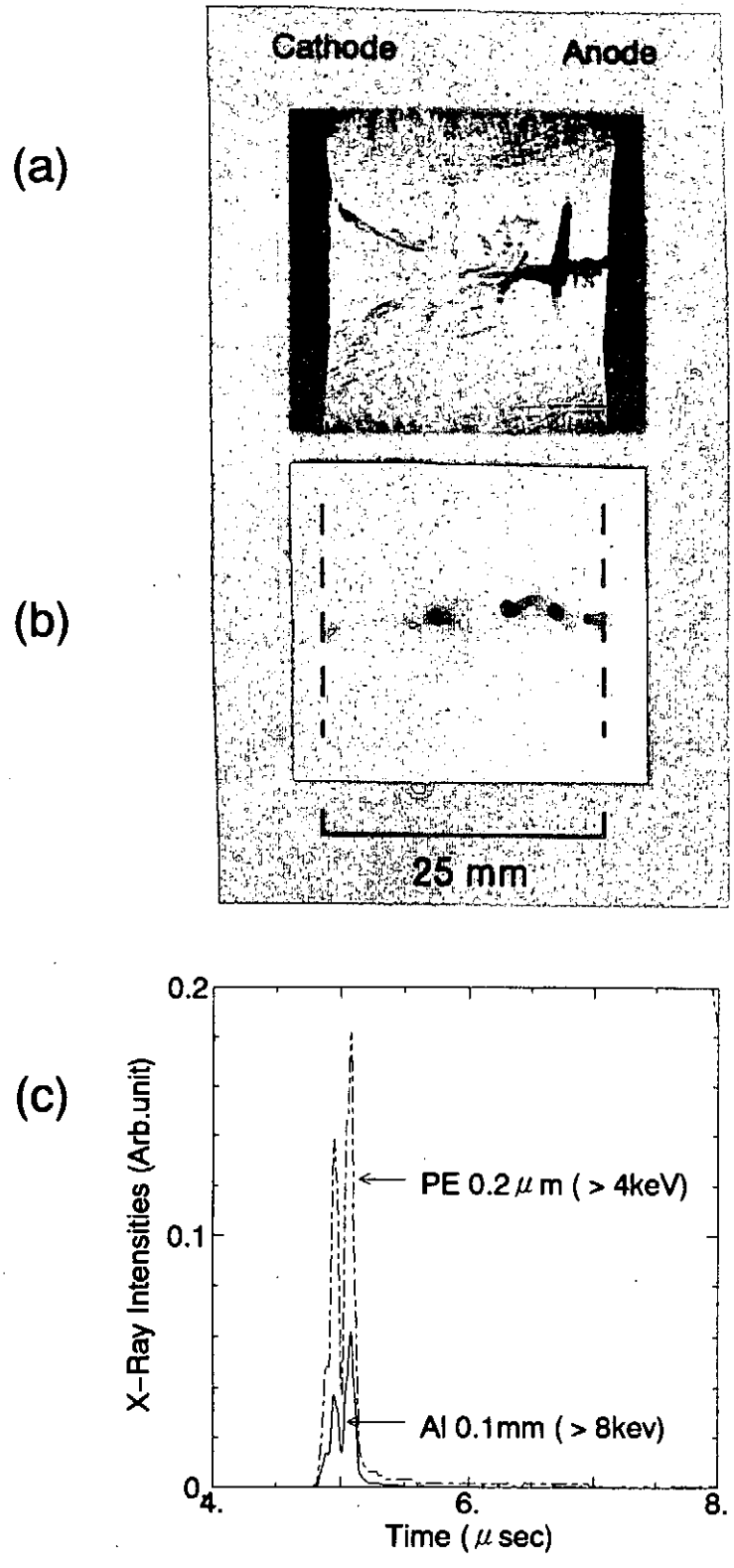

Fig. 5. Comparison of (a) shadowgraph (b) x-ray image and (c) x-ray signals taken in a same shot.

plobes. The observed plasma has shrunk nonuniformly on its surface in earlier implosion phase, and separated to several local pinches by the nonuniformity. Between local pinches the plasma forms nodes, and the delayed implosion occurrs. X-ray radiations are classified into spots and clouds from those shapes. The spots spatially corresponds to nodes. At the node the plasma is three dimensionally compressed and forms high density and high temparature state. Another spots will be irradiated from micro-pinches produced by sousage mode instability in local pinches. The x-ray cloud is not so intense and is formed between the spots. It may have some relation to m = 1 mode instability observed in the expansion phase.

References

[1] J. Shiloh, A. Fisher and N. Rostoker, Phys. Rev. Lett. 40, 515 (1978).

[2] M.G. Haines, Nucl. Instrum. Methods 207, 179 (1983).

[3] D.R. Kania and L.A. Jones, Phys. Rev. Lett. 53, 166 (1984).

[4] K. Takasugi, A. Takeuchi, H. Takada and T. Miyamoto, Jpn. J. Appl. Phys. 31, 1874 (1992).

Effect of Operating Gas on The X-ray Radiation from a Gas-puff Z-pinch

Hideaki Suzuki,[+] Keiichi Takasugi

Kinya Moriyama[+] and Tetsu Miyamoto

Atomic Energy Research Institute, Nihon University

[+]College of Science and Technology, Nihon University

Abstract

Gas-puff z-pinch plasmas using Ne, Ar and Kr as pinch materials have been produced in the SHOTGUN device. The hardening of x-ray radiation with Z of the operating gas was confirmed. The magnetic energy converted into the kinetic energy of the plasma increased with Z of the gas. It is attributed to strong compression due to radiation cooling in the contraction phase.

I. Introduction

The gas-puff z-pinch[1] has been a conventional method of producing high density and high temperature plasmas. It has an advantage as a pulsed x-ray source of repetitive operation with various combination of the operating gas, and radiation characteristics of mixed gas z-pinch was investigated[2,3]. Spectral characteristics of soft x-ray and XUV radiations have been reported[4-6].

In a plasma with moderate electron temperature the radiative energy loss tends to increase with atomic number Z of the operating gas. The lowering of temperature will cause further contraction of the equilibrium z-pinch plasma[7]. In this paper the global characteristics of x-ray radiations and energy inputs into plasmas with three different operating gases at a fixed condition are reported.

II. Experimental Setup

The experiment was carried out on the SHOTGUN z-pinch device[8]. The storage energy is 4.8 kJ (24 μF - 20 kV), and the gas is injected through a hollow nozzle on the center conductor (anode) using a high speed gas valve. The gas used here are Ne, Ar and Kr whose plenum pressure is fixed to 5 atm. The electrodes are made of carbon, and the spacing is 25 mm.

Scintillation probes with various x-ray filters are used for taking spectral information of the x-ray radiation. A vacuum x-ray diode without filter is used for XUV monitor. A four-pinhole x-ray camera is used for taking x-ray images with different filters, in which Kodak DEF x-ray film is located in attmospheric pressure He. The plasma currents are measured by Rogowskii coils placed on both electrodes.

III. Experimental Results

a. Basic Characteristics

Figure 1 shows current waveforms, XUV and x-ray signals of a typical shot of Ar z-pinch. The maximum plasma current is about 200 kA. The XUV and x-ray radiation occur simultaneously

with current dips, which indicate rapid increase of circuit inductance due to radial collapse of the plasma. The XUV signal shows temporally broad profile compared with x-rays.

The pinch times of three operating gases as a function of delay time of discharge from gas-puff detection τ_d is shown in Fig. 2. The contraction time T gradually increases with τ_d, but no evident difference in operating gas is observed. This indicate that total mass of the pinch material depends not on Z of the gas but only on τ_d.

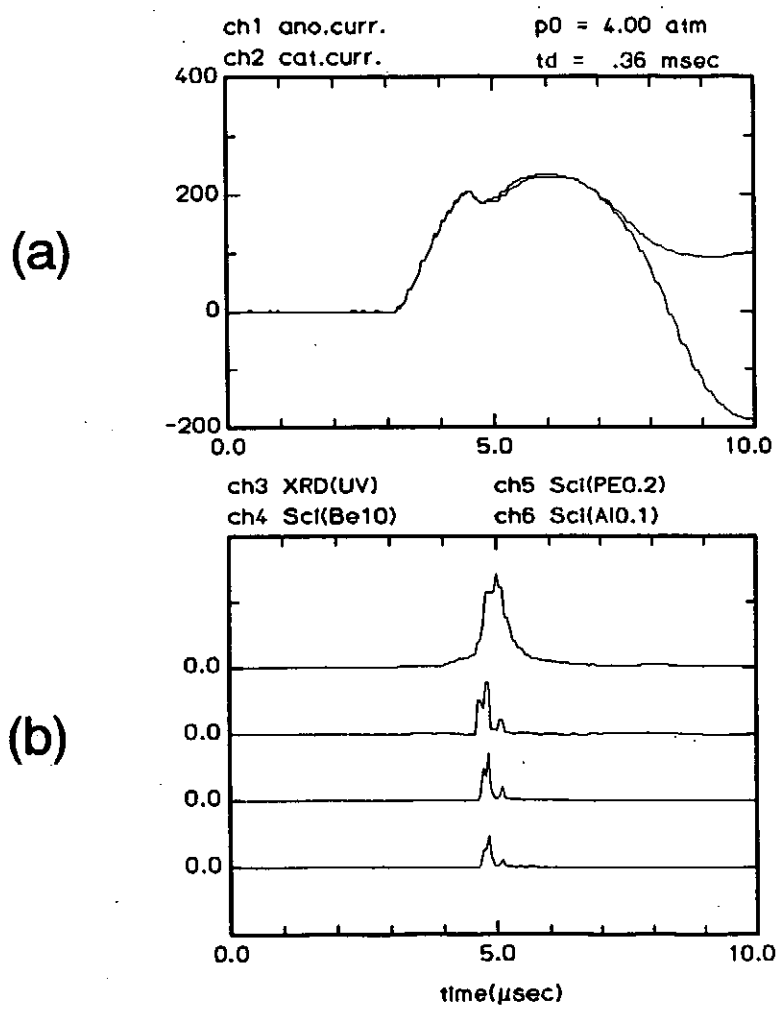

Fig. 1. (a) Plasma currents and (b) XUV and soft x-ray signals of a typical Ar z-pinch.

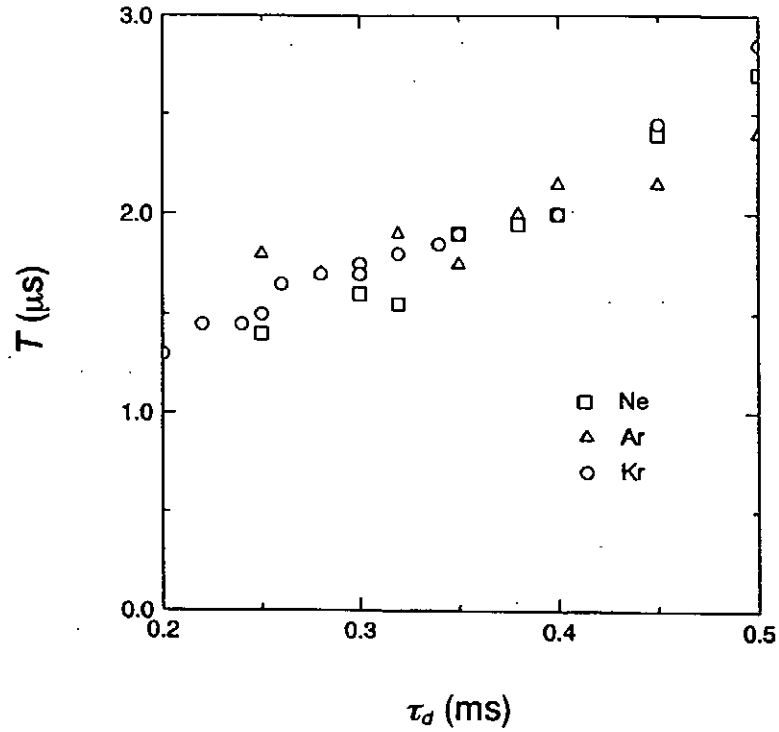

Fig. 2. Contraction time T vs. delay time τ_d for Ne, Ar and Kr z-pinches.

b. X-ray Radiation

Figure 3 shows typical x-ray photographs of Ne, Ar and Kr z-pinches taken with four filters, Be 5 μm, Al 15 μm, Al 0.1 mm and Al 0.5 mm. The photographs of each gas are taken in one shot. In the Ne z-pinch, x-ray image is observed in left two photographs, while in the Ar and Kr, it is observed in three and all photographs respectively. The film is not sensitive to x-rays with the energy exceeding 5 keV, however, it is a clear observation that the hard component of x-ray increases with Z.

Figure 4 compares soft x-ray intensities of Ne, Ar and Kr z-pinches. The x-ray filters used here are Be 10 μm, Al 50 μm, Al 0.1 mm and Al 0.5 mm. All the intensities increase with Z, and the gradient become steeper for harder x-ray. The data is

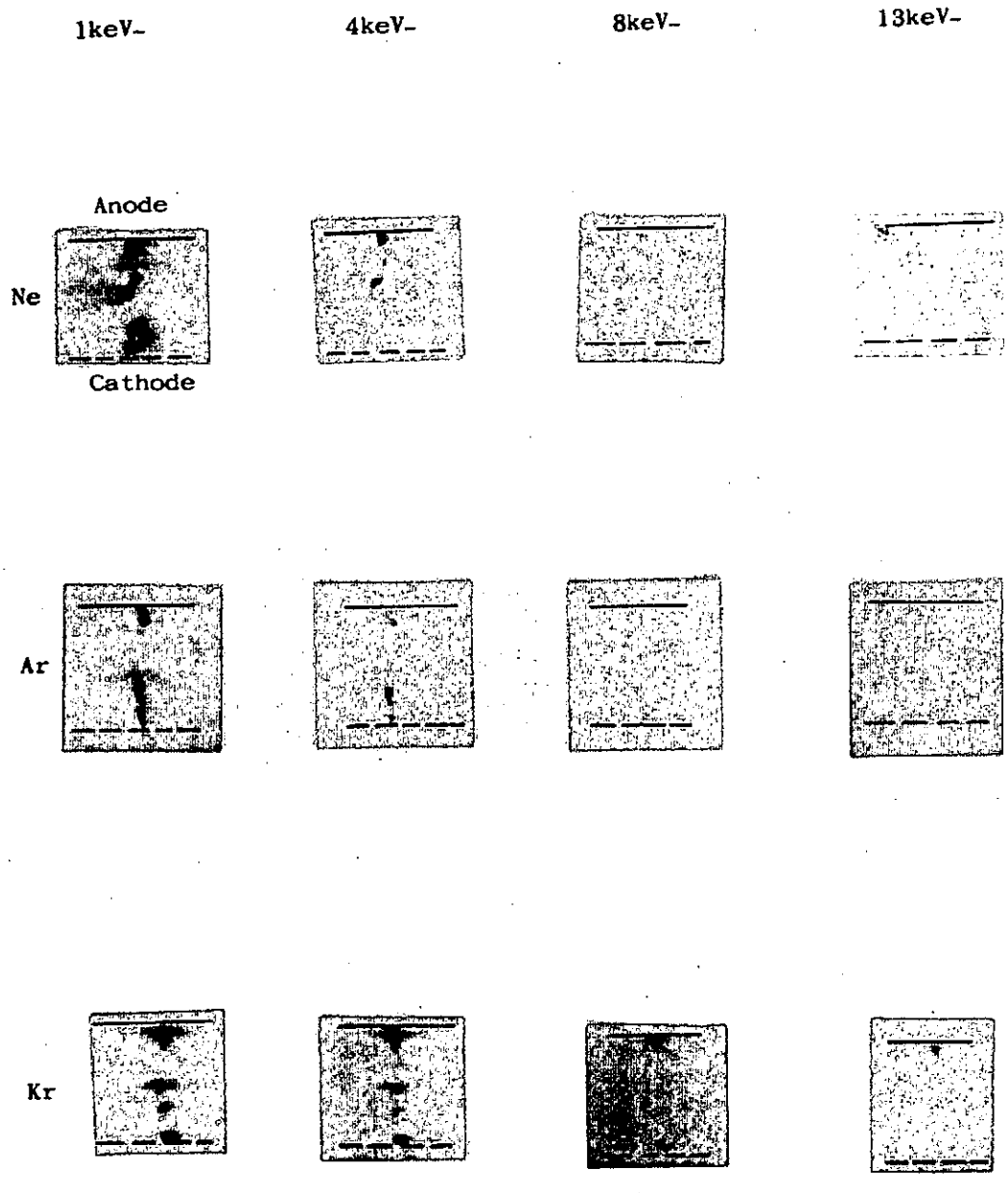

Fig. 3. X-ray pinhole photographs of Ne, Ar and Kr z-pinches taken with different x-ray filters.

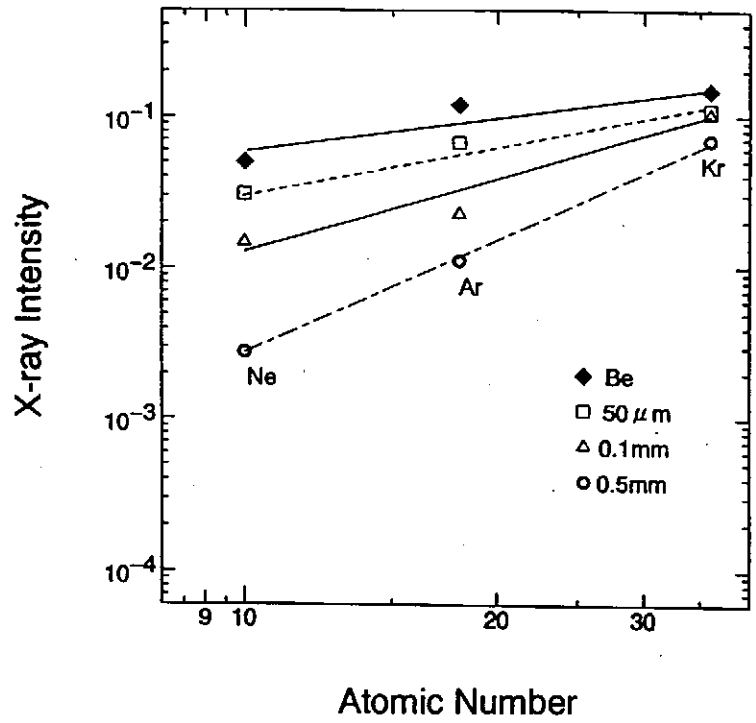

Fig. 4. Scintillation probe intensities of Ne, Ar and Kr z-pinches with four x-ray filters.

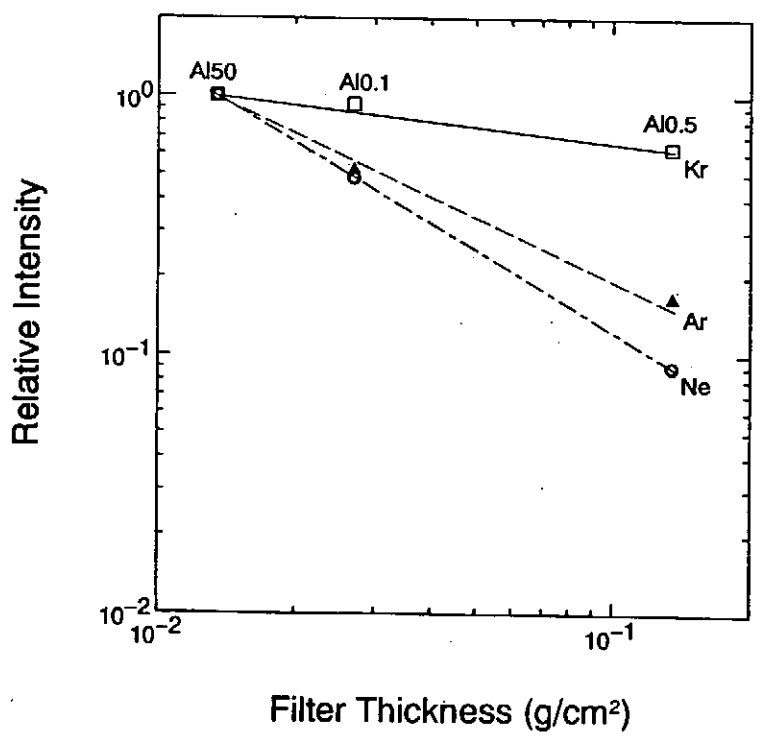

Fig. 5. Relative x-ray intensities of Ne, Ar and Kr plasmas as a function of Al filter thickness.

normalized by the data of Al 50 μm and is replotted for the thickness of Al filter in Fig. 5. Three curves show gentle gradients, which indicates broad spectral radiation in this energy range. The radiation temperatures of the plasmas are 1.5 keV for Ne, 2.9 keV for Ar and 7.8 keV for Kr. Although the temperature is meaningless for optically thin plasmas, it is a direct expression of radiation characteristics for the plasma in which the detailed radiation process is not clear.

c. Energy Input

Figure 6 shows typical current waveforms of Ne, Ar and Kr z-pinch discharges. The peak current levels and the contraction times are almost the same. The current dips, which corresponds to maximum pinch, are shown to become deeper as Z increases. In a rough assumption that the magnetic flux is constant in the short interval of the final contraction, the magnetic energy converted into kinetic energy of the plasma ΔE is[2]

$$\Delta E = \frac{1}{2} L_B I_B^{\,2} - \frac{1}{2} L_A I_A^{\,2} = \frac{1}{2} L_B I_B (I_B - I_A) .$$

Here L is total circuit inductance and I is plasma current. The suffixes B and A denote before and after the maximum pinch respectively. In Fig. 7 the energy ΔE is shown to increase rapidly with Z of the operating gas. These energies are still small fractions of the total energy of the power supply.

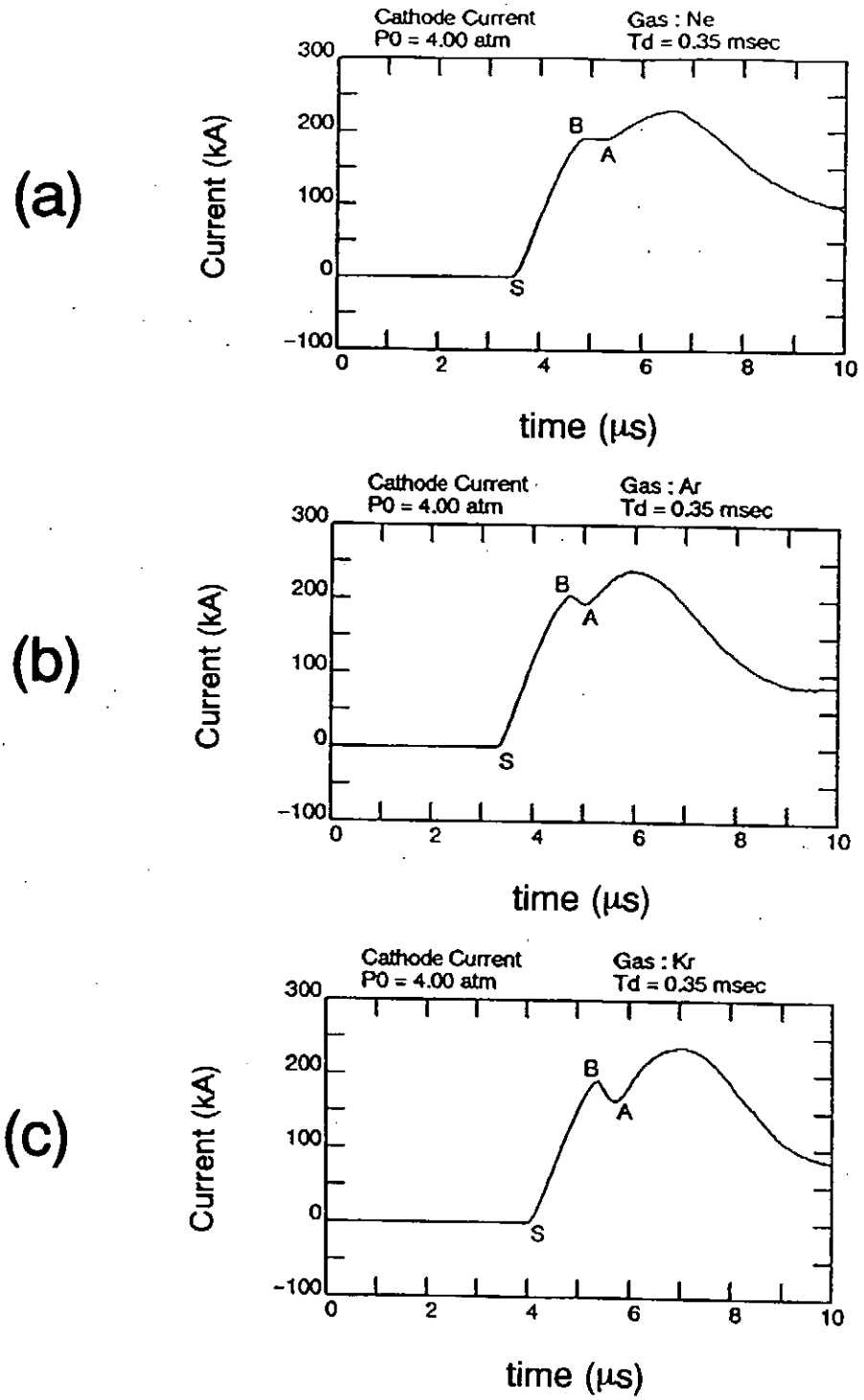

Fig. 6. Current waveforms of (a) Ne, (b) Ar and (c) Kr plasmas. The dip depth changes with the gas.

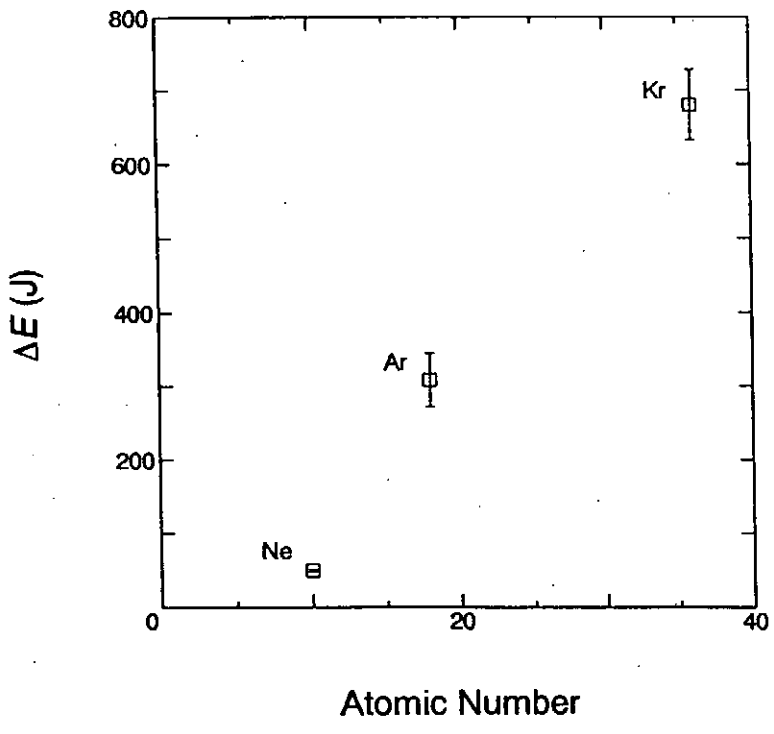

Fig. 7. The magnetic energy converted into kinetic energy of the plasma for three operating gases.

IV. Summary and Discussion

The Ne, Ar and Kr gas-puff z-pinches were generated and the x-ray radiation characteristics were investigated. The hardening of x-ray radiation with Z of the operating gas was confirmed. The radiation temperatures of the three plasmas were evaluated. The temperature was shown to increase with Z.

The magnetic energy converted into the kinetic energy of the plasma was calculated from the current waveform assuming flux conservation during the final contraction. The energy was shown to increase with Z of the gas. This was the direct result of formation of small average radius at the maximum pinch. The high Z gas plasma is radiatively cooled in the radial contraction phase, and it is compressed to a smaller radius,

then gains enegy to become high density and high temperature state.

REFERENCES

[1] J. Shiloh, A. Fisher and N. Rostoker, Phys. Rev. Lett. 40, 515 (1978).

[2] J.E. Bailey, Ph.D. thesis, U.C. Irvine (1983).

[3] J. Bailey, A. Fisher and N. Rostoker, J. Appl. Phys. 60, 1939 (1986).

[4] P.G. Burkhalter, J. Shiloh, A. Fisher and R.D. Cowan, J. Appl. Phys. 50, 4532 (1979).

[5] R.E. Marris, D.D. Dietrich, R.J. Fortner, M.A. Levine, D.F. Price and R.E. Stewart, Appl. Phys. Lett. 42, 946 (1983).

[6] G. Mehlman, P.G. Burkhalter, S.J. Stephanakis, F.C. Young and D.J. Nagel, J. Appl. Phys. 60, 3427 (1986).

[7] J.W. Shearer, Phys. Fluids 19, 1426 (1976).

[8] K. Takasugi, A. Takeuchi, H. Takada and T. Miyamoto, Jpn. J. Appl. Phys. 31, 1874 (1992).

Semi-automated data acquisition-and processing system for a Mach-Zender interferometer

K. Iwai, M. Yosida, H. Kitaoka and K. Hirano
Department of Electronic Engineering
Gunma University
Kiryu, Gunma 376, Japan

Abstract

A simple image acquisition system for an interferometer and image processing technique are described. In this system, commercially supplied tools are used and specific software is developed to perform a semi-quantitative analysis of interferogram. The computer program written in the C language is developed to carry out the thinning of the fringes. The response of the system is evaluated using the contrast transfer function (CTF). The thinning is carried out by the fringes being acquired into the image processing system and detected the maximum luminosity of the fringes with in a limit of the CTF. These techniqes are examined using an interferogram obtained in plasma focus experiment.

§ 1 Introduction

Mach-Zender interferometers are routinely employed to evaluate the spatial distribution of the electron density in plasma physics.[1,2] However, it is a tedeous job to analyse the interferograms by a manual method. Moreover, there is a possibility to include personal errors. Therefore process by automated methods are preferable.

Recently some authors proposed a method in which manual job was widely replaced by a computer processing.[3,4] To detect the maximum of the fringe luminosity, several techniques have been developed. As developed by Hildich, one of the typical method is a thinning which includes a binary image as a pre-processing.[5]

In this paper, a simple semi-automated processing method is described. In this method, we intended to carried out the processing using a commercially supplied CCD camera, an image memory board and personal computer. The spatial response of the system was determined using the contrast transfer function (CTF).

Analysis of the interferograms was as follows.

1 The CTF of the data-acqisition system is estimated.
2 Considering the limit in CTF, an image of the interferogram is formed on the CCD.
3 The image is registered inthe image memory without any pre-processing such as the shading and masking.
4 The thinning of the fringes is carried out and they are numbered.
5 Sometimes interpolation is locally needed to trace the thinning fringes.
6 Results are displayed on a scope or hardcopy device.

In this paper, the interferograms are obtained in the plasma

focus experiment by Mach-Zehnder system in which N_2-pulse laser is used. However, details of the experiment not so important.

We believe that this method is useful to the interferograms obtained in other fields.

§ 2 Experimental

2-1 Interferometer and data acqisition and processing system

The Mach-Zehnder inerferometer in which the N_2 laser was used as a light source employed to evaluate the 2-dimensional electron distribution in the plasma focus device. The image procesing system consisted of a CCD camera (Sony XC-77), a image memory board (Photoron FRM-512), a video monitor, and a personal computer (NEC PC-9801 RA2), a CTR display, and a printer. The image memory board is modefied in a single-shot mode. The interferrograms were formed on a phosphor screen or photographic film and registered in the image memory board through the CCD camera. This system is capable of 6 bits luminosity resolution. The image data can be stored both in the memory of the image memory board or on the floppy disk. The data was processed by the personal computer.

These techniques were examined using a plasma produced a plasma plasma focus device. The coaxial electrode diameters of the plasma focus device are 25 and 80 mm. The length of the electrodes was 80 mm. The condenser bank consisted of 4 x 1.06 μF, 100 KV capacitors. The device was operated at the bank voltage of 60 kV and a working gas pressure of 6 Torr H_2.

2-2 Spatial resolution of the system

We used the CTF to evaluate the spatial resolution of the data acquisition system. The most commonly used a figure of merit for the resolution of a image system is the CTF which is

defined as

$$CTF = \frac{I_{max} - I_{min}}{I_{max} + I_{min}}$$

where I_{max} and I_{min} are the maximum and mimimum luminosity of the fringe of the registered interferogram.

Evaluation of the CTF was carried out using the ITE aperture response chart described in Ref. 8. This is a resolution grid with a squre-wave transmission which arranges regions of 100% transmission and 0% transmission regions alternatively. A part 4.5 x 4.5 cm of the chart is projected on the CCD which was projected on the CCD (512 horizontal x 480 vertical pixels). The CTF as a function of the spacial frequency for the system is shown in Fig.1. It is seen that the maximum CTF of the system is 4 lp/mm approximately. This means that the system operates nearly the Nyquist limit.

§ 3 Data Processing method and results

After the acquisition of the fringes into the image memory in 6 bits luminosity resolution for each pixel, the fringes are scanned and converted into the analog signel. The signal is smoothed by a filter to remove noise. Then the succesive maximums of the signal are detected by the horizontal scanning. We order the detected maximums, and connect the points ordered by same number. This produces a thnning of the fringes. The programs are written in the C language.

In our system, it is impossible to acquire the data stored in 512 x 480 pixels into the memory in the personal computer. Therefore we compress the data into two dimensionl alignment. Connecting the data (in X-coordinate) which have the same fringe munber in Y-coordinate, we obtain the thinning interferogram.

An example of an original interferogram of a collapse phase plasma in the plasma focus experiment is shown in Fig. 2 a). Figure 2 b) is the computer-drawn thinning fringes of the interferogram shown in Fig.2 a). The black dots in this figure are center locations (the maximum luminosity) of each fringe.

Local lack of the dots is caused by crooking in acute angles of the fringes in the original interferogrm shown in Fig.1. Because of the limit for CTF, the thinning was not possible in this region. A manual correction is needed in this part. After conncting the dots on the same fringe number we obtain the thinning interferogram as shown in Fig.2 c).

On our system the analysis of a single interferogram takes about 3 minutes using our processing method. On the other hand, Hildich's method takes about 10 minutes with much more manual corrections.

References

1 A. Bernard, A. Condeville, A. Jolas, J. Launspach and J. de Mascureau, Phys. Fluids 18, (1975) 180

2 K. Hirano, Y. Tagaya, K. Shimoda, Y. Okabe and T. Yamamoto, J. Phys. Soc. Jpn. 55, (1986) 2211

3 H. Chen and W. H Chvistiansen, Rev. Sci. Instrum. 56, (1985) 1619

4 H. A. Vrooman and A. A. M. Maas, SPIE vol.1121 Inteferometry (1989) 665

5 C.J.Hildich, Linear Skeletons from Square Cupboards, Machine Intelligence 4, ed. B. Meltzey et al. Univ. Press, Edinburgh PP 403 ~ 420 (1969)

6 S. G. Glendinning and H. Medecki, Rev. Sci. Instrum. 57, (1986) 1284

7 K. Hirano, T. Yamamoto, K. Shimada and H. Nakajima, J. Phys. Soc. Jpn, 58, (1989) 3591

8 K. Wakui and H. Kusaka, J. Inst. TV. Eng. Jpn, 36 (1982) 209 (in Japanese)

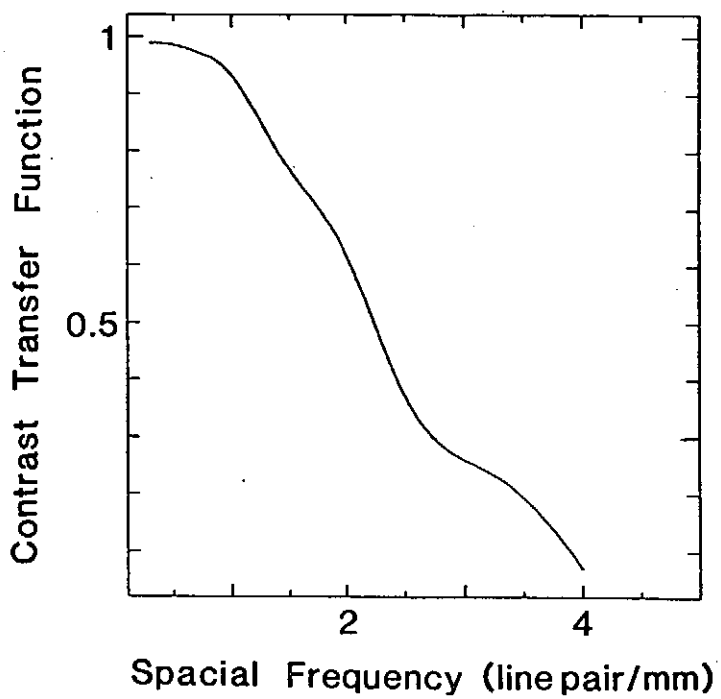

Fig. 1 A contrast transfer function for the image processing system .

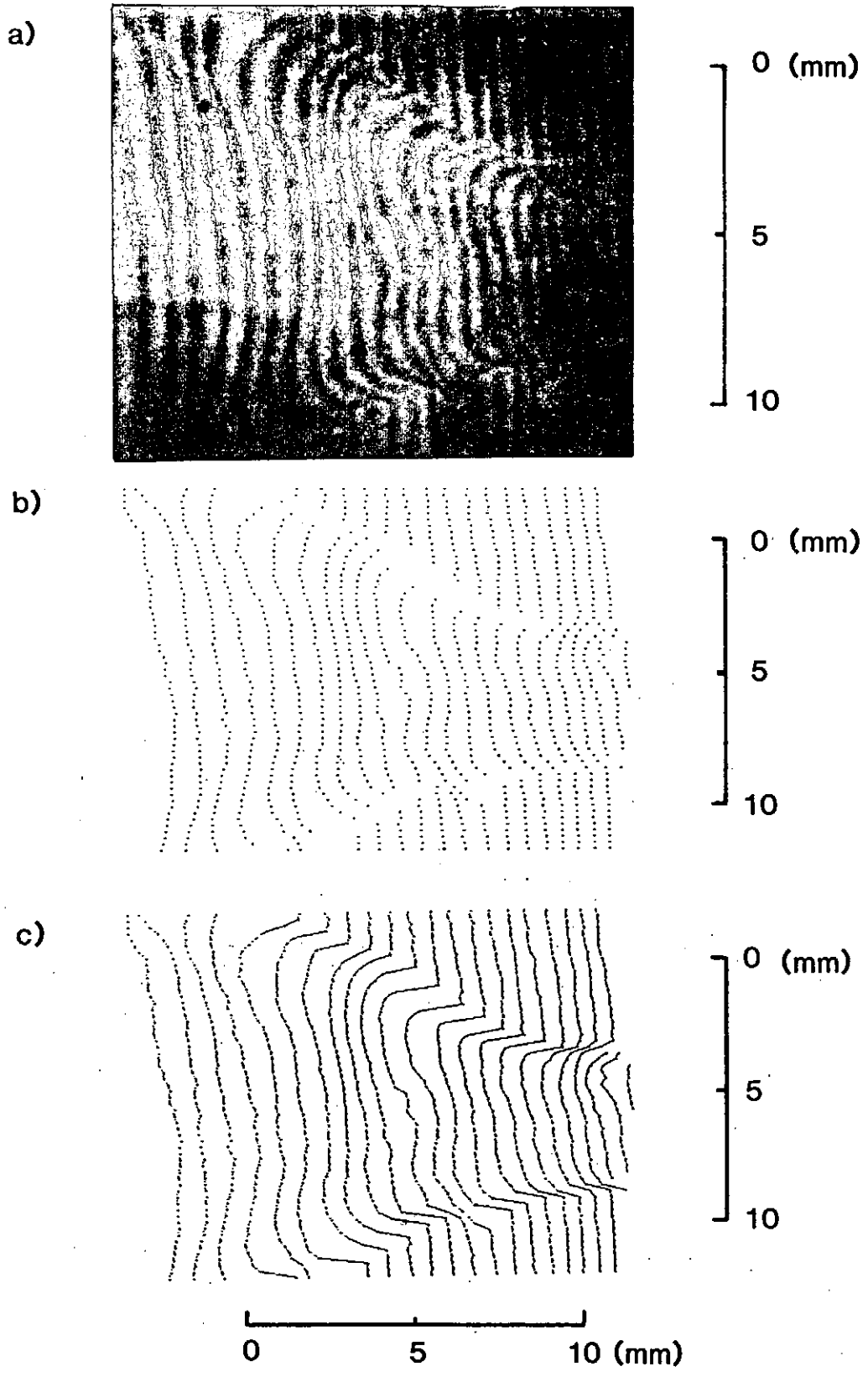

Fig. 2 a) An example of the Mach-Zehnder interferogram.
b) The computer-drawn fringes of the interferogram shown in Fig. 2 a) before connecting the maximum luminosity of the fringes shown by black dots.
c) The thinning fringe after giving manual correction.

A Simple, Semi-quantitative Method for Measuring Pulsed Soft X-rays

Y. Takahama, J. Du, T. Yanagidaira and K. Hirano
Department of Electronic Engineering
Gunma University
Kiryu, Gunma 376, Japan

Abstract

A simple semi-quantitative measurement and image processing system for pulsed soft X-rays with a time and spatial resolution is proposed. Performance of the system is examined using a cylindrical soft X-ray source generated with a plasma device.

The system consists of commercial facilities which are easily obtained such as a microchannel plate-phosphor screen combination, a CCD camera, an image memory board and a parsonal computor. To make a quantitative measurement possible, the image processing and observation of the phosphor screen current are used in conjunction.

§ 1 Introduction

Pulsed X-rays are easily produced in laser plasmas and high current discharge plasmas. Those X-ray sources show remarkable intensity in the soft x-ray region. It is indispensable to observe those sources by a quantitative method with the time and spatial resolution. Several authors have investigated such measurement systems so far. However, few systems have been examined to observe pulsed soft X-ray emitted from dense plasma.[1-3]

In this paper, a simple semi-quantitative measurement and image processing system for pulsed soft X-rays with a time and spatial resolution is developed. The system consists of commercial facilities which are easily obtained such as a microchannel plate-phosphor screen combination, a CCD camera, an image memory board and a personal computor.

Calibration for the soft X-ray intensity should be carried out using a standard X-ray source with a desirable energy. However, a suitable source is sometimes not available. To make a qantitative measurement possible, the image processing and observation of the phosphor screen current are used in conjunction.

The system for the soft X-ray measurement and the characteristics of the plasma focus device are described in § 3. In § 4 performance of the system, experimental results and discussion are presented.

§ 2 Notations

We describe below notation used in this paper.

n_{ps} : intensity of soft X-rays source, photons/s mm² (mard)².

n_{pm} : intensity of the soft X-rays on the MCP, photons/s mm².

n_p : luminosity density of visible image on the phosphor screen per unit time.

n_e : electron yield by n_{p_m} on MCP .

N_e : total electron numbers arrived on the phosphor screen.

$G(V_e)$: electron multiplication efficiency of the MCP at the applied voltage V_e.

$X_p(V_p)$: quantum efficiency of phosphor at applied Voltage V_p.

β : intensity of image registered on the image memory per unit area.

$\eta(\lambda)$: transmission coefficient of Be for the soft X-rays.

$\mu(\lambda)$: detection efficiency of the MCP for the soft X-rays.

§ 3 Apparatus

3-1 Image acquisition system

A schematic diagram of the semi-quantitative image acquisition system is shown in Fig. 1. It is intended to compose the system mainly employing ones which can be obtained easily in commercial.

The Image of the X-ray source is formed on the MCP (micro-channel plate, Hamamatsu Photonics, type 2225-11MX) through a pinhole and Be filter (25 μm in thickness) which prevents the visible light also emitted from the source. The spectral response of the Be-MCP combination is given in Fig. 2. It was calculated with taking into account absorption by Be filter and the detection efficiency for MCP.

The X-rays produce electrons and they are multiplied by the voltage applied between the both side of the MCP. Then the electrons are accelerated to the phosphor screen by the voltage of V_p and a image of the visible light appears. The visible image displayed on the screen is resgistered in an image memory

board (Photon FDM4-256) through a CCD camera (Sony XC-77). The MCP-phosphor system can be gated by the shuttering duration of ~5 ns in FWHM.

The image data can be stored both in the memory of the image memory board and on the floppy disk. The data are processed by the personal computer (NEC PC-9801RA2). A preferable data processing, such as the 3-dimensional display, is possible by this system.

The camera was operated in a mode in which the sensitivity of the CCD was proportional to the luminosity of the object. The image memory board was modified to be operated in a single shot mode.

The voltage signal V_p which is obtained on the scope is given as

$$V_p = \frac{eR}{2}\frac{dN_e}{dt} \tag{1}$$

Then integrating Eq. (1), we obtain

$$N_e = \frac{2}{eR}\int_0^t V_p(t)\,dt \tag{2}$$

The signal is used to obtain the total number of electron which make the image on the phosphor screen.

3-2 Plasma focus device as a soft X-ray source

A Mather type plasma focus device was employed to generate soft X-rays. The coaxial electrode diameters were 25 and 80 mm, respectively. The length of the electrodes was 80 mm. The inner electrode was hollow. The condenser bank consisted of 4 x 1.06 μF, 100 kV capacitors. The device was operated at the bank voltage of 60 kV and a gas pressure of 6.0 Torr H_2. Details of the device were described in a previous

publication.[4] The schematic diagram of the plasma focus device and the tools for measurement is shown in Fig. 3.

Soft X-ray emission was observed by three window-removed PIN photodiodes (Hamamatsu Photonics, S1722-01) and/or three scintillator-photomultiplier combination (NE-142 and Hamamatsu Photonics 1161). The location is shown in Fig. 3.

§4 Experimental Procedure

On the system shown in Fig. 1, the intensity of image registered on the image memory, β is given as a function of the luminosity density of visible image on the phosphor screen per unit time, n_p

$$\beta = f(n_p) \tag{3}$$

When the CCD is used as an image detector, $f(n_p)$ becomes Cn_p, where C is a constant. On the other hand, blackening characteristics should be taken into account when photografic film is employed as a passage of the image acquisition.

"Total intensity" of the image registered in the image memory is

$$\begin{aligned} B_0 &= \int_S \int_0^t \beta \, dS \, dt \\ &= \int_S \int_0^t f(n_p) \, dS \, dt \\ &= \int_S \int_0^t f\{X_p(V_p) \, G(V_m) \, n_e\} \, dS \, dt \end{aligned} \tag{4}$$

Where S is the space in which the image is formed. Now, we assume that $\beta = Cn_p$, then

$$\begin{aligned} B_0 &= C \int_S \int_0^t n_p \, dS \, dt \\ &= C X_p(V_p) \int_S \int_0^t G(V_m) \, n_e \, dS \, dt \end{aligned}$$

$$= CX_p(V_p)\, N_\bullet$$

$$= CX_p(V_p)\,\frac{2}{eR}\int_0^t V_p(t)\,dt \qquad (5)$$

Therefore, we obtain $CX_p(V_p)$ as following.

$$CX_p(V_p) = \frac{B_0}{\frac{2}{eR}\int_0^t V_p(t)\,dt} \qquad (6)$$

Otherwise, $f^{-1}(\beta)$ which is the inverse function of f, should be calculated using sensitivity of the optical materials as mentioned above.

In Fig. 1, we can describe β as

$$\beta = Cn_p = G(V_m)\,CX_p(V_p)\,n_\bullet$$

$$= G(V_m)\,CX_p(V_p)\int_\lambda \eta(\lambda)\,n_{pm}\,d\lambda$$

$$= G(V_m)\,CX_p(V_p)\int_\lambda \eta(\lambda)\,\mu(\lambda)\,n_{ps}\,d\lambda$$

$$= G(V_m)\,CX_p(V_p)\,\overline{n_{ps}}\int_\lambda \eta(\lambda)\,\mu(\lambda)\,d\lambda \qquad (7)$$

where we assumed that n_{pm} is independent of λ in the observed region of the wavelength $\Delta\lambda$. On the other hand, taking the size of the pinhole and other geometries into account, n_{pm} is

$$\overline{n_{ps}} \fallingdotseq \left(\frac{R_2}{R_1}\right)^2 \frac{10^{-3}}{\frac{\pi}{4}\left(\frac{d}{R_1}\right)^2}\,\overline{n_{ps}} \qquad (8)$$

where d is the diameter of the pinhole, 25 μm and R_1, 268mm and R_2, 211mm are given in Fig. 1.

Substituting Eq. (7) into Eq. (8), we obtain finally,

$$\overline{n_{PS}} = \alpha C n_p = \alpha\beta \qquad (9)$$

where

$$\alpha = \left(\frac{R_2}{R_1}\right)^2 \frac{10^{-3}}{\frac{\pi}{4}\left(\frac{d}{R_1}\right)^2} \frac{1}{G(V_m)\, CX_e(V_e) \int_\lambda \eta(\lambda)\, \mu(\lambda)\, d\lambda} \tag{10}$$

The spectral response of the system is determined by that of MCP-Be combination. On the other hand the dynamic range and the spatial resolution are under investigation.

§5 Experimental Results

5-1 Plasma evolution and soft X-ray emision in plasma focus

As shown in Fig. 4 (a) which is observed with an image converter camera, the current sheet reaches the end of the inner electrode and collapses radially and forms a plasma column. At the maximum compression, the plasma radius was ~2 mm. Then the column was disrupted after a short stable phase. With the disruption, a voltage spike (higher than 100 kV) was observed.[5]

After he compression phase, the soft X-ray emission which has several peaks is observed as shown in Fig. 4 (b) (2). Those peaks correspond to the maximum compression, the disruption of the pinched plasma, and emissions from the inner electrode in later phase.[6] The soft X-rays at the maximum compression is emitted from the pinched plasma column. The second peak corresponds to the disruption. At the third peak, no soft X-ray source was recognized in the plasma, but the face of the inner electrode emitt characteristic X-rays.

In this paper, the target of measurement is the first one.

5-2 Processing of the soft X-ray data

Figure 4 (b) (1) shows the phosphor current which was simultaneouly obtained with the soft X-ray signal in Fig. 4 (b) (2). The first peak of the phosphor current corresponds to the

maximun compression of the plasma which is a cylindrical soft X-ray source. Therefore, the integration of the first peak over the time is Eq. (2). We obtain N_0 by the numerical integration of the peak as

$$N_0 = 1.68 \times 10^6 \quad (11)$$

The framing photogragh which was taken with the image acquisition sysytem with the shutter opened is shown in Fig. 4 (b) (1). The spot in the center is the X-rays generated by the plasma cylinder.

After the image processing for 3-dimensional display using the system, we obtain Fig. 5. The purpose of this section is to get a vertical axis with an absolute unit for the X-ray intensity. The vertical axis originally displays a relative X-ray intensity by 6 bits. The integration over the image of the relative x-ray intensity corresponds to Eq. (4). Here, we get

$$B_0 = 12.5 \quad (12)$$

by the numerical integration of Fig. 5. Then, we obtain $CX_p(V_p)$ from Eq.(6) as

$$CX_p(V_p) = 7.44 \times 10^{-6} \quad (13)$$

As $G(V_m)$ in Eq. (10) can be found in the data sheet by the manufacturer of the MCP to be $G(V_m) = 2.66 \times 10^4$. $\eta(\lambda)$ and $\mu(\lambda)$ is given in Ref. 7) and 8), respectively

$$\int_\lambda \eta(\lambda)\mu(\lambda)d\lambda = 36.04 \times 10^{-2} \quad (14)$$

Therefore, we obtain

$$\alpha = 127.23 \quad (15)$$

This makes it possible to give an absolute unit for the vertical axis of Fig. 5.

References

1) A. J. Lieber and R. Snider: Rev. Sci. Instrum. 56 (1985) 821.

2) M. J. Eckart and R. L. Hanks, J. D. Kilkenny, R. Pasha, J. D. Wiedwald and J. D. Hares: Rev. Sci.Instrum. 57 (1986) 2046.

3) D. G. Stearns, J. D. Wiedwald, B. M. Cook, R. L. Hanks and O. L. Landen: Rev. Sci. Instrum. 60 (1989) 363.

4) T. Yamamoto, K. Shimoda and K. Hirano: Jpn. J. Appl. Phys. 24 (1985) 324.

5) K. Hirano, T. Yamamoto, K. Shimoda and H. Nakajima: J. Phys. Soc. Jpn. 55 (1989) 3591.

6) K. Hirano, Y. Tagaya, K. Shimoda, Y. Okabe and T. Yamamoto: J. Phys. Soc. Jpn. 55 (1986) 2211.

7) B. Nahrath: IPF Stuttgart Bercht Nr. IPF-74-11 (1974).

8) W. Parkes, R. Gott, K. A. Pounds: IEEE Trans. Nucl. Sci. NS17 (1970) 360.

Firgure captions

Fig. 1 Block diagram of the data acquisition and processing system for the soft X-ray imaging.

Fig. 2 Spectral response of the MCP-Be filter combination.

Fig. 3 Schematic diagram of the experimental arrangement.

Fig. 4 (a) A streak photograph showing the time evolution of the plasma.

(b) (1) The phosphor current. The hatched area in the first peak corresponds to the maximum compression of the plasma.

(2) Soft X-ray emission simultaneously observed with (1).

(c) (1) Soft X-ray image.

(2) Schematic diagram of the electrode. The hatched area in the face of the inner electrode and the

circle of the dotted line shows the field of view of the data acquisition system.

Fig. 5 The three-dimensional display of the soft X-ray source shown in Fig. 4 (c)(1).

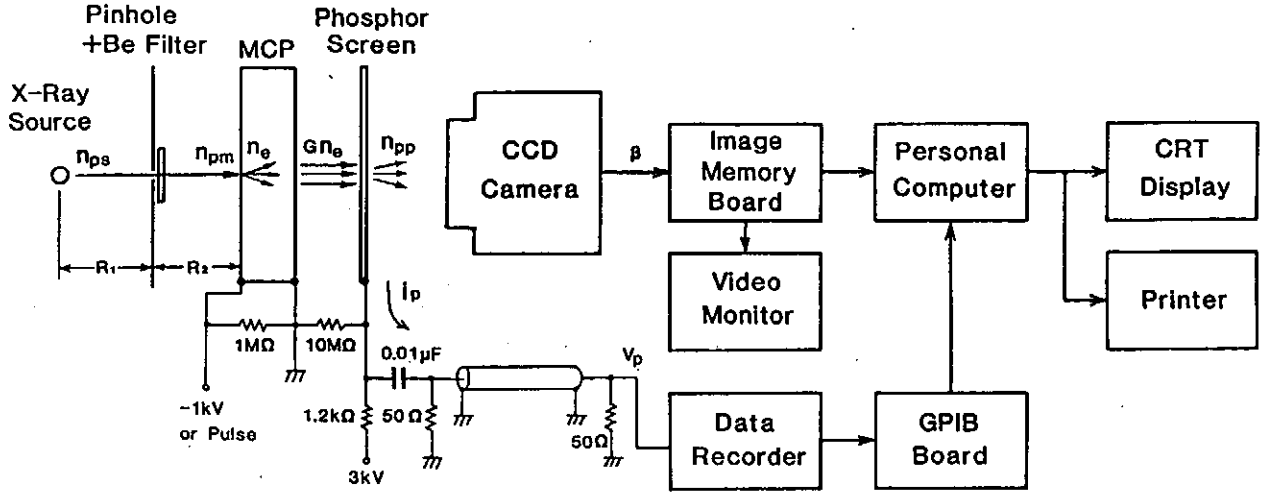

Fig.1

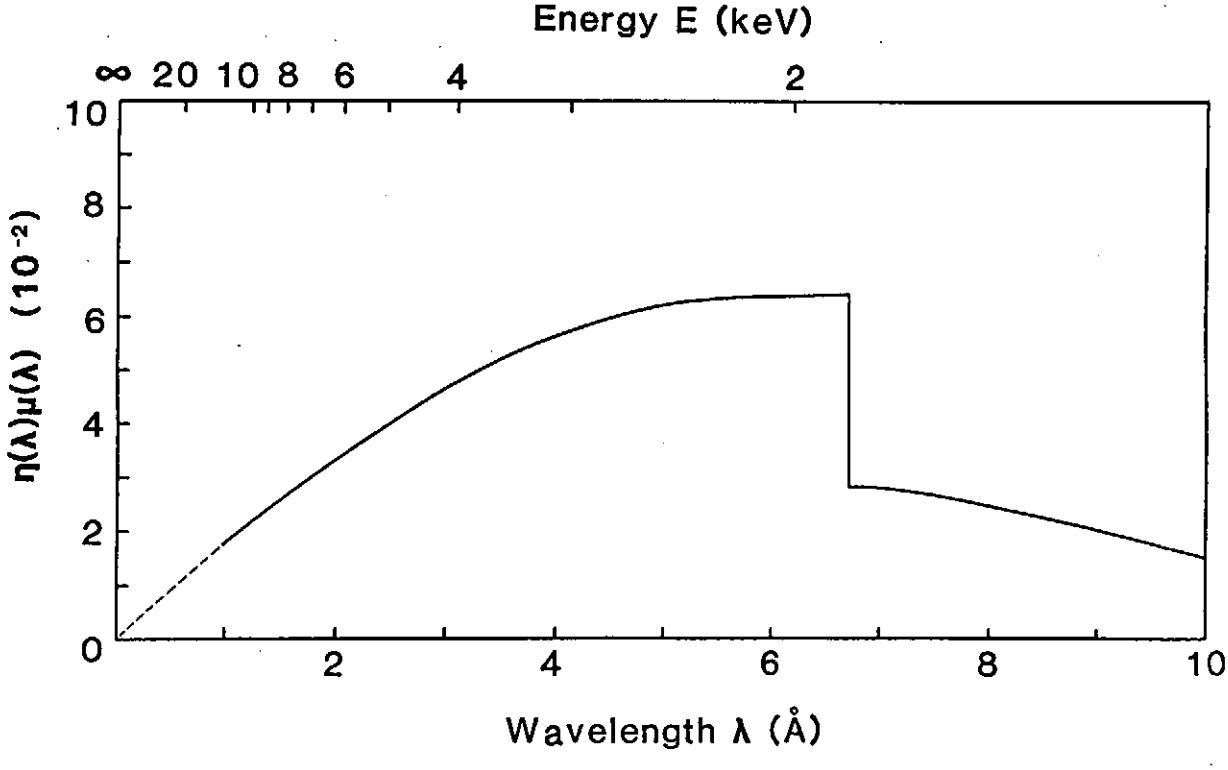

Fig.2

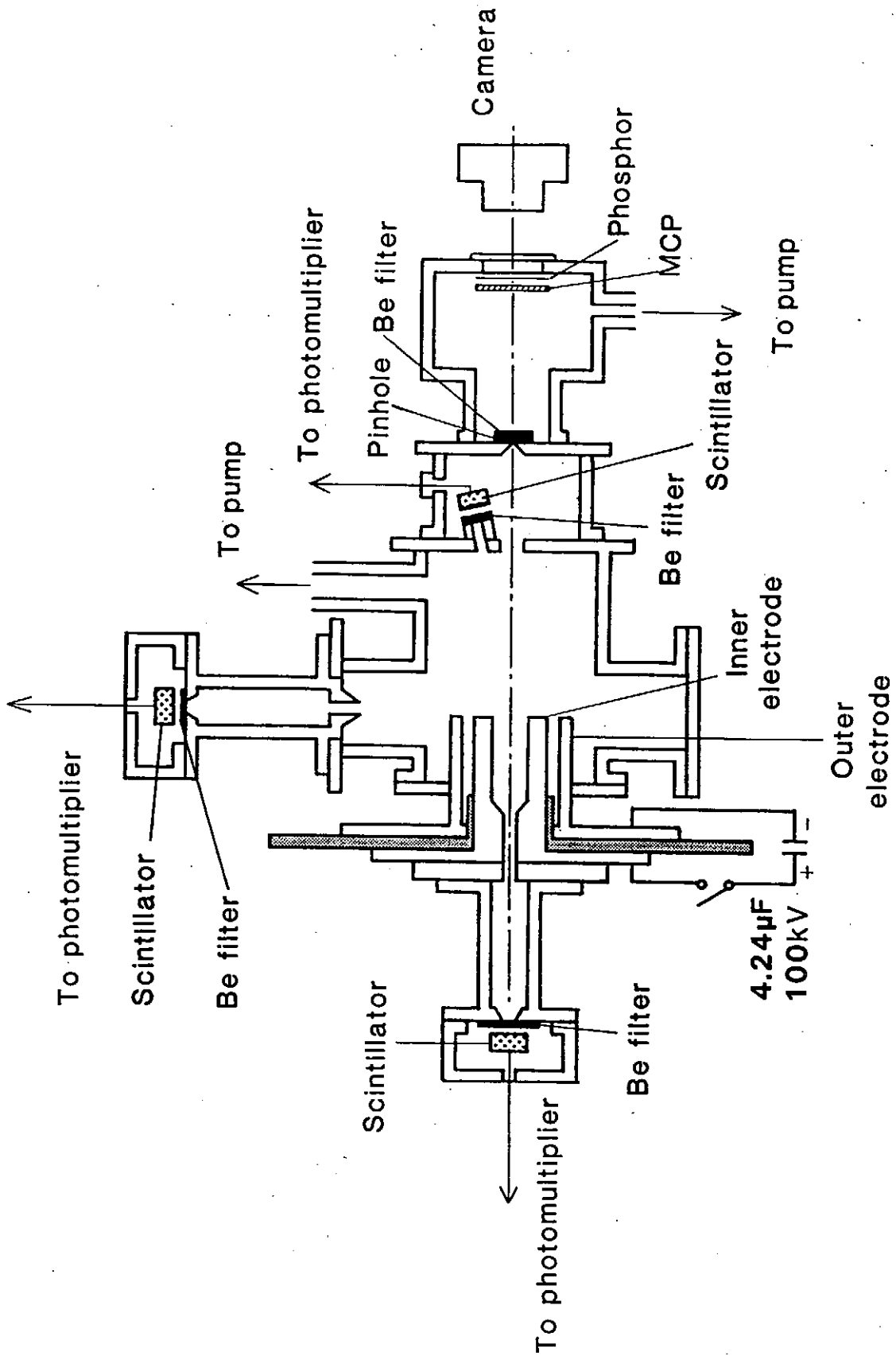
Camera
Phosphor
MCP
To pump
To photomultiplier
Be filter
Pinhole
To pump
Scintillator
Be filter
Inner electrode
Outer electrode
To photomultiplier
Scintillator
Be filter
4.24μF
100kV
Scintillator
Be filter
To photomultiplier

Fig. 3

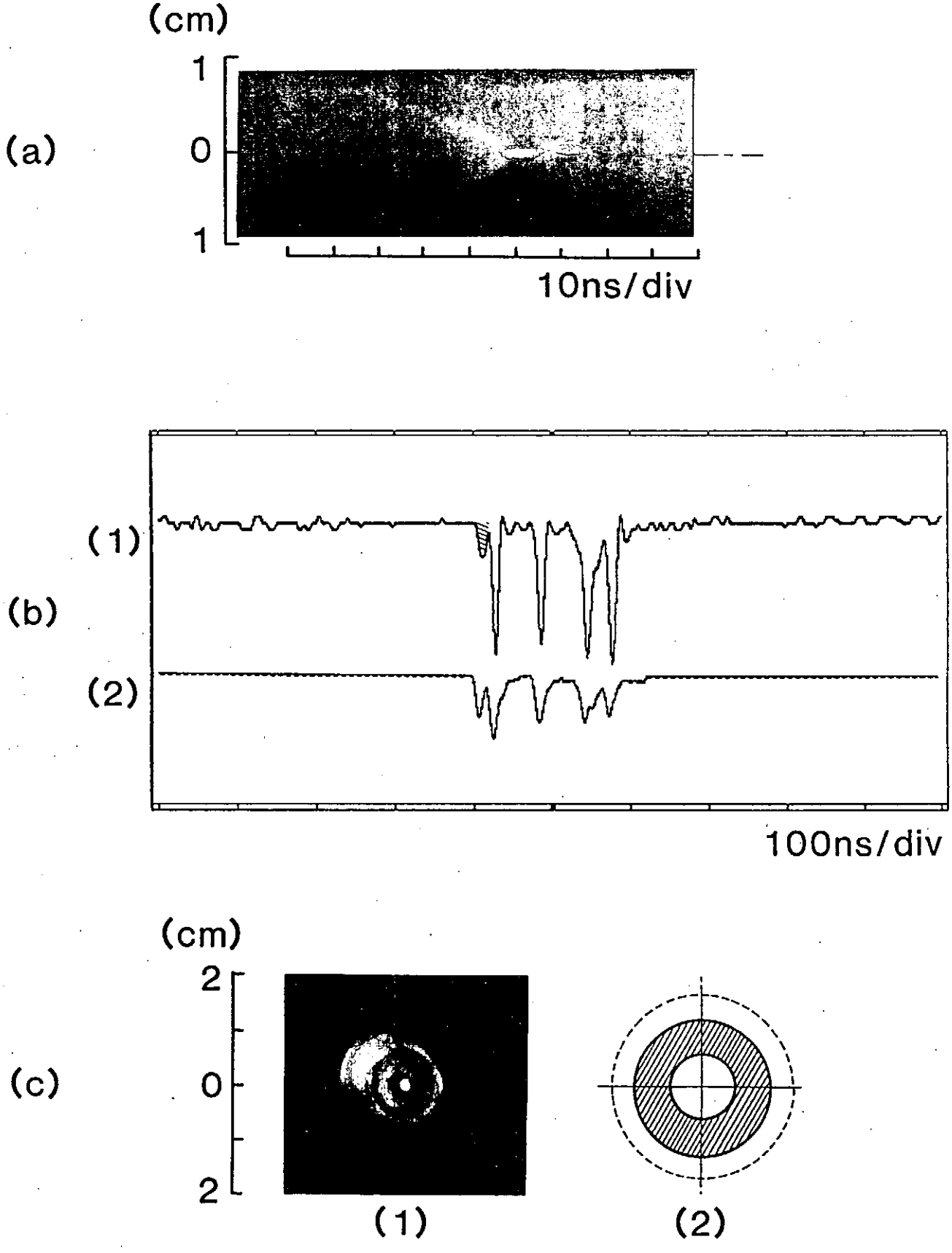

Fig. 4

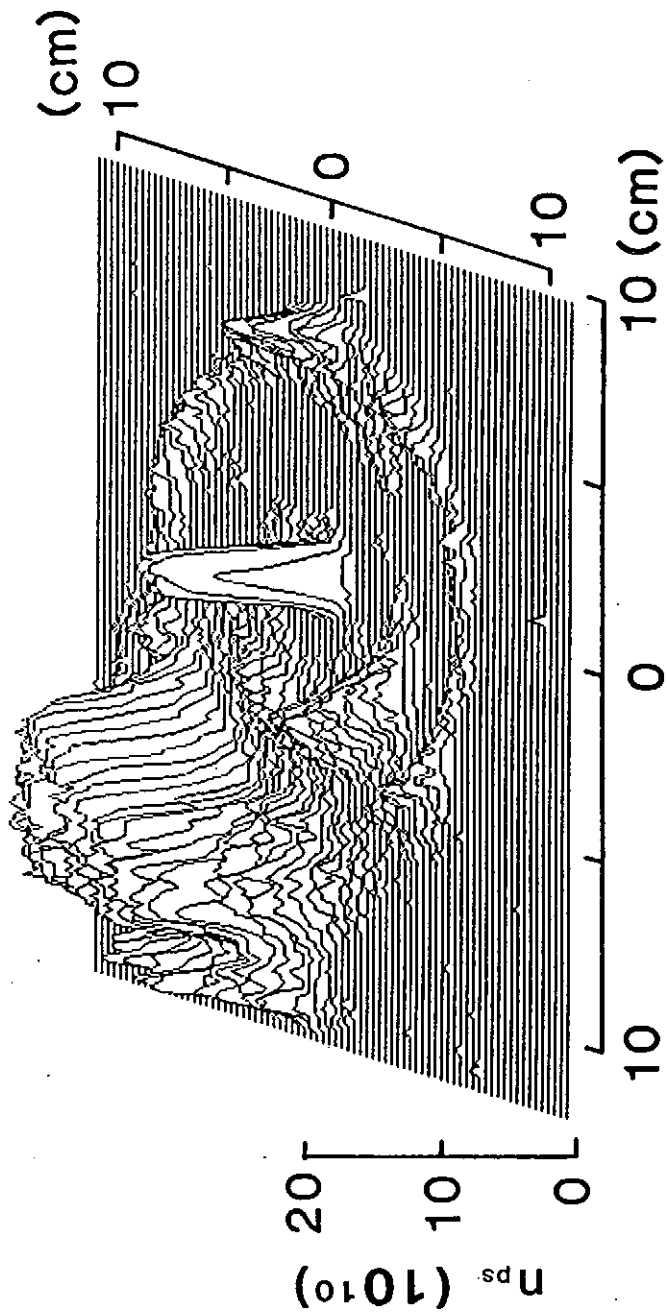

Fig.5

Radiative Collapse in a Z-pinch powered by Blumlein generator

Seizo Furuya, Takahiro Hoshide,

Yoshikazu Hoshina, and Shozo Ishii

Tokyo Institute of Technology

Abstract

We have constructed a pulsed power generator of Blumlein type to examine radiative collapse in carbon fiber pinches. Moreover, we carried out calculating and examination about radiative collapse. Numerical calculations show the reduced critical current for the initiation of radiative collapse.

1 INTRODUCTION

In the Fiber pinch created from a carbon fiber of 7 micrometer in diameter by a pulsed high current, the plasma column usually expands during the initial stage of the discharge. Therefore, the pulsed power generator having a sufficiently high rate of increase of the current is required. We have examined the pinch compression in the carbon fiber pinch powered by a Blumlein generator. Preparation of the generator has been just completed. We are going to measure the soft x-ray from the pinch plasma by various methods to analyze the pinch process. We have carried out the numerical calculation on radiative collapse in the fiber pinch, which results in rapid contraction of the plasma column as the current exceeds a critical value.

2 EXPERIMENTAL APPARATUS

The Blumlein generator constructed is shown in Fig.1. The stored electrical energy in the Marx generator is $6.25kJ$, when the output voltage is $500kV$.

The peak current of $100kA$ rises in about $100ns$.

Fig.2 shows the load chamber for the fiber pinch experiments. The typical waveforms of discharge voltage, current and the x-ray emission detected by a PIN diode are shown in Fig.3.

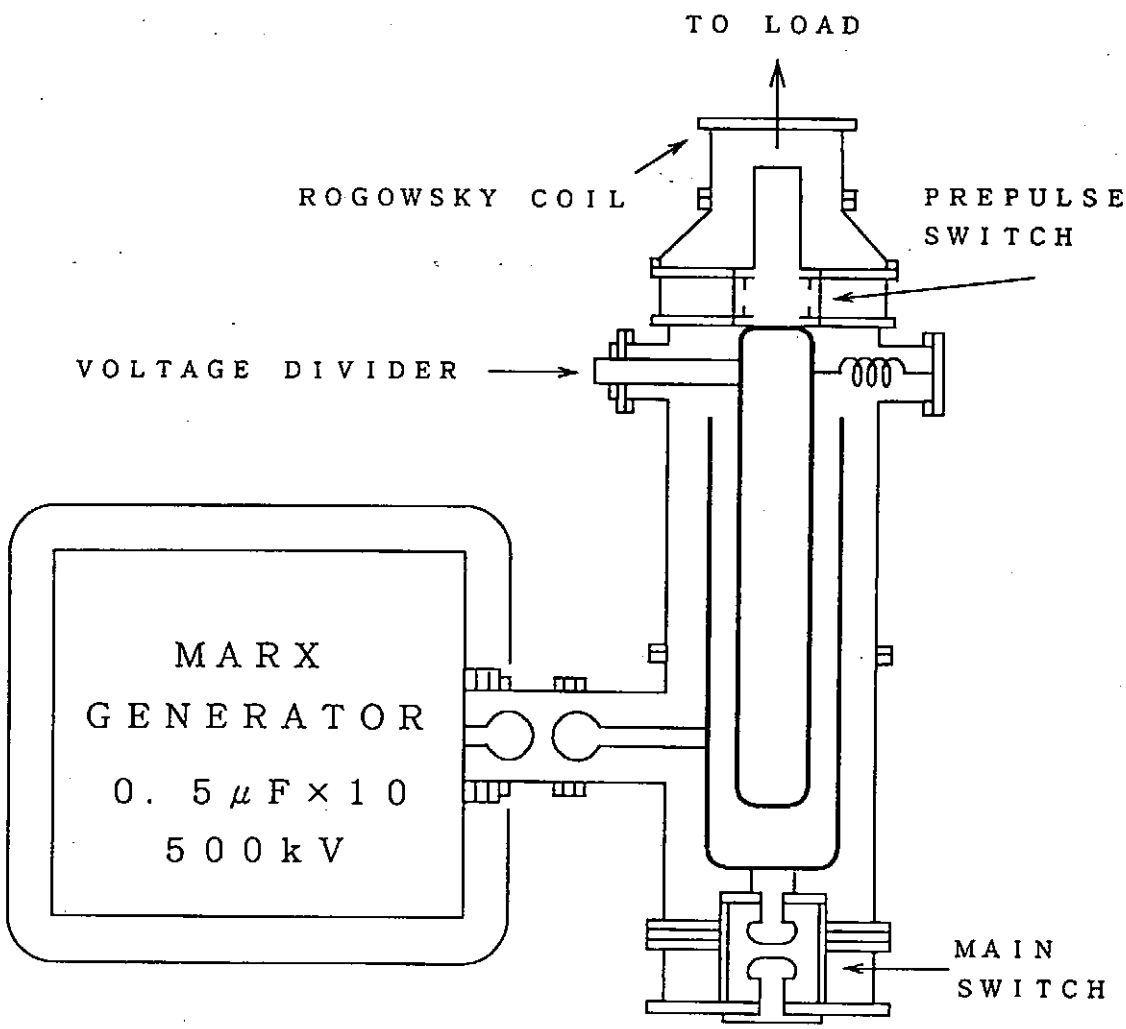

Fig. 1 Blumlein Generator.

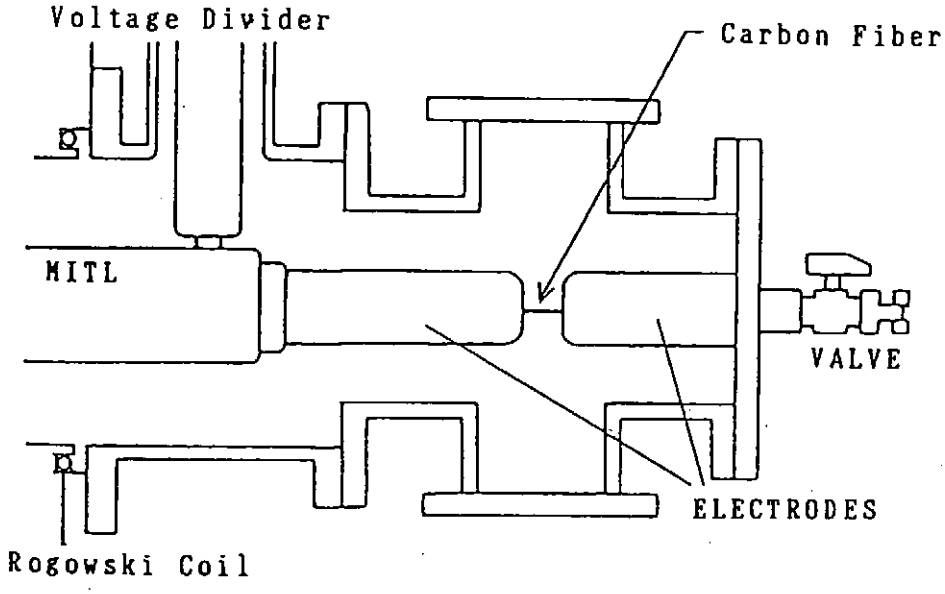

Fig. 2 Load chamber for the fiber pinch experiments.

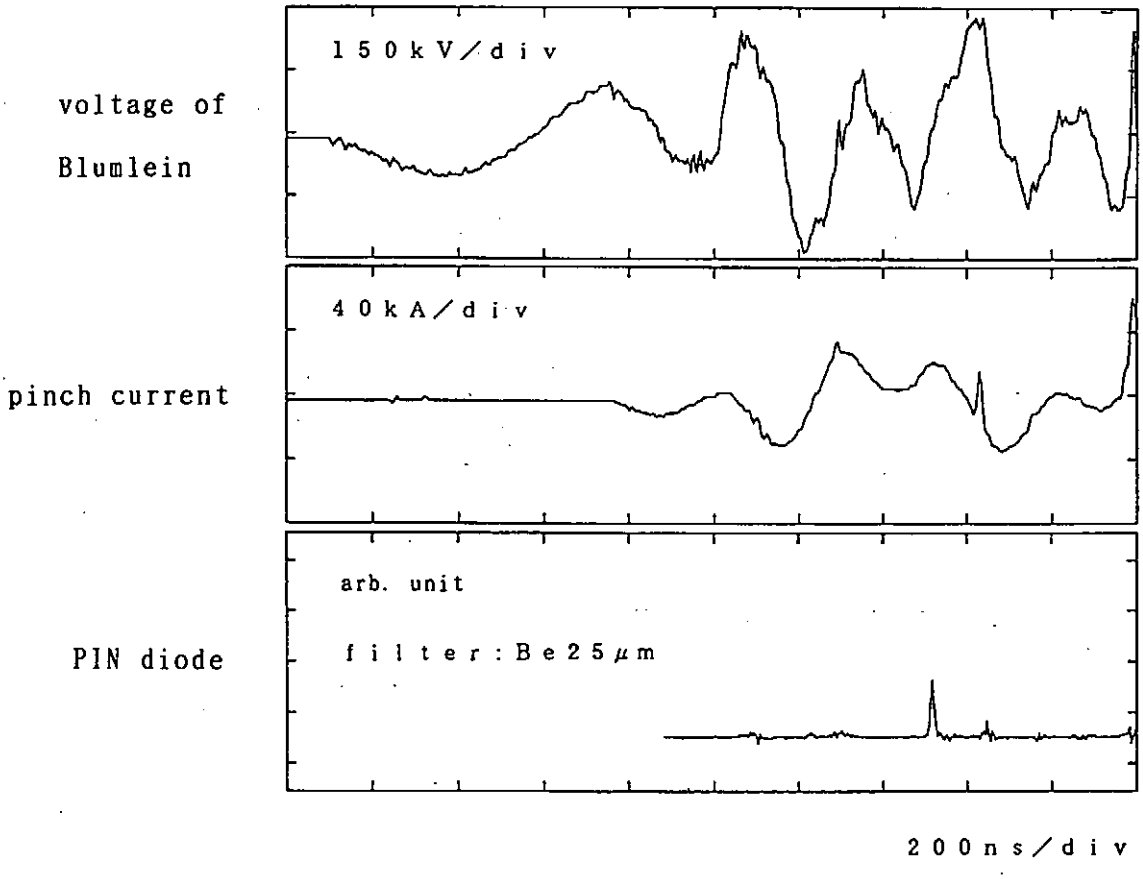

Fig. 3 Waveforms of voltage, current and x-ray emission.

3 RADIATIVE COLLAPSE

The radius of a quasistatic pinch is determined by the balance between joule heating and radiative loss: when the heating exceeds the radiation, the pinch will expand, and vice versa. A steady-state pinch with constant radius is possible only at the Pease-Braginskii current I_{PB}. Below this current the pinch will expand and above this current it will collapse. If the current exceeds I_{PB}, the pinch radius will go to zero in a finite time (the 'radiative collapse').

In the calculating, we consider the Bennet relation

$$\mu_0 I^2 = 8\pi\ (1+Z)\ NkT \tag{1}$$

where I is the pinch current, Z is atomic number, N is the ion number per unit length, k is Boltzmann's constant and T is the mean temperature.

The pinch radius is determined by the power balance between heating and cooling. The power balance equation for unit length of the pinch is

$$\frac{d}{dt}\left\{\frac{3}{2}\ (1+Z)\ NkT\right\} = I^2R - P_r - \frac{\mu_0 I^2}{4\pi a}\frac{da}{dt} \tag{2}$$

where R is Spitzer resistivity, P_r is the joule heating and a is the pinch radius.

Spitzer resistivity R is

$$R = \frac{1.03\times10^{-4}\ln\Lambda}{\pi a^2 T^{3/2}}\quad \Omega\cdot m^{-1} \tag{3}$$

We consider only bremsstrahlung as P_r.

$$P_r = I^2R\left(\frac{I^2}{I_{PB}^2}\right) \tag{4}$$

The Pease-Braginskii current I_{PB} is

$$I_{PB} = 0.433\frac{1+Z}{2Z}\ (\ln\Lambda)^{1/2}\ \mathrm{MA} \tag{5}$$

When $ln\ \Lambda = 10$, we obtain $I_{PB} = 1.4MA$ in hydrogen and $800kA$ in carbon.

The increasing inductance of the collapsing pinch will cause the current to fall. By incorporating the pinch into a realistic circuit shown in Fig.4, this may be calculated by treating the pinch as a varying resistance R_p and a varying inductance L_p in a circuit equation.

$$\frac{q}{C}+R\,i+L\frac{d\,i}{d\,t}+R_P\,i+\frac{d}{d\,t}\,(L_P\,i)\,=0 \tag{6}$$

The results for deuterium and carbon are shown in Fig.5 and 6, respectively. The parameter is the ion number per meter ranging 10^{17} to 10^{19}. In each figure, radiative collapse is indicated by a rapid decrease in radius, and collapse occurs in all cases except for $N = 10^{17}m^{-1}$ in deuterium. For $N = 10^{19}m^{-1}$, it occurs at lowest current.

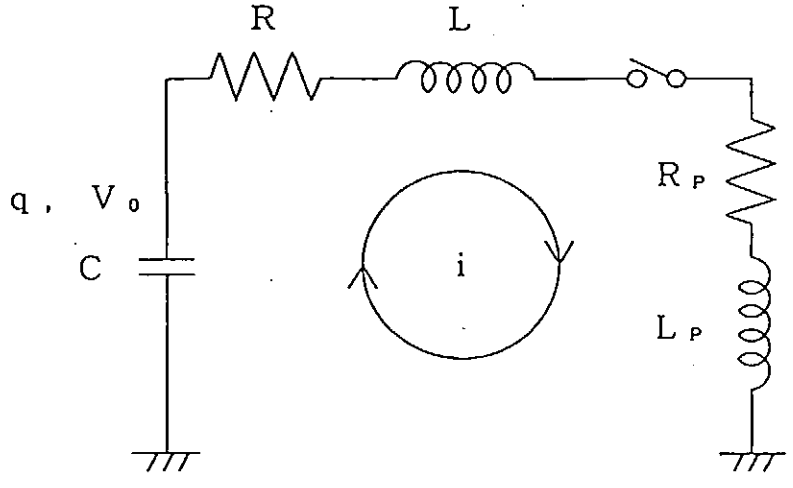

Fig. 4 The circuit model.

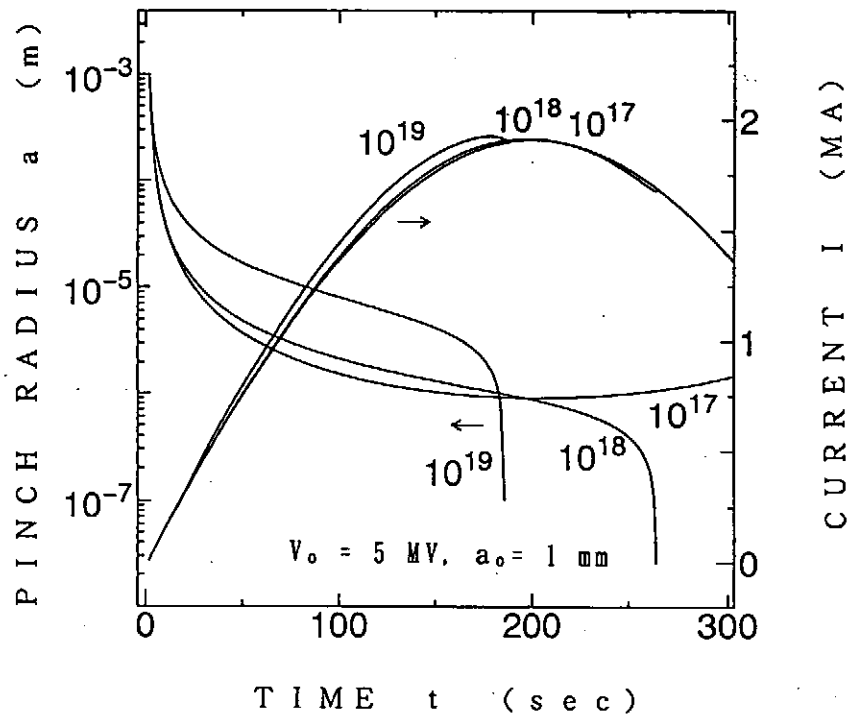

Fig. 5 Radius(a) and current (I) versus time (t) for a pinch in deuterium.

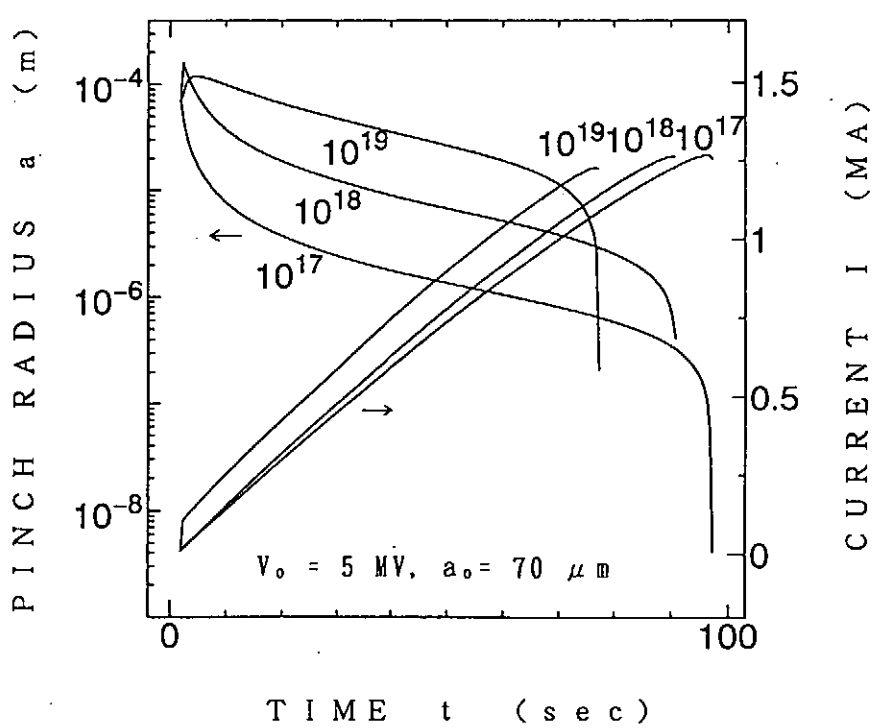

Fig. 6 Radius (a) and current (I) versus time (t) for a pinch in carbon.

4 CONCLUSION

We examined about radiative collapse considered only bremsstrahlung as radiation loss. We used fiber with metal coating on the surface. Therefore, the line radiation power from high ionized ions can not ignore. Radiative collapse initiating at the lower critical current can be observed.

References

[1] J.P.Chittenden and M.G.Haines

Phys.Fluids B2(8),August 1990,pp.1889 to 1897

[2] M.G.HAINES

Plasma Physics and Controlled Fusion,Vol.31,No.5,pp.759 to 778,1989

[3] J.P.CHITTENDEN,A.J.POWER and M.G.HAINES

Plasma Physics and Controlled Fusion,Vol.31,No.11,pp.1813 to 1822,1989

[4] A.E.Robson

Phys.Fluids B3(6),June 1991,pp.1461 to 1466

[5] A.E.Robson

Phys.Fluids B1(9),September 1989,pp.1834 to 1842

[6] A.E.Robson

NUCLEAR FUSION,Vol.28,No.12(1988),pp.2171 to 2178

Soft x-ray radiation from metal vapor puff Z-pinch plasmas

Yoshikazu Hoshina, Toshiaki Suzuki, Kenji Arai,
Qing-Pin Ai, and Shozo Ishii

Tokyo Institute of Technology

Abstract

Dense and high energy density Z-pinch plasmas are created by new way and are examined experimentally. Metal vapor puff Z-pinch is superior to other configurations in control and in operation. In this configuration, the dense plasmas can be created from high z materials and radiate high intensity x-rays. The macroscopic pinch characteristics have been observed by streak photography. Temporal behaviors of x-ray radiation from metal vapor puff Z-pinch have been investigated.

1 Introduction

Z-pinch plasmas easily creating dense and high energy density plasma open up various applications. Intense x-ray radiation from Z-pinch plasma is applied to x-ray laser and intense x-ray source for lithography in semiconductor processing. A gas puff Z-pinch has been attractive as x-ray source and has been tested for many purposes. The advantages of the gas puff Z-pinch are high repetitive and reproducible operation. X-ray intensity and characteristics depend strongly on the initial gas profile and the injection time [1]. The operational time for gas injection is about sub-miliseconds. However, the rise time of typical generator for Z-pinches is sub-microseconds. Therefore, a precise control of the gas profile at the initiation of discharge is impossible. In the gas puff Z-pinch, the materials being able to become plasma are restricted to gaseous material at room temperature. In Vacuum spark, the restriction of the material for plasma

medium is relaxed and solid materials are used. The disadvantage in vacuum spark is poor reproducibility.

To overcome these problems, we have proposed a new scheme of Z-pinch. In this scheme, metal vapor is produced by pre-discharge inside one of the main electrodes. Metal vapor is puffed from a small nozzle. The principle of this system is similar to the gas puff system, but the operation time of the electrically controlled system is faster than that of the gas puff system based on the mechanical control, about several microseconds. The material to become plasma is extended from gas to solid. The degree of freedom in choosing the wavelength range of soft x-ray radiation becomes so large. In this paper, we report on x-ray radiation from the metal vapor puff Z-pinch.

2 Experimental setup

A metal vapor puff Z-pinch apparatus is shown schematically in Fig.1. Lower electrode has a metal vapor production equipment in it. Metal vapor is produced by a pre-discharge in a small cavity. Metal vapor gas profile can be controlled by changing nozzle configurations. Two types of configuration are examined: a nozzle of 1mm in diameter placed at the center of the main electrode and 16 nozzles arranged in a circle of $20mm$ in diameter that is like wire-array pinch configuration. A plasma column length is $10mm$ as determined by the separation of electrodes. The vacuum chamber made of stainless steel is evacuated by an oil-diffusion pump and the operating pressure is $5 \times 10^{-5} torr$. There are four windows in the radial direction viewing the center of the chamber. X-ray and visible radiation are detected through these windows.

The pre-discharge for making metal vapor was powered by the capacitor of $3\mu F$ charged to $15 - 20kV$. The metal vapor puff Z-pinch is driven by a capacitor bank of $27\mu F$. The bank consists of nine capacitor units, each of which has two $1.5\mu F$ capacitors with a pressurized air-gap switch and is charged

to $20kV$. The total stored energy is $5.4kJ$.

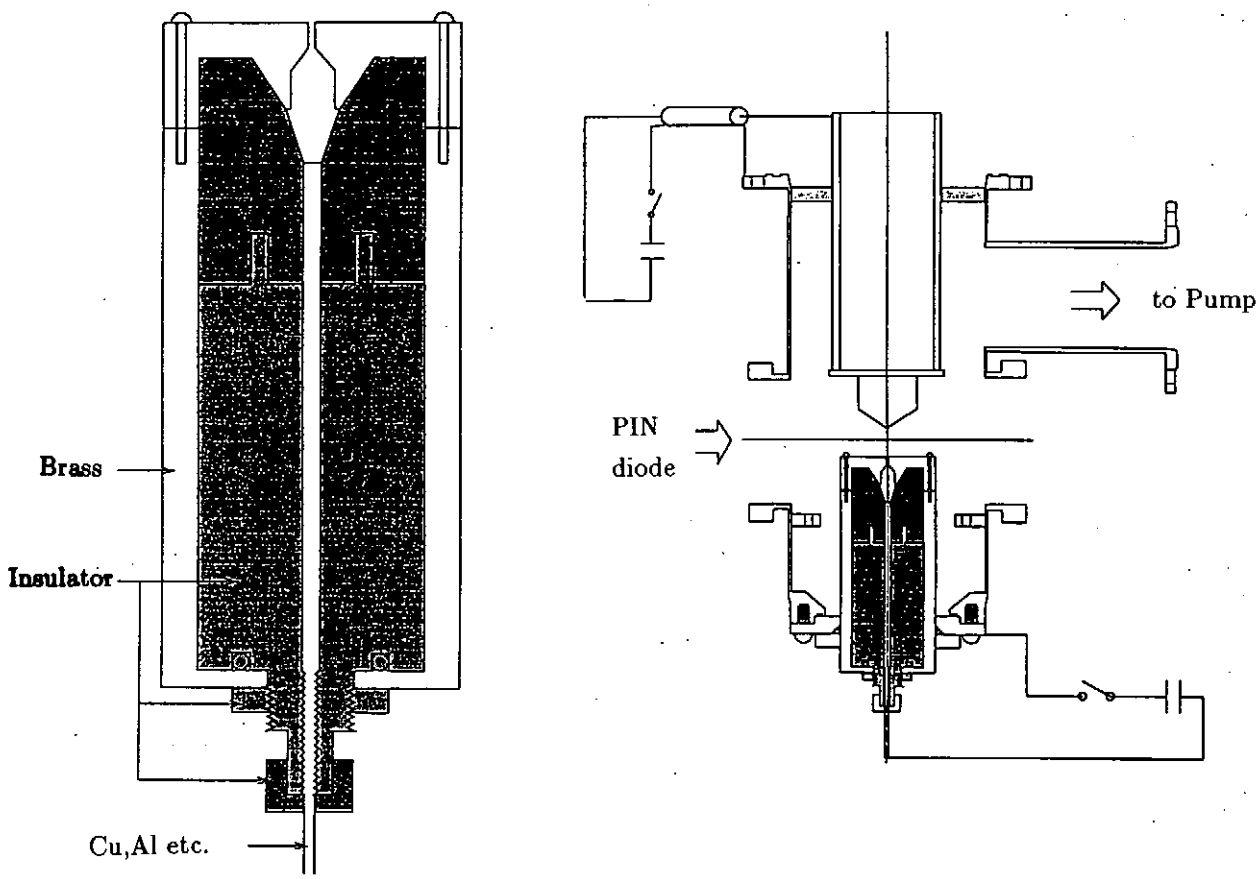

Fig. 1 A metal vapor puff Z-pinch apparatus.

Temporal and spectral behaviors of visible radiation from metal vapor gas have been investigated by a monochromator. The pinch characteristics are diagnosed by streak photography taken through the acrylic window in the radial direction, and by conventional current measurements. A PIN diode (Quantrad Co. 100-PIN-125) has been used as an x-ray detector. If soft x-ray photons are injected into the PIN diode with reverse bias, the signals are detected as a current of the external circuit. The PIN diodes are with faster response than other photo diodes and are sensitive for the soft x-ray wavelength. The wavelength sensitive range of the PIN diodes is from about $0.03nm$ to $3.5nm$ (over 1% in the relative efficiency to maximum). Filters are mounted in front of the PIN diode to cut off visible light radiated from the plasma and to obtain

rough estimation of radiated x-ray photon energy spectrum. An x-ray pinhole camera has been used for spatially resolved x-ray measurement. X-ray spectra in the wavelength range of $8-11\mathring{A}$ are obtained by a flat crystal spectrograph with a KAP (Potassium Acid Phthalate) crystal [2]. The pinhole camera and the spectrograph are shielded from visible light through a beryllium foil. These devices must be in vacuum because soft x-rays are absorbed by air.

3 Results

Copper is mainly used as an evaporating material throughout the experiments. Visible light spectra from metal vapor gas are shown in Fig.2. The line spectra from Cu I and Cu II are observed. And the total intensity of visible light increases as making the charged voltage for pre-discharge higher. The timing of vapor puff is synchronized with current period. As a result, we can control the mass of vapor gas and puff timing with pre-discharge parameters.

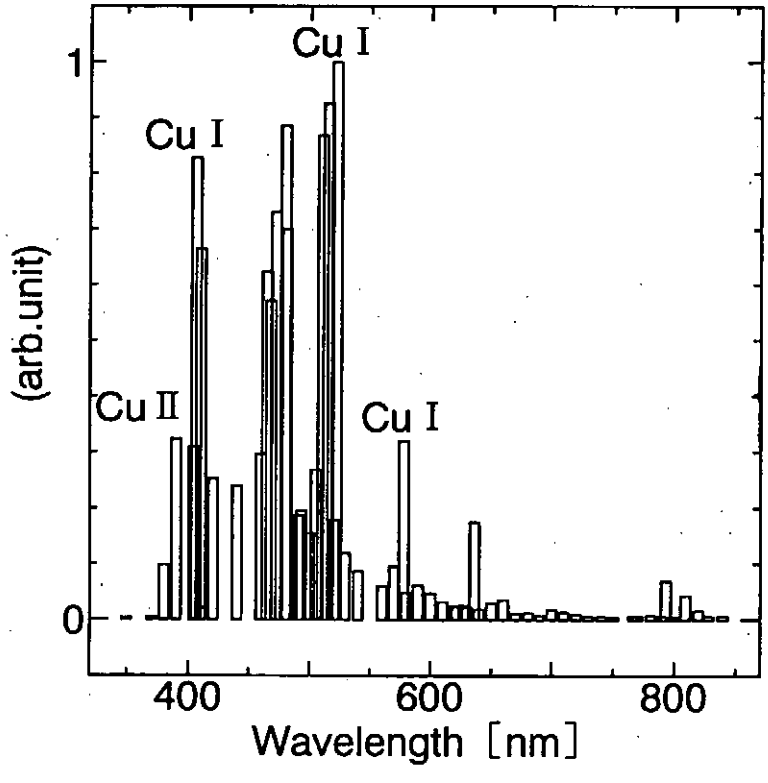

Fig. 2 Visible light spectra from metal vapor gas.

Typical waveforms of the main discharge current and the x-ray radiation detected by the PIN diode are shown in Fig.3. The peak value of the discharge current is about $370kA$. X-ray radiation appears during the current rising and coincides with a dip of plasma current trace. X-ray radiation is observed reproducibly in every shot. The intensity of x-ray radiation is poorly reproducible.

The visible light in the streak photograph is shown in Fig.3. In this case, the initial gas profile is hollow. Radial imploding evolution is observed. Maximum pinch is coincided with the peak of x-ray radiation and is maintained for about $300ns$. When the plasma column length was made longer ($20mm$), plasma was confined in the shorter time (Fig.5).

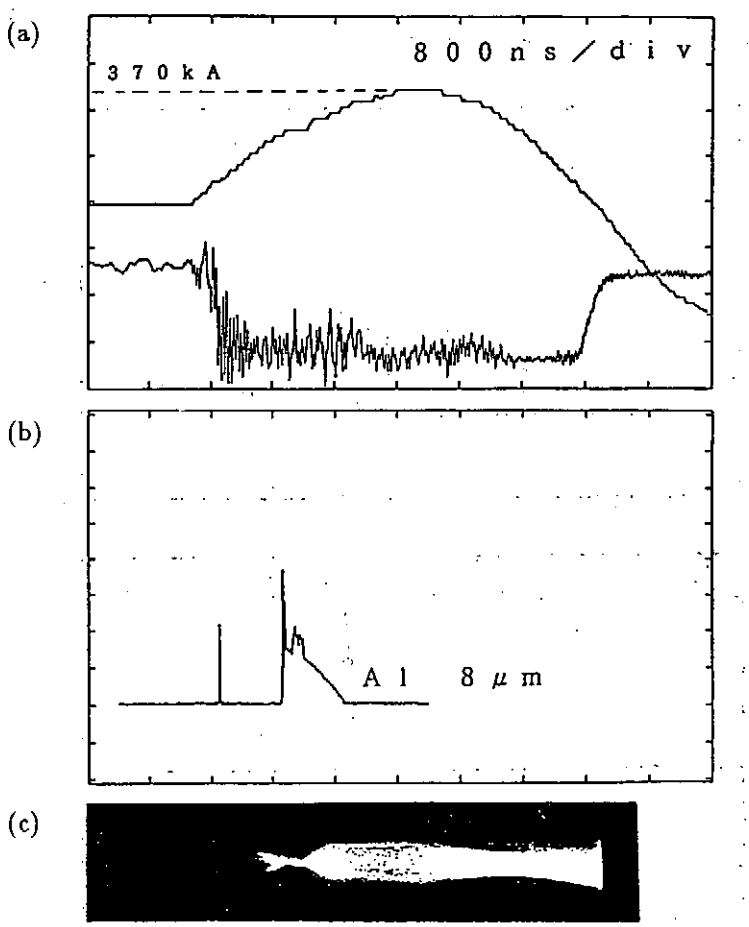

Fig. 3 Metal vapor puff Z-pinch,
(a) pinch current, (b) x-ray signal,
(c) streak photograph of radial profile.

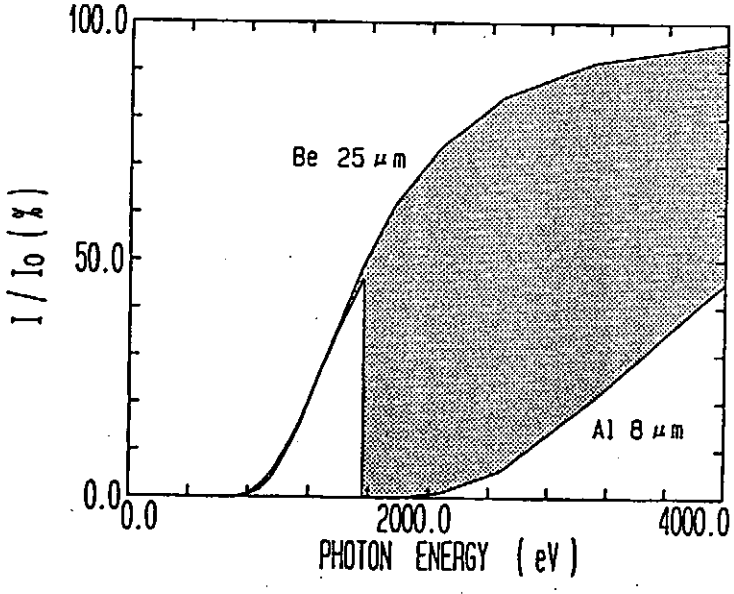

Fig. 4 Absorption characteristics of metal foil windows.

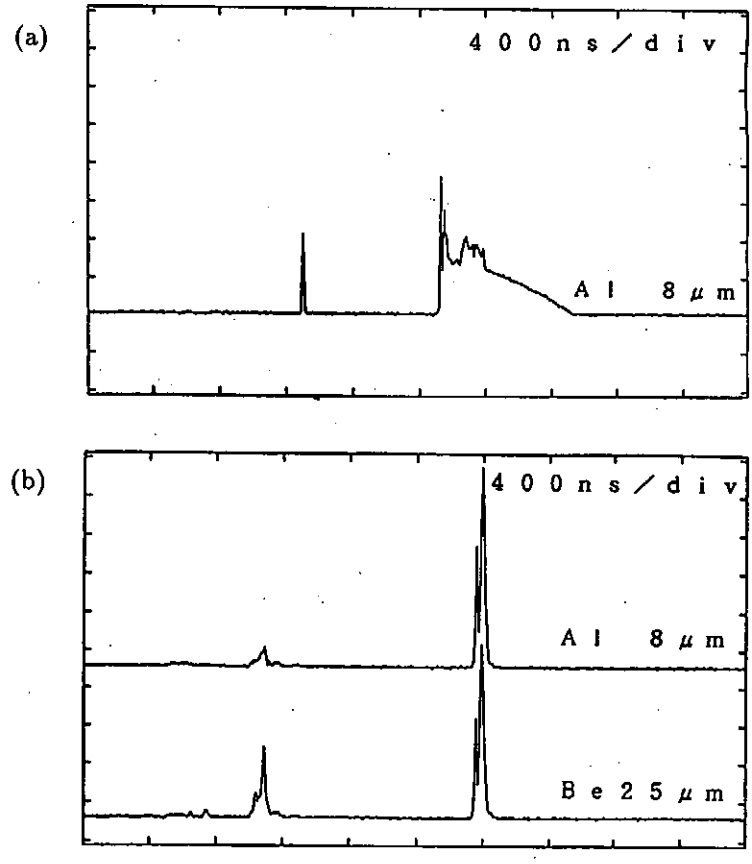

Fig. 5 X-ray signals, at

(a) the plasma column length 10mm,

(b) the plasma column length 20mm.

To analyze time-resolved spectroscopic profiles, x-ray radiation was measured by a pair of two PIN diodes with metal foil windows having different absorption characteristics. As comparing two signals from the diodes with foil windows having different absorption characteristics over the K shell absorption edge of Al ($1.56keV$), one can obtain high energy x-rays more than $1.56keV$ (Fig.4). High energy x-rays were produced mainly by nonthermal process caused by MHD instabilities. Since the signals of two PIN diodes were almost similar, x-ray radiation at the pinch phase was produced by thermal process in the hot plasma rather than by nonthermal process.

4 Conclusion

Dense and high energy density Z-pinch plasmas are created by new way and are examined experimentally. Metal vapor puff Z-pinch is superior to other configurations in control and in operation. In this configuration, a stable plasma column is observed for about $300ns$. X-ray radiation at the maximum pinch was mainly caused by thermal process.

References

[1] Cheng Rong Li and Tsin Chi Yang:
J. Phys. D: Appl. Phys., 24, 48 (1991).

[2] K. Shimoda, T. Yamamoto, S. Takada, H. Sone, and K. Hirano:
Jpn. J. Appl. Phys., 26, 451 (1987).

[3] Y. Hoshina et al.:
NIFS-PROC-7 11 (1991).

Recent Issues of NIFS-PROC Series

NIFS-PROC-1 *U.S.-Japan on Comparison of Theoretical and Experimental Transport in Toroidal Systems Oct. 23-27, 1989* Mar. 1990

NIFS-PROC-2 *Structures in Confined Plasmas –Proceedings of Workshop of US-Japan Joint Institute for Fusion Theory Program–* ; Mar. 1990

NIFS-PROC-3 *Proceedings of the First International Toki Conference on Plasma Physics and Controlled Nuclear Fusion –Next Generation Experiments in Helical Systems– Dec. 4-7, 1989* Mar. 1990

NIFS-PROC-4 *Plasma Spectroscopy and Atomic Processes –Proceedings of the Workshop at Data & Planning Center in NIFS–*; Sep. 1990

NIFS-PROC-5 *Symposium on Development of Intensed Pulsed Particle Beams and Its Applications February 20 1990*; Oct. 1990

NIFS-PROC-6 *Proceedings of the Second International TOKI Conference on Plasma Physics and Controlled Nuclear Fusion , Nonlinear Phenomena in Fusion Plasmas -Theory and Computer Simulation-;* Apr. 1991

NIFS-PROC-7 *Proceedings of Workshop on Emissions from Heavy Current Carrying High Density Plasma and Diagnostics;* May 1991

NIFS-PROC-8 *Symposium on Development and Applications of Intense Pulsed Particle Beams, December 6 - 7, 1990*; June 1991

NIFS-PROC-9 *X-ray Radiation from Hot Dense Plasmas and Atomic Processes*; Oct. 1991

NIFS-PROC-10 *U.S.-Japan Workshop on "RF Heating and Current Drive in Confinement Systems Tokamaks" Nov. 18-21, 1991*, Jan. 1992

NIFS-PROC-11 *Plasma-Based and Novel Accelerators (Proceedings of Workshop on Plasma-Based and Novel Accelerators) Nagoya, Japan, Dec. 1991*; May 1992

NIFS-PROC-12 *Proceedings of Japan-U.S. Workshop P-196 on High Heat Flux Components and Plasma Surface Interactions for Next*

Devices; Mar. 1993

NIFS-PROC-13 『NIFS シンポジウム
「核燃焼プラズマの研究を考える－現状と今後の取り組み方」
1992年 7月 15日、核融合科学研究所』
1993年 7月
NIFS Symposium
"Toward the Research of Fusion Burning Plasmas - Present status and Future strategy-", 1992 July 15, National Institute for Fusion Science; July 1993
(in Japanese)